ROLE OF PHOSPHATIDYLINOSITOL METABOLISM IN RENAL EPITHELIAL MEMBRANE TRAFFIC

by

Shanshan Cui

B.S. in Biological Sciences, Wuhan University, 2005

Submitted to the Graduate Faculty of

School of Medicine in partial fulfillment

of the requirements for the degree of

Doctor of Philosophy

University of Pittsburgh

2010

UNIVERSITY OF PITTSBURGH

SCHOOL OF MEDICINE

This dissertation was presented

By

Shanshan Cui

It was defended on

December 7, 2010

and approved by

Rebecca P. Hughey (Committee Chair), PhD

Carolyn B. Coyne, PhD

Neil A. Hukriede, PhD

Linton M. Traub, PhD.

Dissertation Advisor: Ora A. Weisz, PhD

ROLE OF PHOSPHATIDYLINOSITOL METABOLISM IN RENAL EPITHELIAL MEMBRANE TRAFFIC

Shanshan Cui, Ph.D.

University of Pittsburgh, 2010

Phosphatidylinositol (PI) and its phosphorylated derivatives, phosphatidylinositides (PIPs), are versatile cellular regulators participating in myriad events including signal transduction, cytoskeleton organization, protein targeting and many steps of membrane traffic. Different PIPs exhibit non-overlapping distributions on cellular membranes. This feature contributes to organelle identities and is tightly controlled by kinase/phosphatase-mediated PIP synthesis and turnover. Mechanisms regarding compartment-restriction and detailed functions of many PIPs and PI/PIP metabolizing enzymes remain largely unknown. My dissertation focuses on the cellular targeting mechanism of a PIP kinase and the pathogenesis of a disease caused by mutations in a PIP phosphatase.

Phosphatidylinositol (4,5)-bisphosphate (PIP_2), an apical-surface-enriched PIP in polarized epithelial cells, is primarily synthesized via phosphorylation of phosphatidylinositol 4-phosphate (PI4P) in the presence of type I PI 5-kinases (PI5KIs). Previous studies have suggested that the three isoforms of PI5KI (α, β, and γ) exhibit distinct cellular functions. Data from our lab indicate that these three PI5KIs are differentially localized in polarized renal cells. While the majority of α and γ

isoforms are present on lateral cell surface, the β isoform strikingly localizes to the apical plasma membrane. Using mutagenesis, immunofluorescence, and confocal microscopy, I have found that the apical surface distribution of PI5KIβ is nonsaturable and does not require catalytic activity or the presence of PIP_2. These results provide useful information for future studies on PI5KIβ-regulated cellular activities.

PIP_2 turnover can be catalyzed by a variety of enzymes, one of which is OCRL1. OCRL1 is a PI 5-phosphatase that preferentially hydrolyzes PIP_2, producing PI4P, and is associated with the *trans*-Golgi network, endosomes, and clathrin-coated-pits. Genetic defects of OCRL1 cause Lowe syndrome, a disease manifested by congenital cataracts, mental retardation, and renal tubular dysfunction. By examining cultured renal epithelial cells acutely depleted of OCRL1 via RNA interference, I have found that loss of OCRL1 does not interfere with endocytic trafficking of the multiligand receptor megalin, or uptake of megalin ligands. OCRL1 knockdown did appear to disrupt delivery of newly-synthesized lysosomal hydrolases and alter distribution of primary cilia length in renal epithelial cells. These findings suggest that multiple pathways may contribute to development of renal symptoms in Lowe patients.

TABLE OF CONTENTS

LIST OF TABLES

LIST OF FIGURES

PREFACE

I would like to use this space to express my appreciation to many individuals without whom this work would not have been possible. I would like to start by thanking my wonderful advisor, Dr. Ora Weisz. Ora, your scientific dedication and sharp mind have impressed me many times in the past five years and will keep being a reminder of how I should behave in my future career. Your guidance and suggestions have always been prompt and precise. Your constant support in science and in life has been invaluable during my graduate study. I would also like to give special thanks to every member of my dissertation committee. Drs. Rebecca Hughey, Carolyn Coyne, Neil Hukriede, and Linton Traub, your ideas, suggestions, questions, and critiques in those committee meetings and my dissertation defense have inspired my progress and made me a better scientist.

I would like to thank all the past and present members of Weisz lab, or ‘family’. Five years ago, it was you that made me feel at home in this completely strange country. With you, I have experienced the exciting taste of membrane trafficking research as well as numerous American desserts. I would especially like to thank Jennifer Bruns, Christopher Guerriero, Youssef Rbaibi, Christina Szalinski, and Yumei Lai, who have contributed scientifically to my dissertation work. I would also like to thank all other folks, Di Mo, Polly Mattila, Robert Youker, Bailey Moorhead, Mark Miedel, Kelly

Weixel, Beth Potter, Kerry Cresawn and Mark Ellis, for always being extremely supportive and resourceful. I would like to thank the entire Renal-Electrolyte Division, especially the laboratories of Dr. Rebecca Hughey, Dr. Gerard Apodaca, and Dr. Nuria Pastor-Soler, for sharing experimental materials, instruments, space, and techniques and for maintaining a very pleasant environment to work in. It has been really fun for the past five years. I appreciate the support and help from every member of the Department of Cell Biology and Physiology and would like to give special thanks to Dr. Georgia Duker for sharing with me textbooks and other materials on renal histology, a subject essential to my dissertation.

I owe my parents many thanks. Mom and Dad, I knew exactly how reluctant you were to see me leave for somewhere half the globe away. I apologize for not being around for so long, especially during the rough times of the past year. I thank you for supporting my choices and for taking care of everything at home. I am glad that things are getting better now and wish you health and happiness everyday. I would also like to thank all other relatives and friends in China, US, and many other places. I treasure all the good days that we have shared. Last but not least, I want to thank my husband. Haibin, getting to know you is the best thing that has ever happened to me. My life has never been the same since you entered in. Thanks for always being there for me. Thanks for trying to make me laugh whenever I had a bad day. Thanks for cooking in the past a few weeks when I was busy writing. I love you.

1.0 INTRODUCTION

1.1 STRUCTURE AND FUNCTION OF THE KIDNEY

1.1.1 Anatomy of the kidney

The kidneys are urinary organs found in many types of animals including vertebrates and some invertebrates. During evolution, main functions and efficiency of the kidneys adapted to the living environment of every species, giving rise to functionally and structurally heterogeneous urinary systems in different animals (1). For example, the main function of the kidneys in freshwater fish and amphibians is to get rid of excessive water from the hypotonic aqueous environment, although the amphibians are also able to cope with the land environment by restricting the renal filtration and by other mechanisms. Metabolic wastes of the freshwater animals usually diffuse out directly into the surrounding water without passing through the kidney tubules. Marine animals, on the contrary, live in a constantly hypertonic environment. They therefore need to preserve body water by either developing concentrated isotonic blood or an active system to desalt the sea water. Their kidneys act as excretory organs responsible for clearing metabolic wastes. Some reptiles live in extremely dry environments and their nitrogenous wastes are transformed into the insoluble uric acid, secreted into renal tubules, and excreted without the need of a big volume of waterous solvent. Very little water is lost everyday so that these animals can survive

without drinking water. As direct descendants of the reptiles, birds inherited the uric acid based mechanism to eliminate their metabolic wastes. Mammals, including human, utilize urea as the major form of nitrogenous waste. Urea is water-soluble and needs to be excreted in an aqueous solution. Therefore mammalian kidneys are mini urinary factories producing the end-product urine by filtering the blood and adjusting the filtrate composition by active absorption and secretion (2).

In humans, the kidneys are paired bean-shaped retroperitoneal (lying behind the peritoneum) organs present in the abdominal cavity (1). Sizes and locations of the left and the right kidneys are slightly asymmetric due to the intrinsic organic asymmetry within the abdominal cavity (1). The kidneys and the adjacent adrenal glands are protected by ribs, layers of fat and connective tissue structures.

Encapsulated in a thick strong connective tissue layer called the renal capsule, the kidney gross structure is visually divided into two parts, the cortex and the medulla (1). These two parts differ in both structure and function. The kidneys are most well-known as urinary organs in which the smallest functional unit is called a nephron. There are approximately 1 million nephrons per kidney (1). Each nephron is a blind beginning tube composed of six main sections: Bowman’s capsule, proximal tubule, thin limbs of the loop of Henle (descending & ascending), thick ascending limb of the loop of Henle, distal convoluted tubule, and collecting duct (1). Every section, according to its unique function, exhibits a specific structural relationship to surrounding blood vessels (2). The morphological and functional differences between the renal cortex and medulla are due to uneven distribution of the nephron sections

and blood vessels (2). Additionally, the medulla can be further divided into sub-zones and stripes depending on the renal tubule composition (1).

The kidneys are among the most versatile organs in the body, serving multiple important roles. Besides the main function in waste excretion and urine production, the kidney also participates in other critical processes including the maintenance of acid-base homeostasis, osmolality regulation, blood pressure regulation, metabolic processing and hormone secretion (2).

1.1.2 Glomeruli and renal filtration

The kidney excretory function starts with blood filtration. Bowman's capsule, the blind beginning of the nephron tube, is a bulbous expansion closely surrounding a tuft of capillaries, namely the glomerulus, where filtration takes place. Together, Bowman's capsule, blood vessels (the glomerulus), the intervening basement membrane, and a stalk of supporting mesangial cells form an elaborate spheric structure called the renal corpuscle, which is the filtration unit of the kidney (3). Blood enters the glumerulus via the afferent arteriole which branches into a fenestrated capillary bed allowing passage of serum components through the capillary endothelium (3). Glomerular capillaries are covered by podocytes, specialized visceral epithelial cells continuous with the parietal epithelium of Bowman's capsule at the vascular pole (where blood flows in and out) of the glomerulus. Each podocyte expands its cell body to form numerous end processes or trabeculae interdigitating with processes from neighboring podocytes (3). The spaces between the series of foot processes, also known as pedicels, are spanned by a specialized junctional complex called the

filtration slit diaphragm (3). There is a 320-330 nm thick basement membrane lying between the endothelia of glomerular capillaries and the foot processes of podocytes (3). The basement membrane appears to consist of three heterogeneous layers when examined by electron microscopy. The two lighter staining outer layers are negatively charged and therefore, together with podocyte processes that are also anionic, selectively facilitate passage of positively charged plasma components (2). The electron-dense central layer, at the same time, is enriched with collagen type IV which serves as a molecular filter with a cutoff size of roughly 40KDa (2). After blood has passed through the capillary bed, it exits the glomerulus via the efferent arteriole at the vascular pole. In summary, the fenestrated endothelium, the glomerular basement membrane and the podocyte pedicels with filtration slit diaphragms are the three histological layers that comprise the glomerular filtration barrier. The glomerular filtration rate (GFR) through these three layers is fine tuned by smooth muscle fibers present in the media of afferent and efferent arterioles and contractile intraglomerular mesangial cells (3). Alterations in any part of the delicate filtration barrier can result in diseased conditions.

1.1.3 Proximal tubules and renal reabsorption

The simple squamous parietal epithelium of Bowman's capsule is continuous with the proximal tubule at the urinary pole of the glomerulus. The proximal tubule epithelium consists of simple cuboidal cells with prominent surface specializations important for their functions.

The kidneys generate ~180 liters of filtrate each day, however only one to two liters

are excreted as the urine (3). Most volume of the glomerular filtrate is therefore reabsorbed in kidney tubules. The proximal tubule is where the majority of reabsorption takes place. Materials reabsorbed from the tubular fluid back into the blood circulation include: 65-70% water, 65-70% Na^+ and K^+, ~100% glucose, ~100% amino acids, ~100% citrate, ~100% small peptides, ~80% bicarbonate ions, 40-50% of the Ca^{2+}, and 80-95% of the PO_4^{3-} (3). Histologically, two distinct proximal tubule segments, the proximal convoluted tubule and the proximal straight tubule, can be identified (1). The convoluted portions coil around the glomeruli and occupy much of the cortex while the straight portions cluster with other straight tubules and find their way to the medulla (1).

The renal proximal tubule epithelium faces the luminal fluid with a characteristic apical brush border. The brush border consists of numerous regular plasma membrane protrusions called microvilli, which increase the total epithelial luminal surface area by more than 36 times (3). The dramatic increase in membrane surface area is a big advantage in nutrient reabsorption, which primarily depends on membrane localized receptors and channels. The proximal tubule epithelium is a 'leaky' one that allows paracellular movement of water and Ca^{2+} (3). While protein-based junctional complexes, including tight junctions (which seal off adjacent membranes) and desmosomes (which stabilize cell-cell connections), are present between neighboring proximal tubule epithelial cells, they are considerably thinner compared to those in other renal tubules (3). Also, specific claudins (major transmembrane protein components of the tight junction) that give rise to relatively

leaky tight junctions are found throughout the proximal tubule (4,5). Additionally, aquaporin channels insert to the apical plasma membrane of proximal tubule epithelial cells, allowing water to pass directly through the cells.

The basolateral plasma membrane of the proximal tubule epithelial cells is folded extensively to provide surface area for Na^+K^+ATPase transporters (3). Na^+K^+ATPase actively pumps Na^+ out of the cell and is responsible for creating a cross-membrane electrochemical gradient used to power the secondary active transport events at the apical brush border. A large number of cytoplasmic mitochondria is found at the basolateral invaginations to provide ATP for the enormous energy demands of active transport (3).

The nephron components distal to the proximal tubule have a limited ability to reabsorb water, salt and selected ions. Their main function is to fine tune the volume and composition of urine and regulate GFR though secretion and hormone-mediated responses (2).

1.1.4 Megalin and endocytosis

One of the most important receptors functioning in the renal proximal tubule is megalin. Megalin, also known as Low Density Lipoprotein-Related Protein 2 (LRP2) or GP330, is a 600-kDa type I transmembrane protein and a member of the LDL-receptor family (6). Megalin is able to bind multiple ligands, including proteins, polypeptides, Ca^{2+}, and others. It localizes to the apical/luminal domain of a wide variety of epithelial cells and has distinct functions at different organs. The most studied role of megalin is its involvement in proximal tubule mediated renal

reabsorption.

Megalin is the major receptor involved in the low-molecular-weight protein reabsorption (7). It is found at the renal proximal tubule epithelial brush border membrane where it scavenges multiple protein ligands from the luminal flow. Ligands bound to megalin undergo clathrin mediated endocytosis (7). Endocytosed ligands separate from megalin once exposed to the low pH environment inside endosomes. Free luminal ligands are subsequently destined for lysosomal degradation while megalin is recycled back to the plasma membrane for the next round of ligand binding. Megalin normally undergoes proteolytic cleavages at different sites, generating an N-terminal extracellular fragment shed in the urine and a short C-terminal piece with unknown functions (8,9) Megalin proteolysis can both happen constitutively and be regulated by ligands (8). A role of the megalin intracellular fragment in regulating selected gene expression was hypothesized although there is no direct evidence so far (8).

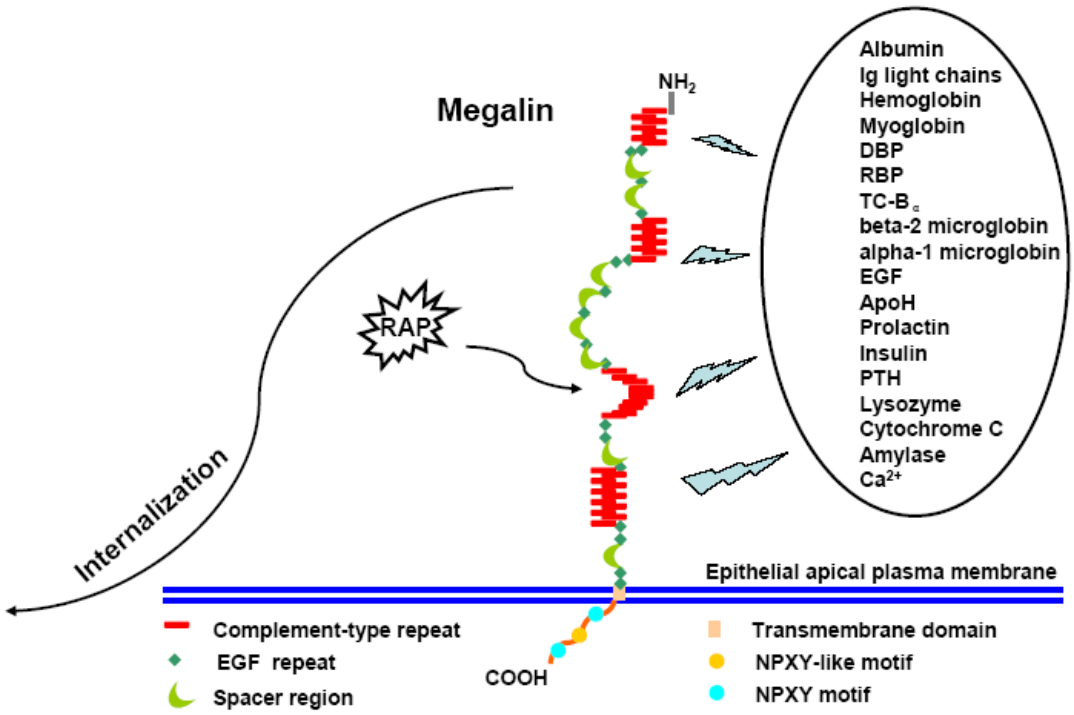

Figure 1.1 Domain structure of the multiligand receptor megalin. Megalin consists of 4 ligand-binding domains (shown in red), a transmembrane domain and a short cytoplasmic tail. Proper folding and localization of megalin require binding to the chaperone RAP. Structural elements as well as a list of ligands of megalin are depicted. This figure is adapted from (10).

Megalin consists of a long extracellular domain, a transmembrane domain and a short cytoplasmic tail (10) (Figure 1.1). The extracellular domain contains four cysteine-rich ligand binding regions separated by epidermal growth factor (EGF)–like repeats and cysteine-poor spacer regions. The cytoplasmic tail contains two NPXY motifs that are required for efficient endocytosis (11,12) and an NPXY–like motif in between, which was reported to be critical for apical sorting and targeting of megalin (13). Proper folding and localization of megalin require the chaperone receptor-associated protein (RAP) (14). The four ligand binding motifs of megalin interact with a variety of low molecular weight proteins and other ligands (10) (Figure 1.1). In addition, megalin is reported to facilitate ligand uptake mediated by a peripheral multi-ligand receptor cubilin (7,10,15,16).

Patients with renal proximal tubule related disorders tend to develop characteristic low molecular weight proteinuria, namely the abnormal excretion of low molecular weight proteins (including many megalin ligands) in the urine, suggesting possible megalin dysfunction. One example of these disorders is Dent disease, which is caused by genetic defects in the endosome-localized chloride/proton antiporter CLC5. (17,18). Reduced renal tubular epithelial expression and disrupted recycling of megalin have been reported to account for the various renal symptoms (including proteinuria, hypercalciuria, and etc.) of Dent patients (17-19). Involvement of megalin in the pathogenesis of other proximal tubule associated diseases, like Lowe syndrome, remains a hypothesis.

1.1.5 Cilia in the kidney

The rates of renal filtration and reabsorption are tightly controlled by a variety of hormones and small molecules (3). Production, release and degradation of those specific regulators are often coupled to changes in the kidney tubular flow rate (3). Renal flow is sensed by multiple types of different structures, one of which being cilia present on tubular epithelial cells (20-22). The importance of kidney cilia and their role in the development of various renal diseases have been appreciated especially in the recent years.

A cilium is a plasma membrane-bound hair-like eukaryotic organelle projecting from the much bigger cell body. Cilia exist as two types: motile cilia and non-motile, or primary, cilia. Inside of a cilium is the axoneme, a microtubule-based structure. The axoneme of motile cilia consist of two central microtubule singlets surrounded by a ring of nine outer doublets (namely a 9+2 axoneme). Inner and outer microtubules are connected by motor and ancillary protein complexes important for regulated movement. The axoneme of primary cilia, however, usually lack the inner pair of microtubules as well as many motion-related structures. It is therefore non-motile and is called the 9+0 axeneme. Axonemes of either cilia type anchor into the microtubule organizing center, also known as the basal body. Motile cilia are present, usually in clusters, on the luminal side of selected organs (e.g. trachea and female Fallopian tubes). They are able to beat and facilitate local content movement. In comparison, primary cilia usually occur one per cell and are present on almost every known mammalian cell type. Their functions have only begun to be revealed in recent years.

The non-motile primary cilia act as “sensory cellular antennae” (23) that respond to various extracellular signals (e.g. mechanical stimuli, lights, odors, and etc.) depending on the function of the cells. These cilia have also been shown to participate in multiple conserved signaling pathways crucial for embryonic development (22,24-26). The ciliary membrane of both cilia types has a unique lipid composition and proteome compared with the bulk plasma membrane (22,24,27). Biogenesis, turnover and maintenance of cilia are mediated by specialized cellular machineries. A process called intraflagellar transport (IFT) is responsible for moving the axoneme materials along the length of cilia. Multiple IFT proteins form complexes (IFT particles) that carry the cargoes and move along the microtubules by attaching to motor proteins (20,22,24). The anterograde IFT, delivering newly synthesized axoneme precursors from the cell body to the growing ciliary tip, and the retrograde IFT, sending disassembled axoneme materials back to the cell body, use distinct IFT complexes/particles and motor proteins to assure opposite directional movements (20,22,24). The net consequence out of these two opposing processes determines the status of every single cilium (growing, retrieving or at an equilibrium). Dynamic regulations on both the anterograde and the retrograde transports ultimately determine the cilia length and morphology, which change under shifted or diseased conditions (21,28-30). The vesicular transport of ciliary membrane proteins to cilia is mediated by a stable protein complex call the BBsome (31,32). The BBsome consists of several conserved Bardet-Biedl Syndrome (BBS) proteins (31,32). Mutations in one or more BBS protein encoding genes have been associated with Bardet-Biedl

Syndrome, a severe disorder affecting multiple organ systems by disrupting cellular cilia functions (21,32-34). Membrane recruitment and proper functions of the BBsome require Rab proteins (Rab8 and Rab11) localized to recycling endosomes as well as the phospholipid phosphatidylinositol (3,4)-bisphosphate (31,35). Detailed mechanisms regarding many aspects of BBsome functioning remain unknown. Genetic defects in cilia themselves or the cilia anchoring basal bodies result in a variety of disorders. As a group, these are often referred to as “ciliopathies”. Bardet-Biedl Syndrome is one example of a ciliopathy (21,33,34).

Cilia found in healthy kidneys are generally primary (non-motile) ones, although renal cells displaying multiple motile “9+2” cilia have been reported to present in injured or diseased kidneys (36-40). Renal tubular primary cilia are present on the luminal side of epithelia. They are thought to be mechanosensors responding to fluid change and possibly facilitating intercellular communications (20-22). Some cilium-specific transmembrane proteins, including polycystin-1 (PC1), polycystin-2 (PC2) and polyductin/fibrocystin, have been reported to participate in the flow-sensing function of renal primary cilia. Post-translational cleavage of these cilium resident proteins and translocation of cytosolic fragments to other compartments (nuclei, cytosol, extracellular space, and etc.) have been associated with the mechanosensory and paracrine roles of renal cilia (20-22). Flow induced deflection of the cilium results in an immediate calcium influx mediated by PC1 and PC2 (20-22). This calcium signal subsequently initiates cascades of cellular events. Defects in PC1, PC2 or other important cilium resident signaling molecules result in loss of the

calcium signaling and abnormal renal functioning, for example renal cyst formation observed in certain diseases (20-22,33,34). Thanks to the extensive research on primary cilia in recent years, the number of diseases attributed to cilia malfunctioning is growing quickly, indicating the importance of cilia in many critical organ systems. Several cultured kidney cell lines, including MDCK (Madin Darby Canine Kidney) cells, retain the ability to form apical primary cilia when polarized in culture. These cilia have similar functions to those found *in vivo* (41).

1.2 STRUCTURE, FUNCTION, AND METABOLISM OF PHOSPHATIDYLINOSITIDES

1.2.1 Structure of phosphatidylinositol and phosphatidylinositides

Phosphatidylinositol (PI) is a negatively charged phospholipid that represents a minor component of the cytosolic face of cellular membranes. Its glycerol backbone is linked to a sixfold alcohol, inositol, via a phosphate group (Figure 1.2A). The inositol ring can be phosphorylated on positions D-3, D-4 and D-5, giving rise to a family of derivatives called phosphatidylinositides (PIPs) (Figure 1.2A,B).

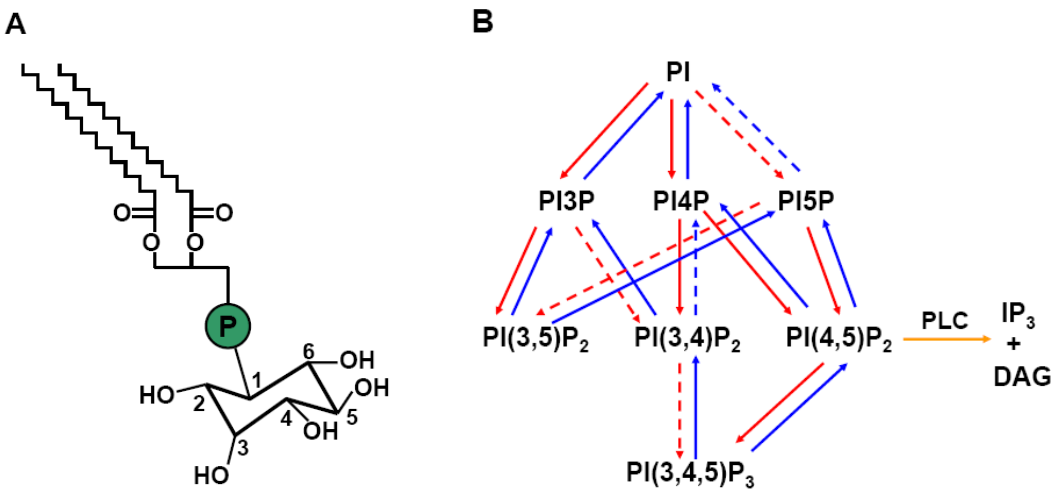

Figure 1.2 PI structure and metabolism. The molecular structure of phosphatidylinositol is shown on the left. Phosphorylation of the 3,4, and/or 5 position via the pathways depicted on the right generate physiologically relevant PIP lipid species. Note that PIP_2 can be "degraded" either by dephosphorylation to yield PI4P or by phospholipase-C mediated cleavage to yield inositol 1,4,5-tripsphosphate (IP3) and diacylglycerol (DAG). Dotted arrows indicate reactions confirmed only *in vitro*. Red arrows: kinase pathways; blue arrows: phosphatase pathways. This figure is adapted from (42).

So far there are 7 known PIPs found in a wide spectrum of living species ranging from unicellular organisms to mammals (43). Those PIPs include: phosphatidylinositol 3-phosphate (PI3P), phosphatidylinositol 4-phosphate (PI4P), phosphatidylinositol 5-phosphate (PI5P), phosphatidylinositol (3,5)-bisphosphate ($PI(3,5)P_2$), phosphatidylinositol (3,4)-bisphosphate ($PI(3,4)P_2$), phosphatidylinositol (4,5)-bisphosphate ($PI(4,5)P_2$ or PIP_2) and phosphatidylinositol (3,4,5)-trisphosphate ($PI(3,4,5)P_3$ or PIP_3) (Figure 1.2B). The conserved nature of PI and PIPs among different organisms indicates that these lipids appeared early during the evolution and are involved in important cellular functions (43).

1.2.2 Functions of phosphatidylinositol and phosphatidylinositides

Foremost, PIPs were viewed as signaling molecules responsive to extracellular stimuli. It has been known for almost half a century that the action of neurotransmitters and hormones results in changes of intracellular PIP populations in selected cell types (43,44). In 1983, inositol 1,4,5-trisphosphate (IP_3) was identified as a second messenger capable of increasing cytoplasmic Ca^{2+} (45,46). This milestone discovery initiated a decade of intensive research leading to identification of many important components of the IP_3 pathway, including the IP_3 receptors, and revelation of the general mechanism of IP_3/Ca^{2+} signaling (45,47-49). Briefly, upon activation of various cell surface receptors (including receptors for growth factors, antigens, neurotransmitters, odorants or light, etc.) by extracellular stimuli, specific isoforms of the plasma membrane bound enzyme phospholipase C (PLC) are activated to hydrolyze cell surface PIP_2 to produce IP_3 and diacylglycerol (DAG), both

of which act as second messengers (45,49). DAG remains at the cell surface and activate protein kinase C (PKC) which passes on the signaling by phosphorylating other proteins. Meanwhile, IP_3 diffuses through the cytosol and binds to IP_3 receptors present at the smooth endoplasmic reticulum (sER) membrane, resulting in release of Ca^{2+} from the sER lumen into the cytosol, which in turn triggers a cascade of intracellular changes and activities (49). Ca^{2+} also cooperates with DAG to activate PKC at the plasma membrane (50).

While the signaling related roles of PIPs are widely accepted and studied, other PIP functions started to emerge and be appreciated by the scientific world in the early 1990s. When a mammalian PI 3-kinase, which phosphorylates the D-3 position on the inositol ring, was cloned (43,51,52), it was found that the kinase exhibited strong sequence homology to Vps34p, a yeast protein important for the vacuolar protein delivery in the strain of *Saccharomyces cerevisiae* (43,53,54). Subsequent studies on PIP regulating enzymes and binding proteins have led to our current knowledge about the diversified functions of PI and PIPs in multiple cellular events besides signal transduction.

One important feature of the PIPs is that each member of the family has its distinct cellular localization, For example, PI4P is primarily localized to the Golgi membrane, PI3P is mostly found on early endosomes, and PIP_2 is predominantly present on the plasma membrane. This feature facilitates identity establishment and maintenance of cellular membrane compartments and ensures delicate regulation of local events. The mechanism of how the highly dynamic PIPs are compartmentally confined is not

fully understood, however regulated synthesis and turnover have been suggested to play a role. (43,55). PIPs are able to recruit various proteins to the membrane by binding to specialized motifs within those proteins. Conserved PIP-binding motifs, each of which only binds selective PIP species, have been found in many cytosolic proteins [Table 1.1; (43,56)]. PIP-mediated protein nucleation represents a crucial initiating step in many important cellular events. One example is the function of PIP_2 in clathrin mediated endocytosis at the plasma membrane (57-60). Additionally, the activity of some proteins changes upon binding to specific PIPs, suggesting that PIPs can also act as allosteric regulators (43). Also, PI/PIP phosphorylation and dephosphorylation have been proposed to facilitate the changes of membrane curvature during trafficking events including membrane fission and fusion (43,61).

Table 1.1 PI binding modules. Typical sizes and preferred targets of seven conserved PI binding domains are listed. This table is adapted from (56).

Domain	Typical size (amino acids)	Preferred target(s)
PH	~125	Diverse phosphoinositides, depending on specific structures, some highly specific
FYVE	60-70	PI3P
PX	~130	PI3P (with a few exceptions)
PROPPIN	~500	$PI(3,5)P_2$ (sometimes also PI3P)
ENTH	~150	PIP_2 (but sometimes a little promiscuous)
ANTH	~280	Phosphoinositides, relatively low specificity
IMD	`250	Phosphoinositides and other acidic phospholipids

PH: pleckstrin homology
FYVE: Fab1, YOTB, Vac1, EEA1
PX: Phox homology
PROPPIN: β-propeller that binds phosphoinositides
ENTH: epsin N-terminal homology
ANTH: AP180 N-terminal homology
IMD: IRSp53/missing-in-metastasis

The PIP populations at any given cellular membrane are dynamic. Efficient PIP synthesis and turnover are crucial to normal cellular functions. PIP metabolism is mediated by a large group of kinases, phosphatases and phospholipases. Each enzyme has its specific substrates, products, regulators and cellular localization. Enzyme-mediated PIP metabolism happens constitutively in the cell and responds to specific signals as well.

1.2.3 PI kinases

Phosphorylation on the inositol D-3, D-4 and D-5 positions is catalyzed by a group of highly specific lipid kinases, the PI kinases (Table 1.2). Depending on substrate selectivity, PI kinases can be roughly divided into three groups: PI 3-kinases, PI 4-kinases, and PI 5-kinases. Within each group, the kinases are further categorized into different types depending on the amino acid sequence homology (Table 1.2).

1.2.3.1 PI 3-kinases PI 3-kinases selectively phosphorylate the D-3 position of the inositol ring. This group of kinases consists of 3 sub-classes, namely class I, II, and III enzymes, differentiated by sequence analysis and by their sensitivity to the kinase inhibitor wortmannin. Specifically, class I PI 3-kinases mainly phosphorylate PI4P and PIP_2 and are inhibited by low nanomolar concentrations of wortmannin (43). Class II PI 3-kinases can phosphorylate PI, PI4P and PIP_2 *in vitro*, however their *in vivo* substrate preferences are largely unkown (43,62). These (class II) enzymes are inhibited by micromolar concentrations of wortmannin. The class III 3-kinase, named PI3KIII in the mammalian nomenclature, only phosphorylates PI and is responsible for production of the majority of PI3P in mammalian cells (43,63). PI3KIII is sensitive

to wortmannin at low nanomolar concentrations. In contrast, Vps34p, the yeast homolog of PI3KIII, can only be inhibited by wortmannin at much higher micromolar concentrations (64-66). Every PI 3-kinase has its specific cellular localization. Cellular functions of these enzymes have started to be revealed and they include roles in signal transduction, endocytic and biosynthetic protein deliveries (43,67-73).

1.2.3.2 PI 4-kinases There are 2 distinct types of kinases, PI4K type II and type III, that specifically phosphorylate PI to produce PI4P (the original type I enzyme was later found to be a PI 3-kinase) (43). PI4KIIIα and β are homologues of yeast proteins STT4 and PIK1, respectively (74-80). Cellular localizations and functions of STT4 and PIK2 are non-overlapping in yeast (81-83). Similar characteristics have also been reported for PI4KIIIα and β (43,76,84-86). Mammalian type II PI4Kα and β were found to lack the signature PIK domain found in other PI 3-/4-kinases, and therefore belong to a novel family of lipid kinases (43). Their yeast ortholog is Lsb6p (87,88). PI4KIIα is a primarily Golgi-membrane localized protein and the major producer of PI4P in mammalian cells (43,89). It has been reported to function in membrane traffic processes involving the *trans*-Golgi network (TGN) (90). Meanwhile, PI4KIIβ is a largely cytosolic protein recruited to plasma membrane ruffles in response to extracellular stimuli (89). The membrane translocation and subsequent activation of PI4KIIβ is Rac dependent (89). A separate class of kinases has been identified to phosphorylate the D-4 position of selected PIPs. They were originally discovered in an effort looking for PI5Ks (therefore named type II PI5Ks back then), but were subsequently found to actually be PI 4-Kinases (91-96) and named PIP4KIIs to avoid

confusion. There are three isoforms in this group. Isoform α, the earliest discovered isoforms, is able to phosphorylate PI3P and PI5P, but not PI(3,5)P2 or PI (43,96-98). This group of PI4Ks only exists in metazoa and is found at the cytoplasm, the nucleus, the ER, and actin cytoskeletal structures (99-105). They have been suggested to play a role in regulated secretion and signal transduction, although the detailed mechanisms remain elusive (94,99,106).

1.2.3.3 PI 5-kinases There are 2 classes of PI 5-kinases that differ in substrate specificity. One includes the yeast protein Fab1p and the mammalian ortholog PIKfyve (43,107). These 2 kinases phosphorylate the D-5 position of PI or PI3P. They both contain a FYVE domain which specifically binds PI3P and therefore contributes to the kinases' cellular localizations to PI3P-rich compartments (43,108). Fab1p has been shown to be required for yeast vacuolar functions (109-111) while PIKfyve, similarly, plays a role in the mammalian endosomal functions (112).

The other class of the PI 5-kinases consists of the type I 5-kinases (as mentioned above, the original type II PI5Ks were later found to be PI4Ks and renamed), which phosphorylate the D-5 position of PI4P and are the major producers of cellular PIP_2. Mammalian cells express three isoforms of type I PI5K (α, β and γ), each consisting of a relatively homogeneous ~400 amino acid central kinase domain and more flexible amino- (N-) and carboxyl- (C-) terminal tails (43,113). The kinase domain contains a small activation loop that contributes to substrate specificity (99,105). Additionally, PI5KIγ exists predominantly in two splice forms (PI5KIγ635 and PI5KIγ661) that differ by a 26-amino-acid C-terminal extension (113,114). The α and

β isoforms of mammalian type I PI5K were cloned by 2 separate groups at around the same time from mouse or human and named in a reversed manner (113,115,116). The human nomenclature is used in the present introduction and all later chapters according to the GenBank guidelines.

PI5KIs all appear to be plasma membrane bound, but exhibit distinct distributions in polarized cells; their recruitment to specific cell surface domains is not fully understood. Their functions in membrane traffic have started to be revealed. Conflicting results have been reported regarding the role of different PI5K isoforms in endocytosis of nonpolarized cells (115,117). In polarized renal cells, our lab has observed that PI5KIβ is apically localized and selectively regulates biosynthetic delivery of a subset of apical cargoes (118). Increased PIP_2 mediated by PI5KIβ overexpression has been shown to decrease apical surface epithelial sodium channel (ENaC) levels in polarized epithelial cells presumably by stimulating epsin (a clathrin adaptor) mediated endocytosis from the apical plasma membrane (119). Separately, PI5KIγ 661 has been suggested to function in delivery to and endocytosis from the basolateral surface of polarized Madin-Darby canine kidney (MDCK) cells via direct interaction with and activation by the μ2 subunit of AP-2 complex (114,120,121). PI5KIα and β were shown to interact with AP-2 as well (121). The yeast homologue of mammalian type I PI5Ks is MSS4 (122,123). MSS4 is an essential yeast protein shown to be involved in actin cytoskeleton organization (43,122-124). Type I PI5Ks and PIKfyve can both be autophosphorylated. Their lipid kinase activity is inhibited by autophosphorylation (125,126).

Although several mechanisms have been implicated for membrane recruitment of PI5KIβ, the signal(s) that mediates apical targeting of the kinase in polarized cells remains unknown (99,105,127-129). This question will be examined in chapter two of my thesis. Determination of the apical targeting signal(s) will be very useful in identifying the domain-specific interactors of PI5KIβ and in elucidating how the enzyme specifically regulates apical membrane traffic in polarized cells.

1.2.4 PI phosphatases

To complete the delicate network regulating PI/PIP metabolism, phosphatases that remove the inositol-bound phosphate groups are needed to balance the PI kinase activities discussed above. A long list of PI phosphatases has been identified (Table 1.2). Each one of them has its unique domain structure and substrate preference. Their cellular localizations and functions have been studied and considered together with our knowledge on PI, PIPs, PI kinases and PIP binding proteins. Using systems biology approaches, the increasing amount of information available for PI/PIPs and their related proteins can help us understand how the various PI/PIP-related cellular events are globally and as well locally coordinated (130). Meanwhile, protein-protein/protein-lipid interactions and macromolecular machineries discovered along the way can potentially serve as molecular targets of pharmaceutical studies.

Based on their substrate selectivity, PI phosphatases are divided into three groups, the PI 3-phasphatases, the PI 4-phosphatases and the PI 5-phosphatases, although selected enzymes are capable of hydrolyzing phosphate groups present on more than one inositol positions (for example, synaptojanin 1 and 2 are dual-function

mammalian enzymes that can hydrolyze both D-4 and D-5 phosphate groups on PIP_2 to produce PI) (43,131,132) (Table 1.2). Based on their domain structures, the phosphatases are further categorized into sub-families. The relatively conserved domain types found in PI phosphatases include: 1) phosphatase activity-related domains, e.g., the Sac domain and the conserved substrate-selective phosphatase domains; 2) PIP-binding domains, for example the FYVE (Fab1 YOTB Vac1 EEA1) domain, the PH (pleckstrin-homology) domain, and the PH-GRAM (pleckstrin homology glucosyltransferases, Rab-like GTPase activators and myotubularins) domain; 3) membrane-binding domains like the C2 (conserved region 2) domain; 4) protein-interacting domains, including the SH2 (phosphotyrosine-binding module 2) domain, the coiled-coil domain and the PRD (proline-rich domain) (43,130). While domain types 2), 3), and 4) are all involved in cellular targeting of PI phosphatases, type 2) is by far the most common localization cue. PI-phosphatases with different domain combinations exhibit specialized substrate preferences and targeted to non-overlapping cellular compartments. Locally, these phosphatases coordinate with PI-kinases and other regulators for tight spatial-temporal controls of PI/PIP metabolizing events. Roles of PI-phosphatases in a variety of cellular processess, including signal transduction, membrane traffic, and cytoskeleton remodeling, are being revealed. Despite extensive research, many aspects regarding the detailed regulations and functional redundancies remain open questions (43,130).

1.2.5 PI/PIP related human diseases

Considering the versatility of PI/PIPs in numerous cellular activities, it is not surprising

that impaired PI/PIP synthesis, turnover or localization often results in diseased conditions. Cellular PI/PIP metabolism is tightly controlled by PI kinases and phosphatases. Therefore genetic defects of these enzymes have been associated with a wide variety of human disorders.

Shown in Table 1.2 are human diseases identified to relate to known PI kinases or phosphatases. Most of these diseases are severe and life-threatening, consistent with the involvement of PI/PIPs in many foundamental cellular events. Organs often affected by these diseases include the central and peripheral nervous system, the eyes, the skeletal muscle and the kidney. The pathogenesis of most known PI/PIP related disorders is not fully understood.

Table 1.2 Mammalian PI kinases and phosphatases: their substrates, products and relationships to human diseases. Note that the myotubularin-related protein family includes active lipid phosphatases, for example MTM1, and pseudophosphatases, such as SBF1 and SBF2. Pseudophosphatases do not exhibit catalytic activity due to lack of a crucial cysteine residue. Information in this table is mostly based on (43,130,133).

Enzyme	*In vivo* substrate(s)	Product(s)	Human genetic diseases
KINASES			
PI3Ks			
PI3KIα,β,γ,δ	PI4P, PIP_2	PI(3.4)P_2, PIP_3	Cancer (α,β)
PI3KIIα,β,γ	PI, PI4P, PIP_2	PI3P, PI(3,4)P_2, PIP_3	--
PI3KIII	PI	PI3P	Bipolar disorder (tentative?)
PI4Ks			
PI4KIIIα,β	PI	PI4P	Bipolar disorder (α)
PI4KIIα,β	PI	PI4P	--
PIP4KIIα,β,γ	PI3P, PI5P	PI{3,4}P_2, PIP_2	Bipolar disorder, schizophrenia (α); mouse PIP4KIIβ knockout causes hypersensitivity to insulin and reduced body weight
PI5Ks			
PI5KIα,β,γ	PI4P and others (?)	PIP_2 and others (?)	Lethal congenital contractual syndrome type 3 (LCCS3) (γ)
PIKfyve	PI, PI3P	PI5P, PI(3,5)P_2	Francois-Neetens fleck cornea dystrophy (CFD)
PHOSPHATASES			
3-Pases			

Table 1.2. (continued)			
PTEN	PIP_3, $PI(3,4)P_2$	PIP_2, PI4P	Cowden syndrome (CS) and Bannayan-Zonana syndrome (BZS), cancer, macrocephaly/autism
MTM1,R1,R2	PI3P, $PI(3,5)P_2$	PI	X-linked myotubular myopathy (XLCNM) (MTM1), Charcot-Marie-Tooth 4B1 (CMT4B1) (MTMR2)
MTMR3,4,6,7,8	PI3P, $PI(3,5)P_2$	PI	--
MTMR9,10,11,12	Inactive phosphatases	--	--
SBF1,SBF2 (MTMR13)	Inactive phoaphatases	--	Charcot-Marie-Tooth 4B2 (CMT4B2) (SBF2)
4-Pases			
INPP4A	$Ins(3,4)P_2$, $Ins(1,3,4)P_3$, $PI(3,4)P_2$	Ins3P, $Ins(1,3)P_2$, PI3P	Not clear in human; a frame shift mutation in mouse INPP4A gene results in the *weeble* mutant mice characterized by neuronal loss
INPP4B	$PI(3,4)P_2$; *in vitro*, also $Ins(3,4)P_2$, $Ins(3,4,5)P_3$	PI3P; Ins3P, $Ins(3,5)P_2$	--
TMEM55A,B	PIP_2	PI5P	--
SACM1L	PI3P, PI4P	PI	--
5-Pases			
SKIP	PIP_3, PIP_2	$PI(3,4)P_2$, PI4P	--
PIB5PA/PIPP	PIP_2, $Ins(1,4,5)P_3$, $Ins(1,3,4,5)p_4$	PI4P, $Ins(1,4)P_2$, $Ins(1,3,4)P_3$	--
INPP5B	PIP_2, PIP_3, $Ins(1,4,5)P_3$, $Ins(1,3,4,5)P_4$	PI4P, $PI(3,4)P_2$, $Ins(1,4)P_2$, $Ins(1,3,4)P_3$	--
OCRL1	PIP_2	PI4P	Lowe syndrome, Dent 2 disease
INPP5D/SHIP1	PIP_3, $Ins(1,3,4,5)P_4$	$PI(3,4)P_2$, $Ins(1,3,4)P_3$	Acute myelogenous leukemia (AML)

Table 1.2. (continued)			
INPP5E	PIP_3, PIP_2	$PI(3,4)P_2$, PI4P	Ciliopathies, e.g. Joubert syndrome (JS) and MORM (mental retardation, truncal obesity, retinal dystrophy and micropenis) syndrome
INPPL1/SHIP2	PIP_3 and others (?)	$PI(3,4)P_2$	Diabetes type II, metabolic syndrome
SYNJ1,2	PIP_2	PI	Bipolar disorder (SYNJ1)
INPP5F	PIP_2>PIP_3	PI4P, $PI(3,4)P_2$	--
FIG4	$PI(3,5)P_2$ and others (?)	PI3P	Charcot-Marie-Tooth 4J (CMT4J); mouse FIG4 knockout results in the pale tremor mice characterized by massive neurodegeneration

Several hypotheses have been made regarding how certain PI/PIP related diseases develop. A 2008 review by Nicot and Laporte (133) provided a very nice description and dissection of human diseases caused by defects of endosomal PI/PIPs. They pointed out a hypothetical “common pathological mechanism” of endosome-related PI/PIP disorders, which are diseases caused by impaired metabolism of endosome localized PI3P and $PI(3,5)P_2$ (133). In their model, compromised membrane fission and retrieval resulting from abnormal levels of $PI3P/PI(3.5)P_2$ are the underlying reasons for defective nerve myelination in CMT4B1/B2 (MTMR2/MTMR13 defects), accumulation of late endosomal compartments in selected cell types of the CFD and CMT4J patients (PIKfyve and FIG4 defects respectively) and altered skeletal muscle cell membrane remodeling in XLCNM (MTM1 defect) (133). They also suggest that certain types of cancer and psychiatric disorders caused by defective PI3Ks are results of impaired cell antophagy (133). This hypothesis is supported by research data showing that PI3Ks are involved in autophagy and that autophagy is altered in cancers and neurological diseases (133-137).

Other disorders that have been associated with defective PI/PIP metabolizing enzymes include LCCS3 [a severe form of arthrogryposis hypothetically caused by defective neuronal membrane traffic as a result of PI5KIγ mutations that eliminate the kinase activity (138)], type 2 diabetes [suggested to result from the abnormal increases in INPPL1/SHIP2 amount and activity, which result in impaired insulin and insulin-like growth factor 1 (IGF-1) signaling, brain dysfunction and insulin resistance

(139-141)], acute myeloid leukemia [since loss of INPP5D/SHIP1 has been associated with unregulated proliferation of CD34(+) cells in AML patients (142)], cancer as well as other diseases associated with the tumor suppressor PTEN (143,144) and Lowe syndrome [caused by OCRL1 defects (145)]. A detailed introduction to Lowe syndrome can be found in the next section. Recently, mutations in the PI 5-phosphatase INPP5E have been related to defective primary cilia functions and subsequent abnormalities in the eyes, the brain and the kidneys of human and mouse (29,30). This novel implication of PI/PIP metabolism in cilia structure/signaling and ciliopathies can potentially open a new field to study the PI/PIP related diseases that are currently not well understood.

1.2.6 Lowe syndrome

Lowe syndrome, also known as Oculocerebrorenal Dystrophy, was first described in 1952 by Lowe and colleagues as a “clinical entity” manifested by “organic-aciduria, decreased renal ammonia production, hydrophthalmos, and mental retardation” (146). As more patients were described subsequently, diagnostic symptoms of Lowe syndrome have evolved into the current triad including congenital cataracts, mental retardation and renal tubular dysfunction. An X-linked pattern of family inheritance was also documented, consistent with the later localization of the Lowe disease gene OCRL to the chromosomal location Xq 26.1 (147-152). Lowe syndrome is a rare panethnic genetic disorder with an incidence of 1 in every 200,000 to 500,000 newborns worldwide (153). The pathophysiology of Lowe syndrome comprises changes and defects in a wide variety of organ systems. The severity of many

symptoms varies broadly among different patients.

As an X-linked recessive disease, Lowe syndrome almost always affects males (although chromosomal translocations affecting the *OCRL* gene locus have been reported to cause Lowe syndrome phenotypes in a very small number of female cases). It is often diagnosed at very early stages (at birth or in the first years of life) based on physical abnormalities. All known Lowe patients are born with bilateral cataracts and have impaired vision (154,155). Impaired lens development has been reported in human fetuses with inherited Lowe mutations (153,155). Glaucoma, keloids, strabismus and even blindness are common in those patients too (153,154). Hypotonia is usually evident during the early infancy of Lowe patients and progresses into the adulthood, resulting in problems including impaired mobility, skeletal deformation, feeding difficulty, coughing inability, and pneumonia (153,154,156,157). Moderate to severe mental retardation develops in most of the Lowe syndrome boys whose facial characters usually include small deep-set eyes, prominent foreheads and abnormally lengthened faces. Renal tubular dysfunction is normally detectable by 12 months after birth. Plasma and urinary creatinine levels, however, remain in the reference range until the patients reach their early teens (153,154,158). Chronic kidney dysfunction is associated with many Lowe patients in their late teens and 20s. A high rate of infantile mortality has been noted for Lowe syndrome. These early deaths are often linked to severe metabolic impairments due to excessive urinary loss of water and electrolytes, however fatal infections, neurological symptoms and sometimes unknown reasons have been associated with deaths as well (153). Lowe

patients who survive infancy normally live into the 2nd or 3rd decade of their lives and sometimes further. The lifespan of a Lowe patient is rarely longer than 40 years (153,154). Deaths are often due to the kidney failure derived from chronic renal problems, however other complications can be fatal as well (154).

The renal tubular dysfunction associated with Lowe syndrome is characterized by urinary loss of pathological levels of low-molecular-weight proteins, amino acids, calcium, bicarbonate, phosphate, L-carnitine and excessive water (153,159,160). Massive wasting of these important nutrients results in conditions including systematic acidosis (due to the loss of bicarbonate), bone problems like rickets and osteomalacia (due to the loss of calcium and phosphate), and dehydration (due to the excessive loss of water) (153). Additionally, older Lowe patients often have glomerular sclerosis, nephrocalcinosis, and/or nephrolithiasis (154). Pathological renal features including epithelial atrophy, filled tubular lumens and fibrosis have also been reported (153,154).

The currently available treatments for Lowe syndrome involve replacement therapy (to compensate for the urinary loss), surgery (to correct eye problems and other defects), dialysis [kidney transplantation remains an option although very few cases have been reported (153,161)], and physical therapy (to alleviate mobility constraints) (153,156). Genetic counseling, maternal detection and prenatal examination are often suggested to families at risk (153,154,156).

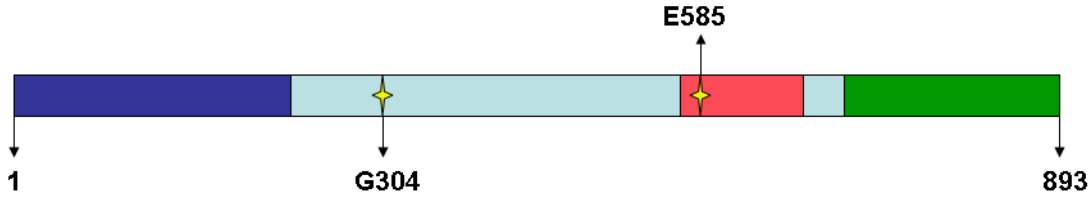

Figure 1.3 Domain structure of OCRL1 isoform b. Dark blue: N-terminal domain; light blue: 5 phosphatase domain; green: RhoGap domain; Red: ASH domain. Yellow stars indicate amino acids mutated in chapter 3. OCRL1 isoform a has an extra 8-residue stretch in the C-terminal RhoGap domain. This figure is adapted from (162).

OCRL, the disease gene of Lowe syndrome, encodes the PI 5-phosphatase OCRL1 (147,163,164). The domain structure of OCRL1 (162) (Figure 1.3) consists of a short N-terminal domain, a central PI 5-phosphatase homology domain, an ASH (ASPM, SPD-2, Hydin) domain (which will be discussed in detail later) and a C-terminal Rho-GAP like domain (inactive due to the lack of a catalytic arginine residue, but suggested to be important for OCRL1 enzymatic activity) (162,165,166). In mammalian cells, OCRL1 primarily localizes to the *trans*-Golgi network and endosomal compartments (162,167-169). It can also be found in clathrin coated pits and is present at plasma membrane ruffles upon growth-factor stimulation (170,171). How mutations in the *OCRL* gene result in Lowe symptoms remains largely unknown although megalin malfunction has been suggested by several groups as a reason for the characteristic low-molecular-weight proteinuria (18,172). Interestingly, *OCRL* knockout mice do not develop Lowe syndrome phenotypes and are largely healthy (173,174). This is due to intrinsic expression of the functional redundant PI

5-phosphatase INPP5B in these mice (173,174). Loss of the OCRL1 activity can not be compensated in humans because of low expression levels of INPP5B (173,174).

OCRL mutations have been found in a subgroup of patients originally diagnosed with Dent disease, another X-linked recessive disorder affecting only the kidneys but typically not other organs (175-178). These patients do not carry mutations in the Dent disease gene *CLCN5* and have been re-categorized into the novel group of Dent 2 patients (175-178). Why Dent 2 *OCRL* mutations do not cause extra-renal defects is unclear. Domain-restricted mutations and alternative splicing have been hypothesized as the underlying mechanisms (176). Dent disease symptoms are similar, but not identical (for example, Dent patients rarely develop kidney tubular acidosis), to the renal manifestations of Lowe syndrome (153,177). The *CLCN5* gene encodes the chloride/proton antiporter CLC-5 whose cellular functions include endosomal acidification (179-181). Abnormal renal tubular expression and localization of megalin have been reported in both Dent patients and the *CLCN5* knockout mice (17,18). Impaired megalin functions have therefore been suggested to account for the proteinuria as well as other renal symptoms found in Dent patients (17,18).

Notably, urinary megalin shedding was reported to decrease in both Lowe and Dent patients (18). It will be interesting to examine whether, like in the case of Dent disease, megalin defects are associated with the renal manifestations of Lowe syndrome as well. Separately, a novel ASH domain was recently reported to present at the C-terminus of the OCRL1 5-phosphatase domain (182,183). The ASH domain has

been found in many ciliary proteins, although its exact cellular functions remain elusive (182). The identification of OCRL1 as an ASH-domain containing protein potentially suggests a novel direction of Lowe syndrome-related studies to look into the relationship between this disease and cellular cilia. Chapter three and four of my thesis focus on elucidating the renal pathogenesis of Lowe syndrome using renal epithelial cells as the model. A variety of experiments were performed to separately evaluate cellular functions of megalin (chapter three) and primary cilia (chapter four) in response to acute OCRL1 depletion [mediated by RNA interference (RNAi)]. Results of these experiments should contribute to our understanding of Lowe syndrome and to development of therapeutic interventions to this severe genetic disorder.

1.3 SUMMARY

PI and PIPs are important cellular regulators. Besides their long-appreciated functions in signaling, these lipids also have crucial roles in membrane traffic. Delicate control of the dynamic cellular PI/PIP pools is dependent upon a variety of metabolizing enzymes, namely the PI kinases and phosphatases. Thanks to extensive research efforts, our knowledge about the structures and functions of PI kinases/phosphatases is increasing steadily. However, due to complexity of the PI/PIP regulation network, many questions remain unanswered. Among them are how specific PI/PIP metabolizing enzymes are compartmentally restricted and how specialized cellular localizations contribute to the functions of those enzymes. These

questions are particularly intriguing when cells assume polarity (*in vivo* or in culture) and therefore, compared to their non-polarized counterparts, exhibit more divergent cellular compartmentalization and functional specialization.

A large group of human disorders has been attributed to genetic defects in selected PI/PIP metabolizing enzymes. These diseases often lead to severe consequences since PI and PIPs are involved in many fundamental cellular processes. The kidneys are among the most disease-prone vital organs and are affected by mutations in genes including those encoding the PI phosphatases OCRL1 and INPP5E. The often present renal tubular dysfunction has led to the hypothesis that functional defects in selected kidney-tubule resident proteins, likely receptors (for example megalin), are responsible for the disease-genesis. However there is not enough evidence so far to verify this hypothesis. Interesting enough, recent studies have linked renal cilia abnormalities to mutations in the PI/PIP regulating gene *INPP5E*. Given the established role of cilia in renal tubular flow-control and the fact that many PIPs are critical signaling and trafficking regulators, it is likely that there is an unsolved mechanism connecting PI/PIP metabolism to the cilia related signaling cascades and membrane traffic in renal tubular cells. Researching and understanding this mechanism can help us appreciate the currently not-so-well-understood roles of PI/PIPs in cilia genesis, maintenance and functioning and can potentially reveal valuable information on pathogenesis as well as therapeutic control of known and unknown PI/PIP diseases.

The three aims of my thesis are: 1) to determine the role of megalin in the renal

pathogenesis of Lowe syndrome; 2) to understand the relationship between OCRL1 and renal primary cilia, and to evaluate this potential relationship in Lowe syndrome development; 3) to study the apical targeting mechanism of PI5KIβ in polarized renal epithelial cells. By focusing on these aims, I expect to improve our knowledge on compartmentalized regulation of PI/PIP-related events in polarized cells (as discussed above, the current knowledge in this area is far from complete) and to further the long-standing effort in preventing and treating Lowe syndrome.

2.0 DETERMINING THE APICAL TARGETING MECHANISM OF PI5KIβ IN POLARIZED EPITHELIAL CELLS

2.1 INTRODUCTION

The epithelium is the layer or layers of cells lining the surfaces, lumens and cavities of the body. Its main roles include protection, secretion, absorption and sensation. On the one hand, there are widely diversified types of epithelium, each with a specific morphology-structure combination and carrying specialized cellular responsibilities designated by its organic context. On the other hand, as a tissue family, all epithelial types share several characters that distinguish them from other biological tissues. One of these characters is being the physical as well as functional division between luminal/external substances (for example bacteria, air, water, half-digested food, renal filtrate, and etc.) and structures underneath (including a fibrous basement membrane, connective tissue, blood vessels and nerves). The barrier function of epithelia is achieved by formation of intercellular tight junctions, which consist of joined networks of transmembrane protein complexes from two adjacent cells and seal off the intercellular space (184). Tight junctions anchor into the actin cytoskeleton (184). Number and composition of tight junctional protein complexes vary in different epithelia, resulting in distinct sealing strengths that are function-related (184). In a single epithelial cell, the tight junction presents a physical barrier to lateral diffusion of

selected cell surface proteins and lipids (184,185). The plasma membrane is, therefore, divided into two compartments, one on each side of the tight junction. These two compartments are in contact with very different environments and therefore develop distinct cellular roles accompanied by dissimilar structural features. Separation of the luminal/external (apical) cell surface from the rest (basolateral) of plasma membrane is the basis of apical-basal polarity universally found in various epithelial cells. Functional details and structural specializations of the apical and basolateral epithelial membranes vary broadly among organs.

To achieve specialized apical and basolateral functions, the two plasma membrane domains of each polarized epithelial cell develop asymmetric compositions crucial for domain identities. Notably, the asymmetry is not limited to membrane proteins, but also present in lipid components on both the outer and the inner leaflets of plasma membrane (55,186). This is somewhat surprising considering the fact that inner-leaflet lipids can diffuse freely across the tight junction (185). The delicate spatial compartmentalization of PIP family members is clearly manifested in the apical-basal polarity. Specifically, PIP_2, while present on the entire cell surface, is selectively enriched on the apical plasma membrane and crucial for the recruitment and activity of many apical proteins (55,119,186). On the contrary, PIP_3, a minor PIP, is almost exclusively found on the basolateral cell surface and is required for establishment of the basolateral identity (55,186). Elegant studies from the Mostov laboratory have partially tackled this conundrum (55,186). By examining developing MDCK 3D-cysts, his group discovered that the apical localized PI 3-phosphatase

PTEN was critical for apical-basal polarity initiation as well as cyst lumen formation presumably by hydrolyzing any PIP_3 that diffused to the apical surface and spatially segregating PIP_2 and PIP_3 (55,186). In accordance with these results, his lab also showed that the PI 3-kinase activity, which catalyzes synthesis of PIP_3 out of PIP_2, was required for the formation of epithelial basolateral cell surface (186).

Separately, the importance of PIP_3 in sorting and membrane delivery of basolateral protein cargoes has been revealed by several groups. The Sheff laboratory suggested a role of PI 3-kinases in basolateral sorting and AP (adaptor protein complex) -1B (an epithelial-specific clathrin adaptor complex selectively participating in sorting and trafficking of newly synthesized or recycled proteins to the basolateral cell surface) dependent trafficking from the recycling endosomes in polarized epithelial cells (187), Also, Fölsch and colleagues showed that PIP_3 was found in the recycling endosomal membrane of AP-1B positive epithelial cells, and that the presence of PIP_3 was crucial for recruitment of AP-1B to recycling endosomes and for correct sorting and targeting of AP-1B dependent basolateral cargoes in polarized epithelial cells (188). Participation of PIP_3 in basolateral membrane traffic further indicates the importance of this lipid in normal functions of the basolateral plasma membrane.

While generation and maintenance of the basolateral PIP_3 pool have started to be understood, mechanisms regarding formation of the apically concentrated PIP_2 reservoir remain largely unknown. Although PIP_2 can be generated by PTEN-mediated PIP_3 hydrolysis, that is far from the major PIP_2 synthesizing pathway

due to the much higher cellular abundance of PIP_2 compared to that of PIP_3. In fact, the majority of cell surface PIP_2 is synthesized via phosphorylation of PI4P by type I PI 5-kinases (43).

The three known isoforms of PI5KI, α, β and γ, are cytosolic proteins that associate with cell membranes. They share a domain structure featuring a conserved central kinase homology domain and relatively flexible N- and C- termini [(43,113); Figure 2.1A]. The γ isoform exists predominantly as two alternative splice variants differentiated by a 26-amino-acid C-terminal unstructured tail [(114); Figure 2.1A]. The kinase domain of each isoform contains a 22-amino-acid stretch, the activation loop, which determines the substrate specificity (for PI4P) (99,105). All three PI5KI isoforms are capable of binding μ-2 subunit of the classical cell surface clathrin adaptor AP-2 (114,120,121). Additionally, the nerve-enriched longer PI5KIγ splice variant, γ661, has been shown to specifically interact with the AP-2 β-2 subunit via its short extra 26-amino-acid tail (189). This interaction is regulated by clathrin and is therefore suggested to facilitate temporally controlled regional production of PIP_2, which then interacts with and functionally regulates virtually all known cytosolic proteins involved in clathrin coated pit assembly (189). Studies on involvement of PI5KI isoforms in endocytosis of nonpolarized cells have yielded conflicting results (115,117,120). Barbieri et al. found that PI5KIα, not Iβ, was required for the endocytosis of epidermal growth factor (EGF) receptor in NR6 fibroblasts (117), whereas Padrón et al. observed that overexpression of either PI5KIα or Iβ increased endocytosis of transferrin receptors, membrane association of AP-2 complexes, and

the number of clathrin coated pits in CV-1 cells (115). In addition, through knockdown studies, Padrón et al. also concluded that PI5K1β played a primary and irreplaceable role in constitutive endocytosis in CV-1 and HeLa cells (115). Surprisingly, the same study found no involvement of PI5KIγ in endocytosis within their nonpolarized system (115), contrary to more recent studies suggesting a role for the γ isoform in basolateral endocytic traffic in polarized cells [(120), and see below].

In polarized epithelial cells, the enrichment of PIP species in distinct plasma membrane domains has added an additional layer of complexity to cellular localizations and functions of type I PI5Ks. As mentioned previously, our lab showed that PI5KIβ strikingly localized to the apical plasma membrane of polarized MDCK cells and selectively regulated surface delivery of a subset of newly synthesized apical cargo proteins (118). Also, overexpression of PI5KIβ was able to stimulate endocytosis of the apical proteins ENaC and megalin, presumably by increasing apical PIP_2 (119,174). In contrast, PI5KIγ661 was found to localize to the basolateral surface of polarized epithelial cells where it associates with AP-1B and regulates basolateral trafficking events as well as adherens junction dynamics (114). Therefore, apical and basolateral membrane traffic events seem to be modulated by separate isoforms of PI5KIs. However what triggers the polarized localizations of PI5KI family members remains elusive.

Previous studies have indicated that the activation loop as well as multiple dibasic-amino-acid motifs present in the kinase homology domain are required for the membrane attachment of all isoforms of type I PI5Ks (99,105,129). It has also been

reported by Dr. Yin's group that Ser/Thr as well as tyrosine phosphorylation status (which responds to and changes upon different stress signals) of PI5KIβ directly correlates with the membrane bound versus cytosolic ratio of the enzyme and as well as with lipid kinase activity (127,190). Regarding the apical-basal polarized localizations of different PI5KI isoforms, very little information is currently available. Considering that the central kinase domain is highly conserved among PI5KIs, it is likely that the polarized targeting signals reside within the more variable N- and/or C-tails. Interestingly, one study indicated that the C-terminus of PI5KIβ was required for the enzyme's polarized localization to the uropod of neutrophils, a different polarity model (128). It is not known whether the same sequence functions similarly in polarized epithelial cells.

Determination of apical targeting signal(s) is critical for identifying apical-specific PI5KIβ interacting proteins and for understanding the roles of this kinase in apical membrane traffic. By comparing localization signals and other structural features between the β and γ isoforms, I expect to be able to answer some fundamental questions regarding polarized epithelia. These questions include: 1) why PI5KIβ and γ localize to separate plasma membrane domains in polarized epithelial cells; 2) why apical and basolateral PIP_2 levels are considerably different when PI5KIs with very homologous kinase domains are present; 3) whether there are distinct requirements for PIP_2 and/or other proteins/lipids by apical versus basolateral endocytic events; 4) whether the potential difference in PIP_2 (or other molecules) requirement accounts for the different endocytic rates observed from the two epithelial cell surface

compartments (191). Additionally, understanding of type I PI5K functions in epithelial cells can provide useful information for studies in other polarized models (e.g. neurons and migrating cells).

2.2 RESULTS

2.2.1 Three isoforms of the type I PI5K exhibit non-overlapping localizations in polarized renal epithelial cells

To determine the expression levels of type I PI5K isoforms in mCCD cells, RT-PCR using specific primers against PI5KIα, β or γ was performed. The PI5Kγ primers were able to amplify both the shorter and the longer transcript variants. As shown in Figure 2.1B, all three kinases were detectable in the mCCD lysate under our RT-PCR conditions. While PI5KIα and γ are relatively abundant in mCCD cells, PI5KIβ is expressed at a lower level. Samples generated with actin primers or no RT enzyme added were included as the positive or the negative control respectively.

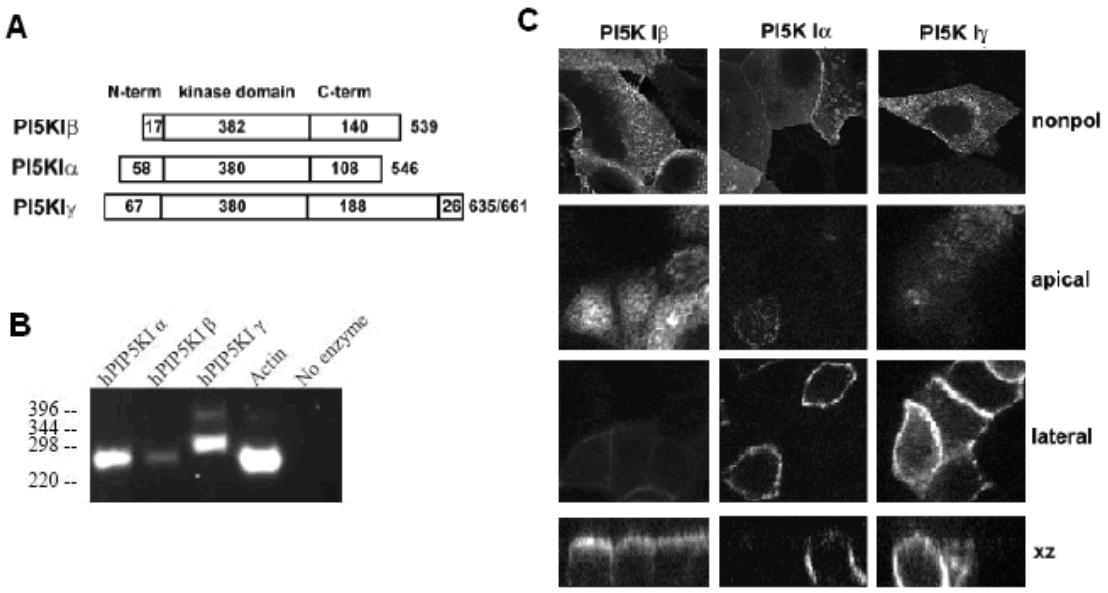

Figure 2.1 Type I PI5K isoforms. A: amino, kinase, and carboxy terminal domains of the three type I PI5K isoforms are depicted. The number of amino acids in each domain is shown. B: RT-PCR using mCCD cell lysate to detect endogenous expression levels of the three PI5KI isoforms. C: mCCD cells plated sparsely on coverslips (top row) or plated on transwells for three days were infected with adenoviruses encoding HA-PI5K1α (mouse), HA-PI5K1β (mouse), or HA-PI5K1γ661 (human) prior to fixation and processing for immunofluorescence imaging using an anti-HA-epitope antibody. Confocal sections of the polarized cells are shown to demonstrate kinase localization to the apical (second row) and/or lateral (third row) regions of the cells. XZ sections of deconvoluted images are shown on the bottom row. Figure 2.1B was generated by Christina M. Szalinski (C.M.S.) from University of Pittsburgh; figure 2.1C was generated by Christopher J. Guerriero (C.J.G.) from University of Pittsburgh.

We subsequently determined the localizations of type I PI5K isoforms in nonpolarized mCCD cells or polarized mCCD cells grown on transwell filters using immunofluorescence. Due to the lack of high-quality antibodies for all the endogenous PI5KIs, this experiment was done by virally expressing (with a multiplicity of infection (MOI) of 125) exogenous tagged kinases. As indicated by Figure 2.1C, in nonpolarized mCCD cells, all three kinases were found both on the plasma membrane and in the cytosol. When expressed in polarized mCCD monolayers, PI5KIβ appeared enriched on the apical plasma membrane, PI5KIα was mostly on the lateral surface, while PI5KIγ661 was present at the cell periphery and slightly concentrated at the lateral plasma membrane. Similar results were seen in polarized MDCK cells (data not shown). Therefore, in polarized renal epithelial cells, the three type I PI5K isoforms assume distinct distributions that are potentially relevant for their non-overlapping cellular functions.

2.2.2 Endogenous PI5KIβ localizes to the apical plasma membrane of polarized renal epithelial cells

We were able to detect the endogenous localization of PI5KIβ in both polarized mCCD cells and rat cortical renal tissue by immunofluorescence. Shown in Figure 2.2 upper and middle rows are confocal XY images of rat kidney cortex slices either selectively labeled for PI5KIβ or treated in the absence of primary antibodies during immunofluorescence. Compared to the no-primary-antibody control, which does not show any specific staining, samples treated with the PI5KIβ antibody are selectively labeled on the apical surface of epithelia lining both distal (characterized by wide

lumens; Figure 2.2 DT) and proximal (characterized by collapsed lumens; Figure 2.2 PT) tubules. In cultured polarized mCCD cells, PI5KIβ is enriched on the apical plasma membrane as illustrated by XZ confocal images of cells stained with a specific PI5KIβ antibody (Figure 2.2 bottom row). These results are consistent with previous data acquired using HA-tagged exogenous PI5KIβ in polarized renal epithelial cells [(118,119), Figure 2.1].

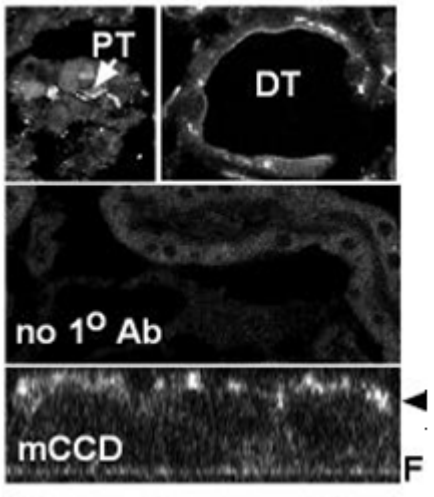

Figure 2.2 Apical localization of endogenous PI5KIβ in renal epithelia. The upper confocal micrographs show anti-PI5KIβ immunolabeling of proximal (left, PT) and distal (right, DT) tubules in a four μm rat kidney cortex slice. Below is a control section without primary antibody but was processed and imaged directly. The bottom panel shows an xz section of filter grown mCCD cells with indirect immunofluorescence staining for endogenous PI5KIβ. Note the apical localization of this enzyme. The arrow head denotes the apical surface whereas F marks the filter. Images of rat kidney tissue slices were provided by Nuria M. Pastor-Soler (N.M.P.) from University of Pittsburgh; images of mCCD cells were provided by C.J.G..

2.2.3 Chronic expression of exogenous PI5KIβ leads to compromised polarity in renal epithelial cells

I generated a GFP-tagged PI5KIβ construct to facilitate cellular detection of the enzyme by immunofluorescence. After generation of clonal stable MDCK cells expressing GFP-PI5KIβ, I screened the clones, picked one that had 30-40% GFP expressing cells and subjected that clone to FACS to recover high and low expressor populations. The high-expressing population originally exhibited 70-80% GFP positive cells; however, the percentage of GFP positive cells dropped to 20-30% after ~ 2 weeks of culture under selection and continued to decrease. Moreover, as shown by confocal XZ images of the remaining GFP positive cells, localization of GFP-PI5KIβ is largely non-polarized (Figure 2.3, both panels). This is inconsistent with the apical localization of the same protein when transiently transfected by electroporation (albeit low expression efficiency) in polarized MDCK cells. The nonpolarized localization of chronically expressed GFP-PI5KIβ may indicate cell toxicity, although ZO-1 (an apical-basal cell polarity marker) distribution in these cells looks normal by immunofluorescence (Figure 2.3).

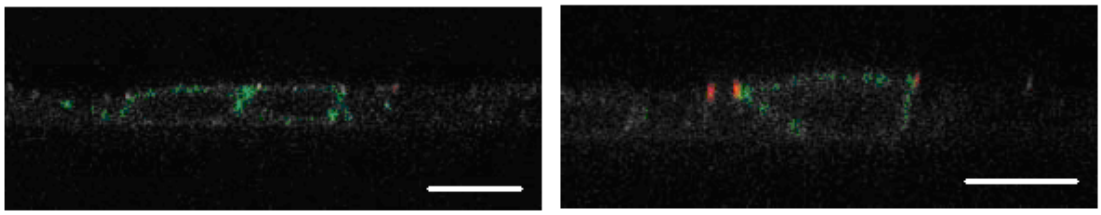

Figure 2.3 Chronic expression of exogenous PI5KIβ causes nonpolarized localization of the kinase in MDCK monolayers. Clonal MDCK cells stably expressing GFP-tagged PI5KIβ were plated at confluence on 12-well transwells and cultured for four days under selection. They were then fixed and stained for ZO-1 using immunofluorescence. Two representative XZ confocal images are shown. Note that the stably expressed PI5KIβ appears nonpolarized on the plasma membrane. Red: ZO-1; green: GFP. Scale bar: 10 μm.

2.2.4 Apical expression of PI5KIβ is not saturable

Determining the saturability of apical PI5KIβ expression can help us estimate what type of apical targeting mechanism is used by this kinase. Therefore, I infected polarized filter-grown MDCK cells with either a control AV or increasing amounts of AV-HA-PI5KIβ. The infected cells were subsequently fixed, subjected to immunofluorescence against the HA-tag and ZO-1, and imaged using a confocal microscope. Cells infected with the control AV did not show any specific staining in the channel of the HA-tag (data not shown). A broad spectrum of single cell expression levels was observed in each MDCK transwell infected with AV-HA-PI5KIβ. In cells expressing relatively high amounts of PI5KIβ, abnormal doming of the apical surface was frequently apparent (Figure 2.4B). As shown in Figure 2.4A,B,

exogenous HA-PI5KIβ was enriched at the apical plasma membrane (above the ZO-1 staining), even in the highest expressing cells. No detectable fluorescence signal was observed in the cytosol. I measured the average and total fluorescent signals (in the HA channel) at the apical and the basolateral plasma membrane domains of 37 randomly chosen cells. The ratios representing apical average to basolateral average were plotted against the total cellular fluorescent signals. As shown in Figure 2.4C, the top left panel, cells expressing low levels of HA-PI5KIβ display extremely variable apical/basolateral ratios (Y values) ranging from ~5 to ~600. This is due to very low basolateral signals (that are hard to pick up by the imaging scope and software) in those cells. The graph was replotted, with adjusted Y axis ranges, to eliminate points with exceptionally high Y values (Figure 2.4C top right and bottom two panels), There is no obvious trend in the distribution of points as the total pixels increase (especially from ~10000 to ~46000), indicating that the apical localization of PI5KIβ in polarized renal epithelial cells is nonsaturable, at least within the expression range tested. This suggests that binding to lipid components, which are usually much more abundant than proteins on cellular membranes, likely contributes to the apical localization of PI5KIβ in polarized epithelial cells.

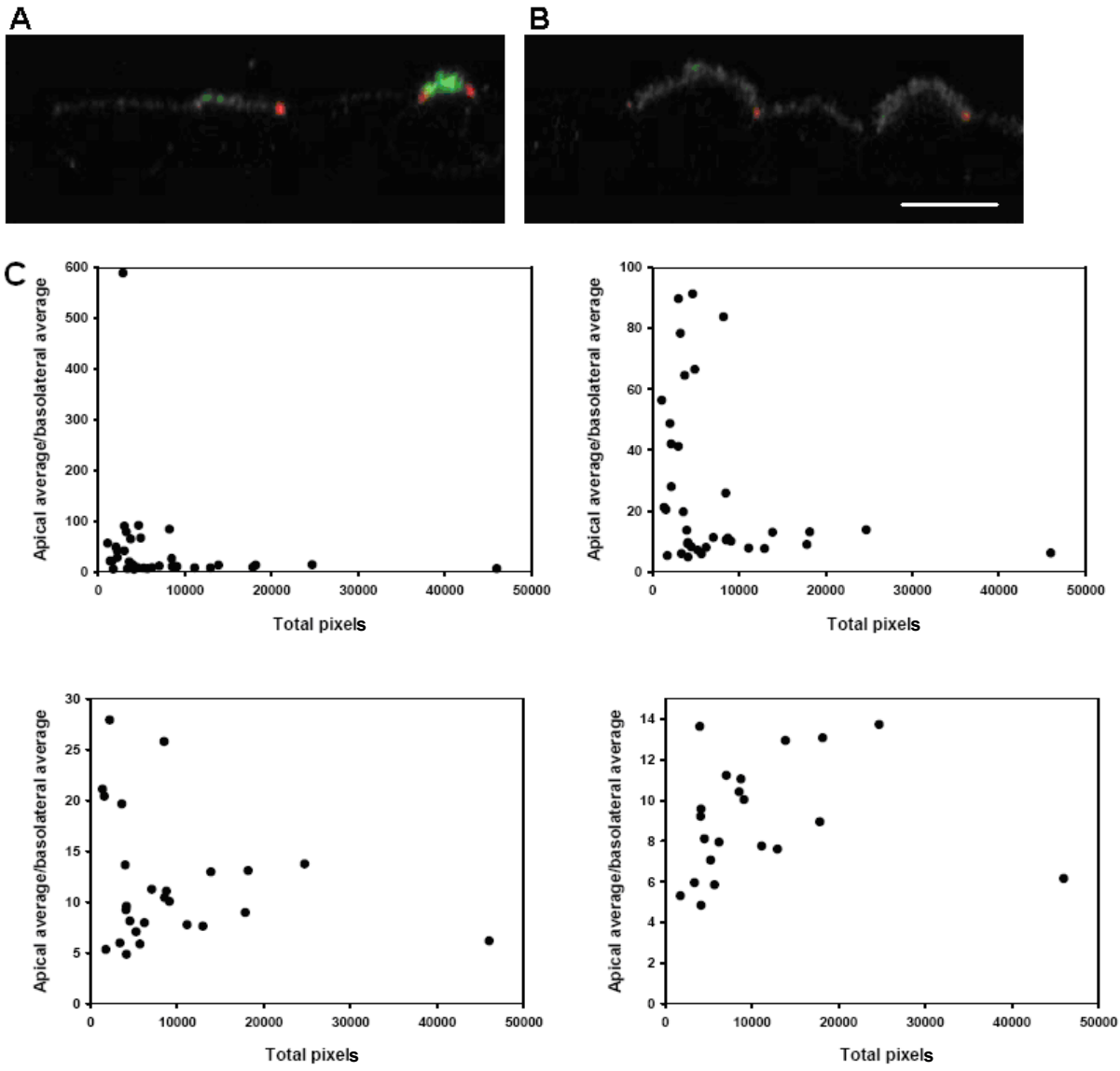

Figure 2.4 The apical plasma membrane localization of PI5KIβ is nonsaturable. MDCK cells were plated at confluence on 12-well transwells and cultured for three days before being infected with AV-HA-PI5KIβ at increasing MOIs. One day after the infection, cells were fixed and stained for the HA epitope and ZO-1 using immunofluorescence. Confocal XZ images of normal looking (A) and domed (B) cells are shown. Note that the virally overexpressed PI5KIβ primarily localizes to the apical plasma membrane of polarized MDCK cells even when cell morphology changes. C: the average and total fluorescent signals (in the HA channel) at the apical and the

basolateral plasma membrane domains of 37 randomly chosen cells were quantitated. The ratios representing apical average to basolateral average were plotted against the total cellular fluorescent signals/pixels. The graph is replotted four times with differing Y scales. Scale bar: 10 μm.

2.2.5 PIP_2 binding does not contribute to the apical localization of PI5KIβ

Because PIP_2 is enriched at the apical surface, I asked whether this lipid contributes to the polarized localization of PI5KIβ. To address this, I conducted a PIP_2 competition experiment in which increasing amounts of the specific PIP_2 binding domain of PLCδ tagged with GFP (GFP-PH-PLCδ) was virally expressed in polarized MDCK cells. Localization of co-expressed HA-PI5KIβ (AV-HA-PI5KIβ infected at MOI 50 for all samples) was determined in cells expressing different levels of PH-PLCδ. If PIP_2 is required for the correct localization of PI5KIβ, sequestration of PIP_2 by excessive PH-PLCδ should be able to dislocate the kinase. When expressed in polarized MDCK cells, as shown by confocal XZ images in Figure 2.5A,B, GFP-PH-PLCδ appeared mostly on the plasma membrane, although there was a diffuse cytoplasmic population as well. The membranous GFP-PH-PLCδ was enriched on apical plasma membrane, consistent with the distribution of PIP_2 on polarized epithelial cell surface. I quantitated average HA-PI5KIβ fluorescent signals at apical and basolateral plasma membrane domains of 32 random cells expressing both PI5KIβ and GFP-PH-PLCδ as well as 6 random cells expressing PI5KIβ and a control AV (images of cells expressing the control AV are shown in Figure 2.5C). The ratio of “apical average

HA-PI5KIβ fluorescence intensity/basolateral average HA-PI5KIβ fluorescence intensity" was determined for each cell and plotted against the total pixels of plasma membrane bound GFP-PH-PLCδ signal in the same cell (Fig 4.5D). Compared to cells infected with the control AV (represented by dots with an X value of 0), increasing cellular expression of GFP-PH-PLCδ (X value) did not have a discernable effect on the polarity of PI5KIβ (Y value). This result indicates that PIP_2 is most likely not involved in the apical targeting of PI5KIβ in polarized epithelial cells.

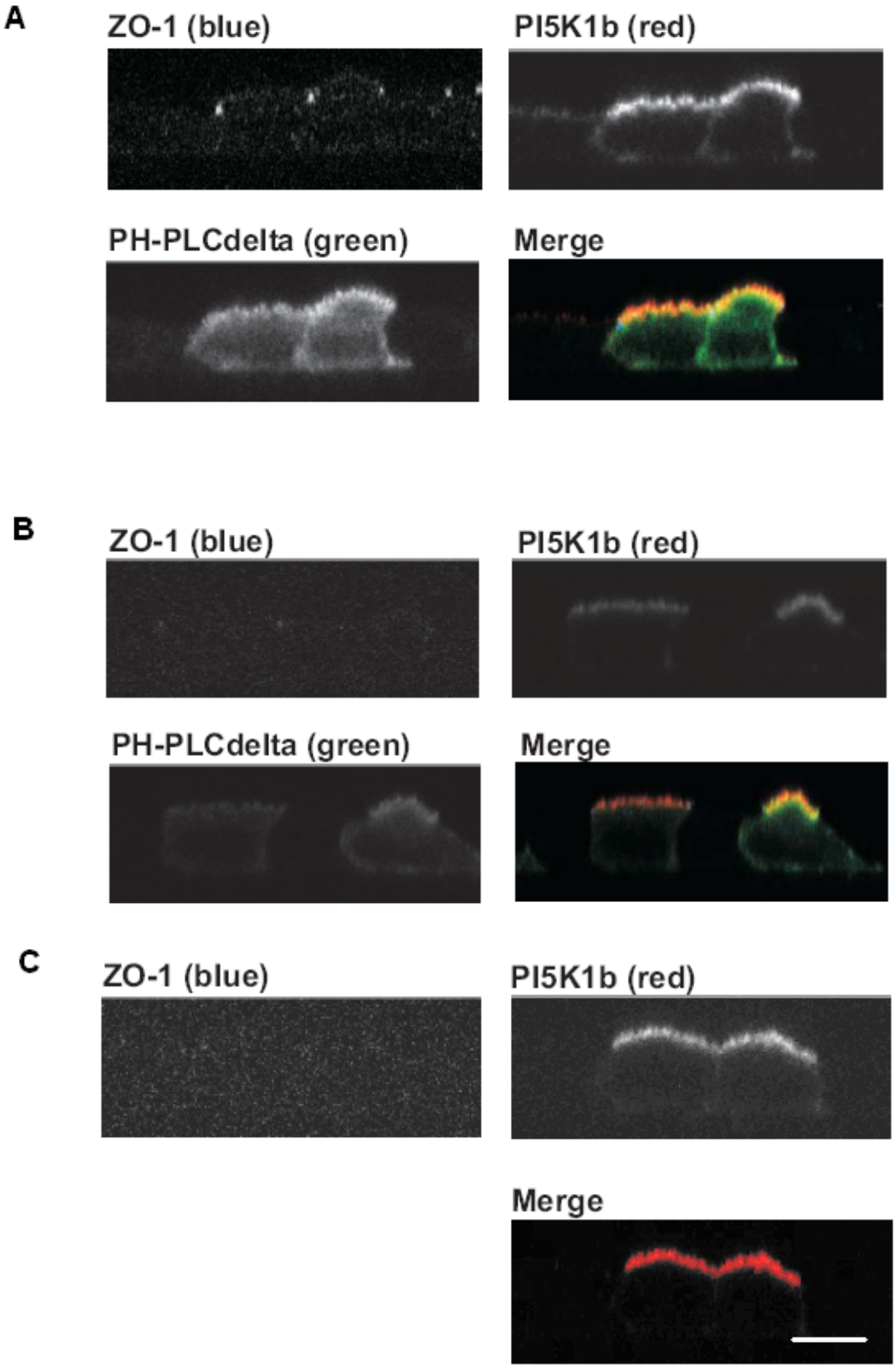
A
ZO-1 (blue)
PI5K1b (red)
PH-PLCdelta (green)
Merge
B
ZO-1 (blue)
PI5K1b (red)
PH-PLCdelta (green)
Merge
C
ZO-1 (blue)
PI5K1b (red)
Merge

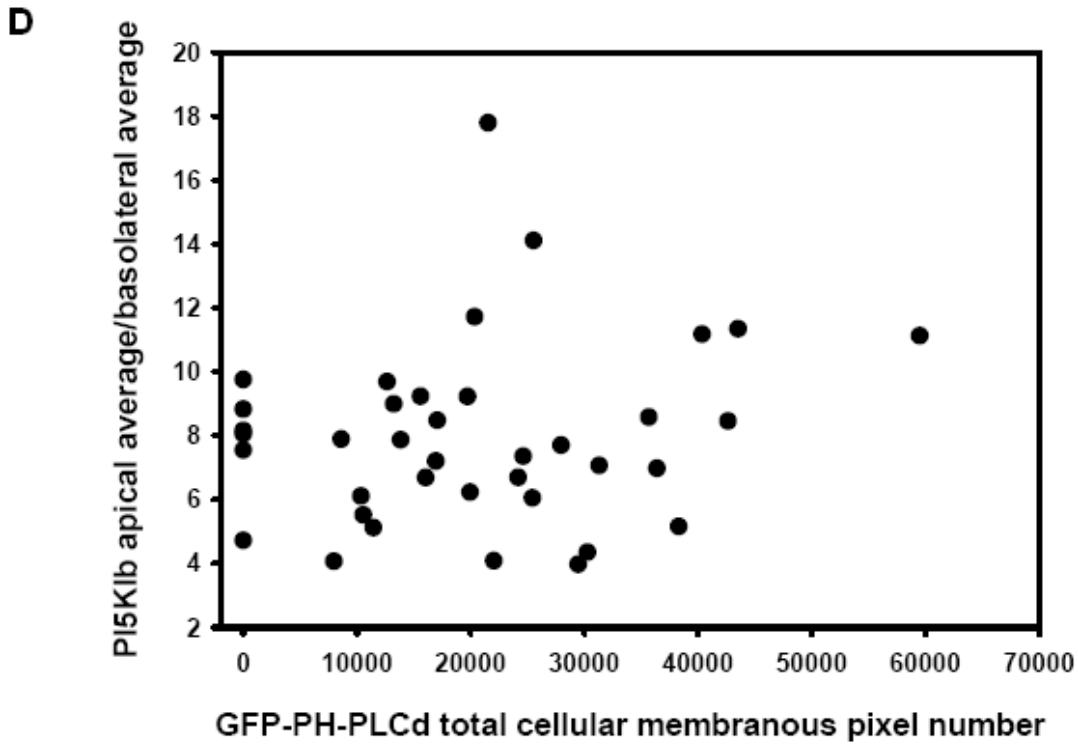

Figure 2.5 High levels of GFP-PH-PLCδ are not able to compete PI5KIβ off the apical plasma membrane. MDCK cells were plated at confluence on 12-well transwells and cultured for three days before being co-infected with AVs encoding HA-PI5KIβ (low MOI) and increasing amounts of GFP-PH-PLCδ (or a control AV). A large variation in single cell expression level was observed in every sample. Shown in A and B are representative XZ confocal images of polarized MDCK cells imaged for ZO-1, HA-PI5KIβ or GFP-PH-PLCδ using immunofluorescence. Merged images are also shown. Note that PI5KIβ is enriched at the apical plasma membrane in cells expressing high (A) or low (B) levels of GFP-PH-PLCδ. C represents confocal XZ images showing the localizations of PI5KIβ and ZO-1 in polarized MDCK cells infected with a control AV instead of AV-GFP-PH-PLCδ. D. the (apical average/basolateral average) ratios of cellular PI5KIβ signals were quantitated as in Figure 2.4C and plotted against the total plasma membrane bound GFP-PH-PLCδ

signals/pixels. 38 random cells were quantitated. Data points from cells infected with the control AV are represented by a zero X value. Scale bar: 10 μm.

2.2.6 Catalytic activity is not required for the apical localization of PI5KIβ

It has been reported before that the activation loop is crucial for both substrate specificity and plasma membrane localization of type I PI5Ks (99,105). In comparison, the kinase activity is not necessary for membrane attachment of PI5KIs (105). It is not known whether the catalytic activity of PI5KIβ is required for apical targeting of the kinase. To address this question, I infected polarized MDCK cells with low MOIs (~50, titrated to achieve comparable expression efficiencies and levels by immunofluorescence and immunoblot respectively using an anti-HA tag antibody) of AVs encoding either the wildtype HA-PI5KIβ or one of 4 known kinase-dead PI5KIβ mutants (HA tagged). The K138A mutation disrupts ATP binding while the D203A and D227A mutations abolish kinase activity via unknown mechanisms. The infected cells were fixed one day after and stained for the HA tag and ZO-1 using immunofluorescence. As shown by XZ confocal images in Figure 2.6A, localization of the D203A and the K138A mutants are comparable to that of the wildtype kinase, indicating that the catalytic activity is not required for the apical plasma membrane localization of PI5KIβ. However, the D227A mutation, either by itself or in combination with D203A, results in a partially cytosolic protein distribution. When probed with an anti-HA antibody by Western blotting, the wildtype HA-PI5KIβ appears to be a doublet, presumably due to constitutive Ser/Thr phosphorylation [Figure 2.6B, (127,190,192)].

Interestingly, as shown in Figure 2.6B, proteins with the D227A mutation (HA-PI5KIβD227A and HA-PI5KIβD203A,D227A) are devoid of the characteristic upper band when blotted for the HA tag, suggesting decreased phosphorylation of these mutants. Notably, despite the increased cytoplasmic pool, HA-PI5KIβD227A remaining on the plasma membrane retains the apically enriched distribution (Figure 2.6A), further indicating that kinase activity, as well as other possible changes associated with the D227A mutation, is not required for the polarized localization of PI5KIβ.

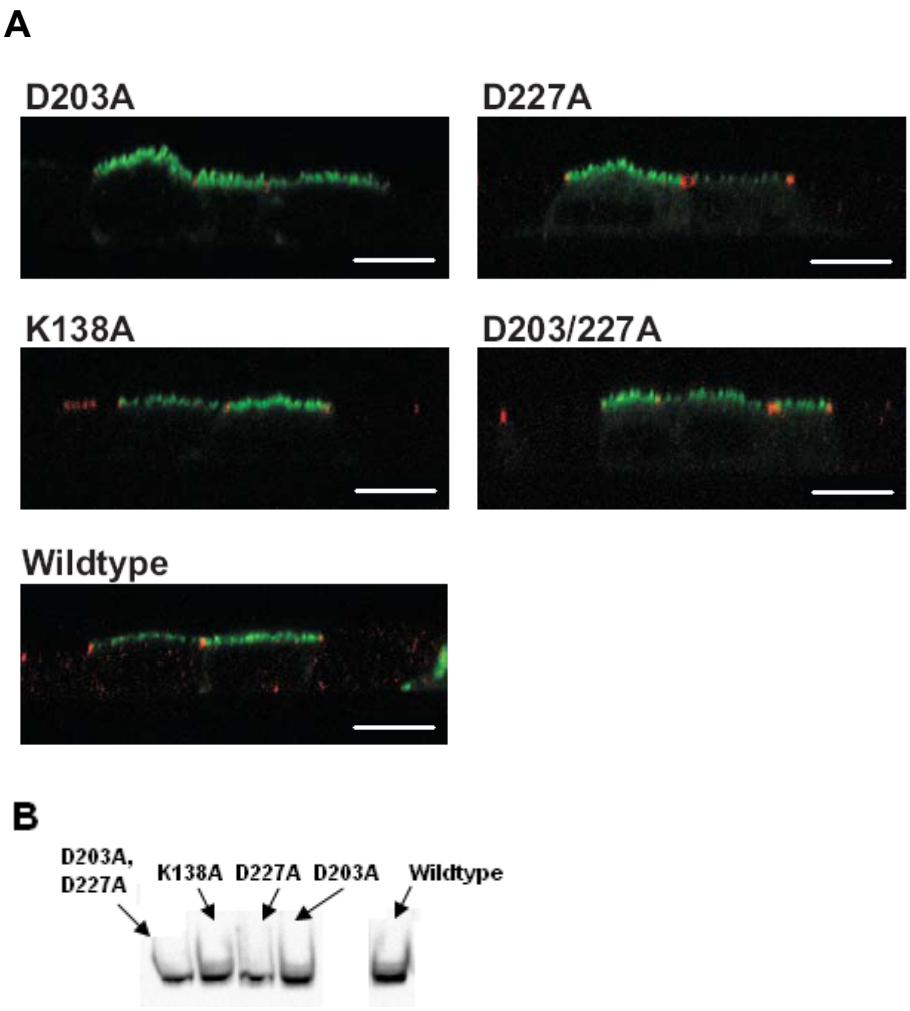

Figure 2.6 Localization of kinase-dead PI5KIβ mutants in polarized MDCK cells. MDCK cells were plated at confluence on 12-well transwells and cultured for three days before being infected with the AV encoding one of the 4 HA-tagged kinase-dead point mutants labeled in the figure (low MOIs). One day after the infection, cells were fixed and probed for ZO-1 (red) and the HA epitope (green). Representative XZ confocal images are shown in A. Note that, compared to the wildtype kinase, the presence of D227A mutation results in partially cytosolic localizations of PI5KIβ mutants, whereas other point mutations have no effect on localization. Scale bar: 10 μm. B: a parallel set of cells infected with different PI5KIβ point mutants were collected and lysed for Western blotting using an anti-HA-epitope antibody. Specific

protein bands representing PI5KIβ are shown. Note that the D227A mutation results in loss of the upper band (please see the text for details).

2.3 DISCUSSION

Our lab is interested in the regulation of PI/PIP metabolism in polarized renal epithelial cells. We have found distinct localizations of the three plasma-membrane-bound PI5KI isoforms in polarized cells, indicating that they most likely function in a non-redundant fashion and participate in distinct local cellular events that require PIP_2. In the present study, my aim was to determine the mechanism leading to highly selective apical localization of PI5KIβ. Understanding this unique localization (in comparison to the more laterally enriched distribution of isoforms α and γ661) can provide information on how PIP_2 metabolism is regulated on the apical plasma membrane and how PIP_2 related processes are differentially modulated at the apical and basolateral cell surface domains of polarized epithelial cells.

2.3.1 The apical localization of PI5KIβ

I have shown here that PI5KIβ selectively localizes to the apical plasma membrane of polarized renal epithelial cells both *in vivo* and in culture. What mediates this characteristic localization remains unclear. As described above, my data indicate that the apical cell surface localization of PI5KIβ is non-saturable. Therefore a lipid component of the plasma membrane is most likely involved in apical targeting of the kinase. My data also suggest that PIP_2 is not required for cellular localization of

PI5KIβ because high expression of the PIP_2 sequestering protein GFP-PH-PLCδ did not reduce apical plasma membrane enrichment of the enzyme. Another possible lipid candidate is phosphatidic acid (PA), which is known to specifically stimulate kinase activity of type I PI5Ks (193,194). A role of PA in membrane recruitment of cellular proteins was reported before (195). In a recent study, a membrane-targeted PA biosensor based on fluorescence resonance energy transfer (FRET) was developed to detect cellular localization of PA (196). Interestingly, PA concentrations detected (by the biosensor) were consistently higher on free plasma membrane domains than on cell-cell contact regions in nonpolarized COS7 cells, especially upon stimulation by growth factors (196). A similar asymmetrical distribution of PA can possibly exist in polarized epithelial cells and facilitate polarized localization of PI5KIβ. To test this possibility, future studies are needed to determine the plasma membrane distribution pattern of PA in polarized cells, perhaps using the same biosensor (196), to examine whether PI5KIβ interacts directly with PA using methods described before (195), and to investigate whether loss of PA (for example by knocking down PA synthesizing enzymes) leads to mislocalization of PI5KIβ in polarized epithelial cells. While the above mentioned experiments are warranted, it is noteworthy that the basal level of PA in unstimulated cells is relatively low due to the presence of various PA-degrading enzymes, including lipins [Mg^{2+}-dependent PA phosphatases; (197,198)] and lipid phosphate phosphatases [Mg^{2+}-independent and *N*-ethylmaleimide-insensitive; (197,199-203)]. Most newly synthesized PA serves as precursors for a number of other cellular products and is rapidly transformed (204).

Therefore, it is unlikely that PA alone is responsible for the enrichment of PI5KIβ at the apical surface of unstimulated cells observed through my study. Other lipid and/or protein factors are possibly involved in the apical targeting of PI5KIβ regardless of the role of PA in this process.

A rapid decrease of GFP-PI5KIβ expression was observed in clonal MDCK stable cells (chronically expressing this construct) under selection. This could result either from apoptosis of cells expressing the kinase or from intrinsic cellular responses that silenced the expression of exogenous PI5KIβ or degraded the plasmid. Loss of the polarized PI5KIβ distribution was also observed in these cells, indicating compromised cell polarity. Since PIPs are critical and versatile regulators of many cellular signaling and trafficking pathways, it is possible that excessive PI5KIβ disrupts the balance between different PIP populations and results in aberrant signaling cascades and/or protein targeting events that eventually lead to impaired polarity. Further research is needed to verify this hypothesis. Interestingly, transient virally overexpression of PI5KIβ, especially at high levels, often causes doming of the apical plasma membrane of polarized (manifested by correct localization of PI5KIβ) epithelial cells (Figure 2.4B). This abnormal phenotype can be a sign of cell toxicity by excessive PI5KIβ and may prelude loss of epithelial polarity and cell apoptosis in chronic expressions.

I have generated truncation mutants of PI5KIβ (GFP-tagged) to examine what portion of the kinase is required for its correct cellular targeting. Since chronic expression of PI5KIβ causes polarity problems, as described above, and transient

transfection yielded very low expression efficiency, completion of these studies will require generation of AVs encoding these constructs. Once the AVs are made, localizations of virally expressed PI5KIβ mutants will be determined by immunofluorescence in polarized epithelial cells and compared to that of the virally expressed wildtype kinase. Domain(s) identified to play a role in apical targeting will be further dissected by additional mutagenesis, AV-mediated expression and immunofluorescence to pinpoint minimal sequence motifs/residues required in polarized cellular localization of PI5KIβ. These motifs/residues can then be used as bait to identify specific apical interactors of PI5KIβ and determine whether any of these interactors contribute to apical targeting of the kinase.

As described above, catalytic activity is not required for apical localization of PI5KIβ in polarized epithelial cells. This result does not rule out the possibility that selected portions of the kinase homology domain are important for apical targeting of the enzyme. However, due to the high level of sequence homology between the kinase domains of PI5KI isoforms, my prediction is that the apical targeting signal(s) of PI5KIβ lie within the N- and/or C- terminal flexible regions. This would be consistent with the reported result that the C-terminus of PI5KIβ contributes to polarized localization of the kinase in neutrophils (128).

2.3.2 Phosphorylation of PI5KIβ

Unlike the wildtype HA-tagged kinase, HA-PI5KIβD227A does not exhibit the upper protein band [suggested to represent the Ser/Thr phosphorylated HA-PI5KIβ (127,190,192)] when blotted with an anti-HA antibody (Figure 2.6B). Phosphorylation

of PI5KIβ has been linked to reduced catalytic activity and compromised membrane association of the kinase (127,190,192). It is therefore curious that D227A associated dephosphorylation, manifested by loss of the upper band, results in loss, instead of an increase, of kinase activity and reduced membrane localization of PI5KIβ [Figure 2.6A, (205)]. A very similar observation was reported by Dr. Yin's group when they treated cells expressing HA-PI5KIβ with H_2O_2 [oxidative stress, (127)] and discovered that the kinase lost the upper band by blot, redistributed to the cytosol, and had decreased lipid kinase activity. Yin and colleagues observed that, in spite of the massive decrease in Ser/Thr as well as net phosphorylation of PI5KIβ, the enzyme was selectively phosphorylated on a Tyr residue upon H_2O_2 treatment (127). They concluded that the effect of Tyr phosphorylation on PI5KIβ kinase activity and localization was much more potent than that of Ser/Thr phosphorylation (127). A similar balance shift between Ser/Thr and tyrosine phosphorylation events might be responsible for the abolished catalytic activity and the partial cytosolic localization associated with PI5KIβD227A. Future studies are needed to evaluate this hypothesis.

2.3.3 Differential localizations of type I PI5Ks

Localization of PI5KIγ661 in polarized epithelial cells is largely nonpolarized with a slight enrichment on the lateral surface (Figure 2.1C). The γ661 isoform has been implicated in basolateral membrane traffic in polarized epithelial cells and has been shown to regulate synaptic endocytosis by PIP_2 synthesis as well as direct interactions with key components of clathrin coated pits (114,120,121,189). If the minimal apical targeting motif of PI5KIβ can be isolated, it will be transplanted into the

γ661 isoform to determine if the sequence is able to re-direct PI5KIγ661 to the apical plasma membrane. Meanwhile, I have generated GFP-tagged domain chimeras of PI5KIβ and γ661 (by mixing and matching their N- terminal, C- terminal and kinase homology domains). These constructs will be subcloned to make AVs as described above. If, as I predict, the apical targeting signal of PI5KIβ is within the N- and/or C-flexible regions, a chimeric construct consisting of the N- and C- tails of the β isoform as well as the kinase domain of the γ isoform should localize to the apical plasma membrane of polarized epithelial cells. If not, either the apical signal is within the kinase domain, or the signal is not transplantable (requiring collaboration from other β-specific sequences within the kinase domain or silenced by a dominant basolateral/non-polarized signal in the γ kinase domain). Further studies are then needed to verify these possibilities.

The β-γ chimeras mentioned above can also be used in functional studies. For example, by expressing a non-polarized chimera with intact PI5KIβ kinase activity in polarized epithelial cells depleted of the endogenous PI5KIβ (and probing for PIP_2 by immunofluorescence using GFP-PH-PLCδ), we will be able to determine whether the higher PIP_2 concentration on apical plasma membrane is simply due to higher activity of the β isoform (supported if apical and basolateral surface GFP-PH-PLCδ signals appear comparable) or is regulated by other mechanisms (supported if the apical plasma membrane still has more PIP_2). Similar strategies can be utilized to evaluate whether differentially localized PI5KI isoforms contribute to different endocytic rates on apical and basolateral plasma membrane domains (191). Moreover, PI5KIα, which

is mostly on the lateral surface of polarized epithelial cells, can also be studied by making chimeras with the apically localized PI5KIβ.

2.3.4 Summary

The present study focuses on apical localization mechanisms of PI5KIβ. My data suggest that an unknown membrane lipid is likely involved in apical targeting of the kinase and that PIP_2 is most likely not that lipid. Other possibilities include PA as discussed above. We are currently in the process of generating AVs encoding PI5KIβ truncation mutants. These mutants will be used to determine the apical targeting signal sequence within PI5KIβ and to identify specific interactors of the kinase that possibly contribute to its cellular localization. We are also generating chimeras of different PI5KI isoforms that localize differentially in polarized epithelial cells. These chimeras will be useful in localization and functional studies of the type I PI5Ks.

3.0 OCRL1 FUNCTION IN RENAL EPITHELIAL MEMBRANE TRAFFIC

3.1 INTRODUCTION

OCRL1, the Lowe disease protein, is a lipid phosphatase that preferentially converts PIP_2 to PI4P by hydrolyzing the 5' phosphate of PIP_2 (163,164). OCRL1 is localized primarily at the *trans*-Golgi network (TGN) and is also associated with a subset of endosomes and with clathrin coated pits, suggesting a potential function of this enzyme in membrane traffic through these compartments (162,167,168,170,206). While mutations throughout the 970 amino acid protein encoded by the OCRL1 gene can result in Lowe syndrome, cell extracts from fibroblasts cultured from Lowe syndrome patients universally exhibit a markedly reduced ability to dephosphorylate PIP_2 (163,207). OCRL1 appears to be the major PIP_2-hydrolyzing enzyme in human kidney proximal tubule cells, and kidney cells derived from Lowe syndrome patients have roughly double the normal cellular contingent of PIP_2 (208). Thus, the OCRL1 phenotype correlates well with loss of phosphatase activity.

Lowe syndrome patients almost universally have renal tubular dysfunction, including acidosis, amino aciduria, phosphaturia, and proteinuria (209). The defect in protein reabsorption has been suggested to result from improper function or trafficking of the cell surface receptor megalin (18,172). Megalin recycles at the apical domain of polarized epithelial cells (6). It binds to numerous protein ligands that

dissociate from the receptor after internalization and are targeted to lysosomes for degradation. In patients with renal tubular dysfunction, ligand handling is somehow compromised, resulting in excess secretion of filtered proteins into the urine. Whether proteinuria in Lowe syndrome patients is due to aberrant megalin trafficking as a result of the defect in OCRL1 activity has not been directly tested experimentally.

In addition to its role in signaling, PIP_2 also regulates cytoskeletal dynamics as well as numerous steps in membrane traffic (42,210). We have previously found that increases in cellular PIP_2 mediated by overexpression of PI5KIβ in MDCK cells stimulated delivery kinetics of a subset of apical membrane proteins by increasing the frequency of actin comets, short branched actin structures (rapidly nucleated by the Arp2/3 protein complex) capable of propelling the movement of transport vesicles in the cytosol (118,211). Similarly, increased PIP_2 has been correlated with an increase in clathrin-mediated endocytosis (115,117,119).

Given the known stimulatory roles of PIP_2 in these processes, it is not immediately obvious how loss of OCRL1 function might lead to renal tubular dysfunction in Lowe syndrome patients. Additionally, it is difficult to describe a mechanism leading to the ancillary renal defects that accompany proteinuria in Lowe Syndrome patients, including acidosis, amino aciduria, and phosphaturia. Nevertheless, the idea that OCRL1 directly regulates megalin traffic has been reinforced by the recent demonstration that some patients with Dent disease, originally described as resulting from defective function of the CLC-5 Cl^-/H^+ antiporter, in fact have mutations in OCRL1 (178,212). There is strong evidence that loss of CLC-5 function leads to

decreased uptake of fluid phase markers and megalin ligands in knockout mouse models (213-219), although direct studies on megalin endocytosis have not been performed. The recent demonstration by De Camilli's group that a small subpopulation of OCRL1 binds to APPL1 in clathrin coated pits has fueled this speculation (170). OCRL1 also interacts with clathrin, α-adaptin and several Rab proteins, including Rabs 5 and 6 (206,220).

Although the OCRL1 protein is ubiquitously expressed in mouse and human tissues and cell lines, only a subset of organs are functionally impaired by OCRL1 mutations (169). It has been hypothesized that expression of other inositol polyphosphatases can compensate for loss of OCRL1 function in some cells. Interestingly, knockout of the OCRL1 gene in mice does not recapitulate Lowe syndrome, as the mice do not develop cataracts or renal tubular dysfunction (173). Expression of the homologous 75 kDa inositol polyphosphate-5-phosphatase INPP5B in mice has been suggested to compensate for loss of OCRL1 function, as INPP5B is expressed at considerably higher levels in mice compared with humans. In support of this idea, knockout of INPP5B in mice had no discernible renal phenotype; however a cross between OCRL1 and INPP5B knockout mice did not produce any viable double-knockout mice (173). However, in contrast to OCRL1, INPP5B is largely localized to the early biosynthetic pathway although it is also present on some early endocytic compartments. INPP5B does bind to APPL1 *in vitro* but unlike OCRL1, does not interact with clathrin or α-adaptin (170,221). Moreover, a recent study argues that OCRL1 and INPP5B do not access the same pools of PIP_2, as

expression of INPP5B does not rescue membrane ruffling in OCRL1 deficient fibroblasts (220).

In the absence of an animal model, we have used siRNA mediated knockdown in human (HK-2) and canine (MDCK) renal epithelial cells to model the disease and examine the consequent effects on the trafficking of megalin and other proteins. MDCK cells establish well differentiated monolayers and provide a good model in which to investigate apical biosynthetic and endocytic traffic; however, they also express significant levels of INPP5B, which could complicate dissection of the cellular role of OCRL1. The human proximal tubule cell line HK-2 is less well differentiated but expresses no INPP5B. We find that knockdown of OCRL1 in either cell line recapitulates key features of cells cultured from Lowe Syndrome cells, including a trend towards increased cellular PIP_2 and alterations in cytoskeletal dynamics. We found no effect of depleting OCRL1 on either biosynthetic or endocytic membrane traffic. However, we did observe increased lysosomal hydrolase secretion in OCRL1-deficient cells, consistent with a role for this enzyme in post-Golgi delivery to lysosomes (168,222).

3.2 RESULTS

3.2.1 Characterization of OCRL1 knockdown in human and canine kidney cells

To examine the consequences of disrupting OCRL1 function in renal epithelial cells, we optimized approaches to knock down the protein using siRNA. We previously showed that biosynthetic delivery in polarized MDCK cells is sensitive to

overexpression of wild type OCRL1 (118). However, because canine cells, like mice, might express a redundant inositol polyphosphate 5'-phosphatase that could compensate for loss of OCRL1, we also developed methods to knock down OCRL1 in human renal proximal tubule HK-2 cells. Endogenous OCRL1 localized largely to the Golgi complex in both of these cell lines (Figure 3.1A and data not shown). Other groups have previously reported that a small subpopulation of OCRL1 also localizes to endosomes and the cell surface (162,168,170). Introduction of siRNA oligonucleotides by electroporation resulted in efficient reduction in OCRL1 levels in both cell lines, as measured by western blotting (Figure 3.1B) or using a PCR-based assay (performed using HK-2 cells only, Figure. 3.1C). Importantly, we could detect no endogenous expression of INPP5B message in either HK-2 or HeLa cells, although our primers efficiently amplified a heterologously expressed human INPP5B cDNA construct when expressed in HeLa cells (Figure 3.1D). Thus, any functions of OCRL1 that are disrupted upon knockdown of this enzyme are unlikely to be restored by compensatory expression of INPP5B in these cells. However, MDCK cells do express significant levels of INPP5B (Figure 3.1D).

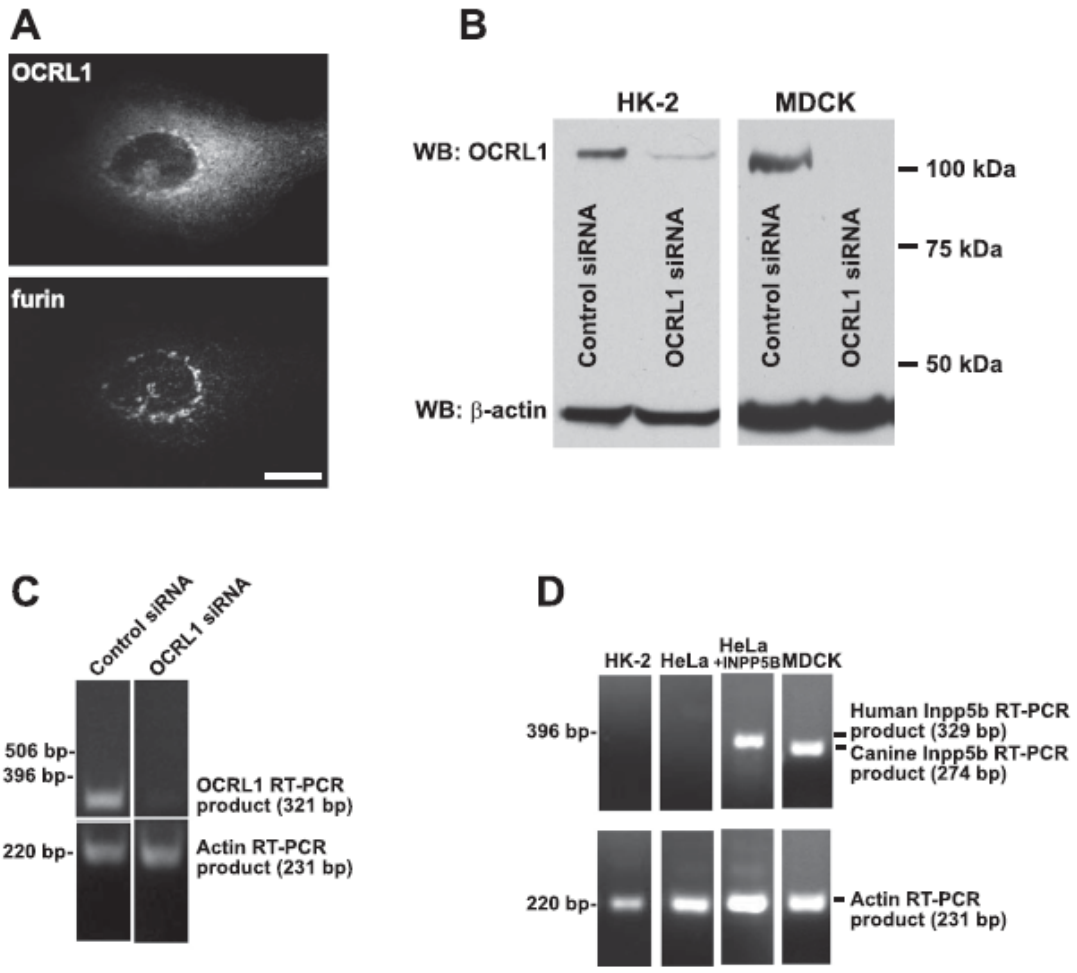

Figure 3.1 SiRNA-mediated knockdown of OCRL1 in human and canine cells. A: MDCK cells were fixed, processed for indirect immunofluorescence to detect OCRL1 and the TGN marker furin, and examined using confocal microscopy. The images are maximum projections of ten confocal slices. Scale bar: 10 μm. B: Low passage MDCK or HK-2 cells were nucleofected with control or OCRL1 siRNA as described in Materials and Methods. Cells were plated directly onto permeable supports (MDCK) or in 12-well dishes (HK-2) for three days. Samples were harvested and analyzed by Western blotting (WB) to detect OCRL1 and actin (as a loading control). The migration of molecular mass standards is indicated on the right. C: siRNA knockdown of OCRL1 in HK-2 cells was confirmed using a PCR-based assay as described in

Materials and Methods. D: Primers specific for human INPP5B were used to amplify mRNA isolated from HK-2 or HeLa cells. HeLa cells transfected with a cDNA encoding human INPP5B were included as a positive control to demonstrate the efficacy of the primers. Figure 3.1A was generated by C.J.G.; figure 3.1D was generated by C.M.S..

Kidney proximal tubule cell lines derived from Lowe syndrome patients have been reported to have elevated levels of PIP_2 compared to normal human kidney cells (208); however, no other studies have reported changes in cellular PIP_2 in OCRL1-deficient cells. This is consistent with the fact that most of the cellular PIP_2 is present at the plasma membrane, whereas OCRL1 is largely excluded from this site. We compared cellular PIP_2 extracted from control and OCRL1 knockdown cells after radiolabeling with $^{32}P_i$ for 4 h. We reproducibly observed a tendency towards increased cellular PIP_2 in MDCK cells treated with siRNA directed against OCRL1, although this was not statistically significant by Student's paired t-test (Figure 3.2A). To determine whether this trend is physiologically relevant, we tested whether knockdown of OCRL1 alters the percentage of cells producing actin comets. Fibroblasts from Lowe patients have previously been demonstrated to have dramatically increased numbers of comets, presumably due to enhanced PIP_2-dependent activation of N-WASP-Arp2/3-mediated polymerization of these branched actin structures (223). To quantitate actin comet occurrence, control vs. OCRL1 knockdown MDCK cells stably expressing GFP-actin were observed by

spinning disc confocal microscopy. Individual fields were imaged over a three min period and the number of cells with actin comets quantitated. Knockdown of OCRL1 resulted in a dramatic increase in the percentage of cells with detectable actin comets over this period, confirming that OCRL1 normally regulates a pool of PIP_2 involved in cytoskeletal dynamics in these cells (Figure 3.2B). Moreover, this pool is apparently not accessible to the INPP5B expressed in MDCKs. This is consistent with recent results demonstrating that expression of INPP5B does not rescue the enhanced membrane ruffling observed in OCRL1 deficient fibroblasts (220).

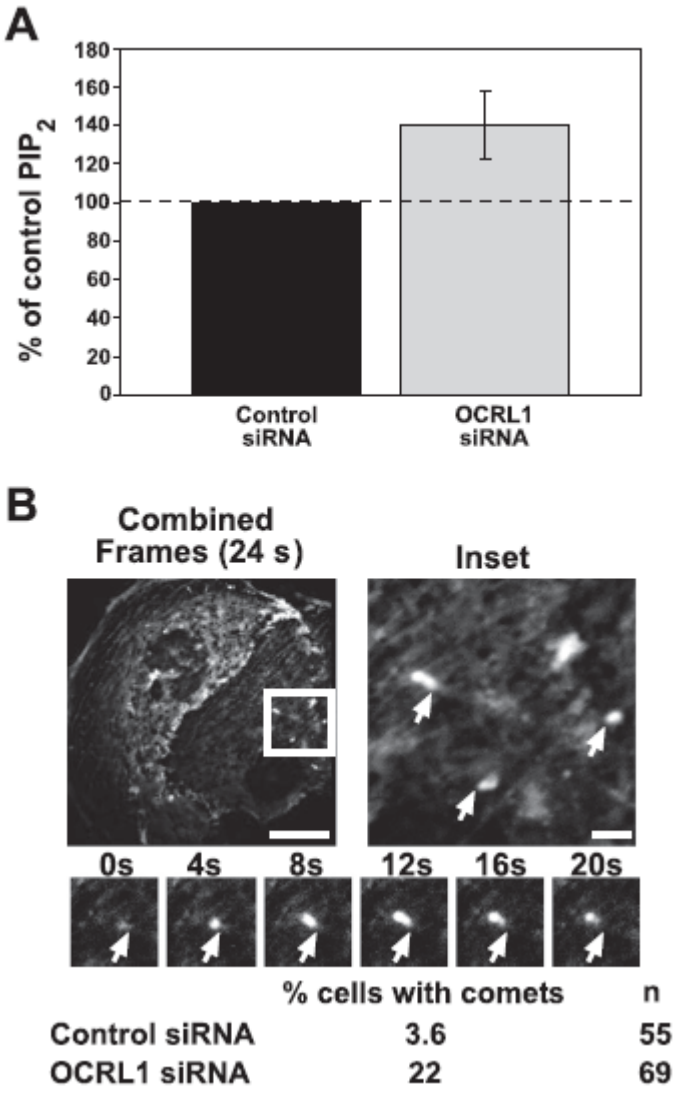

Figure 3.2 PIP_2 levels and actin comet frequency are elevated upon OCRL1 knockdown in MDCK cells. A: MDCK cells were treated with either control or OCRL1 siRNA and plated directly onto filters for three days. Phospholipids were labeled with ^{32}P-orthophosphate and analyzed by TLC to determine relative phospholipids levels as described in Materials and Methods. PIP_2 values in cells nucleofected with OCRL1 siRNA were normalized to control in three independent experiments and the mean +/- SEM is plotted. The difference in PIP_2 levels between the two experimental conditions is not statistically significant by Student's t-test. B: MDCK cells stably expressing GFP-actin were electroporated with control or OCRL1

siRNA and plated onto filters for two days before being transferred to Bioptech 0.17 mm ΔT dishes for an additional day prior to imaging. Images were taken every two seconds. MetaMorph software was used to overlay multiple frames and filter out low level fluorescence to reveal the path of the actin comets in the cell (right panel; arrows). The lower panel shows the path of a single comet. In each image the arrow represents the starting position of the actin comet in the series. The percentage of cells treated with control vs. OCRL1 siRNA that had detectable actin comets during a three min imaging window is noted underneath; n represents the number of cells examined for each condition. Scale bar: 10 μm. Figure 3.2 was generated by C.J.G..

3.2.2 Effects of OCRL1 knockdown on biosynthetic delivery kinetics

We showed previously that elevation of cellular PIP_2 upon overexpression of PI5KIβ in polarized MDCK cells stimulates a post-Golgi step in biosynthetic delivery of the apical marker influenza hemagglutinin (HA) via a mechanism dependent on actin comets (118). In contrast, heterologous expression of OCRL1 or dominant negative inhibitors of Arp2/3 activation inhibited HA delivery. Moreover, HA could be detected at the tips of actin comet-like structures in fixed cells. Because both PI5KI β overexpression and OCRL1 knockdown cause an increase in actin comets, we hypothesized that HA delivery kinetics might be stimulated upon depletion of OCRL1 by siRNA. However, we found no effect of OCRL1 knockdown on HA delivery kinetics in either MDCK or HK-2 cells (Figures 3.3A and 3.3B). In contrast, knockdown of N-WASP resulted in significant inhibition of HA delivery in MDCK cells, whereas

overexpression of PI5KIβ stimulated HA delivery kinetics as expected (Figure 3.3A). PI5KIβ overexpression has a greater effect on the cellular PIP_2 level compared with OCRL1 knockdown [210% of control for PI5KIβ (unpublished result of C.J.G.)], and it is possible that a threshold increase in PIP_2 is required to stimulate HA delivery.

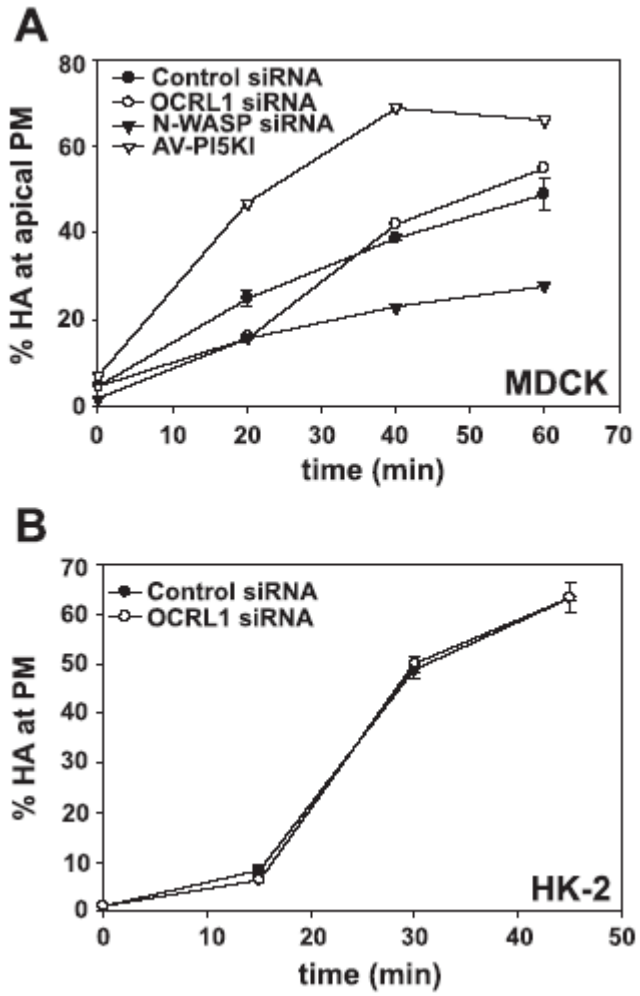

Figure 3.3 Knockdown of OCRL1 does not enhance apical biosynthetic delivery kinetics in MDCK, HK-2 cells. A: MDCK cells were electroporated in buffer containing either control siRNA or an siRNA oligonucleotide directed against N-WASP or OCRL1. The efficiency of N-WASP knockdown was between 15 and 40% based on Western blotting of cell lysates (not shown). The cells were seeded onto Transwell filters for three days and then infected with AV expressing the apical protein HA and either control AV or AV-PI5KIβ. The following day, cells were starved, radiolabeled for 15 min, and chased for two h at 19ºC. Cell surface delivery kinetics of HA were measured after warming to 37ºC using a cell surface trypsinization assay. Similar results were obtained in three independent experiments; results from a single

representative experiment are plotted. B: HK-2 cells treated with either control or OCRL1 siRNA were infected with AV-HA two days after nucleofection. The following day, cells were radiolabeled for 15 min and plasma membrane delivery kinetics of HA quantitated. Similar results were obtained in four independent experiments; results from a single representative experiment are plotted. Figure 3.3 was generated by C.J.G..

3.2.3 Effect of OCRL1 knockdown on low molecular weight protein uptake and megalin internalization kinetics

We next examined whether knockdown of OCRL1 disrupts megalin-dependent uptake of low molecular weight proteins. Patients with Dent disease caused by defective CLC-5 activity have virtually identical urinary proteomes to OCRL1 patients, and dramatically decreased uptake of megalin ligands has been observed in proximal tubule cultures from CLC-5 knockout mice (213). Moreover, megalin expression is reduced in proximal tubules from CLC-5 knockout mice (213) as well as in the renal tubular epithelium of some Dent disease patients (19). However, whether loss of CLC-5 function affects the kinetics or fidelity of megalin trafficking is unknown.

MDCK cells do not express endogenous megalin (13), although they do express LRP, a basolaterally recycling member of the LDL receptor family closely related to megalin. Additionally, these cells express both ARH and Dab-2, adaptor proteins thought to play a role in endocytosis of megalin in the proximal tubule. HK-2 cells express ARH, but not Dab-2 (Figure 3.4A). The ARH doublet observed in MDCK cells

has been previously observed in some other cell types (224). We infected polarized MDCK cells with recombinant adenovirus expressing a GFP- and V5-tagged truncated megalin receptor (AV-mini-megalin). Fluorescence imaging in non-permeabilized cells to selectively label the surface-exposed V5 tag in addition to the total pool of GFP-tagged mini-megalin confirmed that this protein was efficiently trafficked to the apical membrane (Figure 3.4B). We next examined the domain selective binding of ^{125}I-lactoferrin (^{125}I-Lf), a ligand that binds to mini-megalin, in control vs. mini-megalin expressing MDCK cells. MDCK cells grown on Transwell filters were incubated with apically or basolaterally added ligand on ice, then quickly washed several times with ice-cold medium. The filters were removed from their supports and cell surface radioactivity quantitated using a gamma counter. Apical binding to cells infected with AV-mini-megalin was significantly higher than to control cells, confirming that apical ^{125}I-Lf binding is quantitatively mediated by mini-megalin (Figure 3.4C).

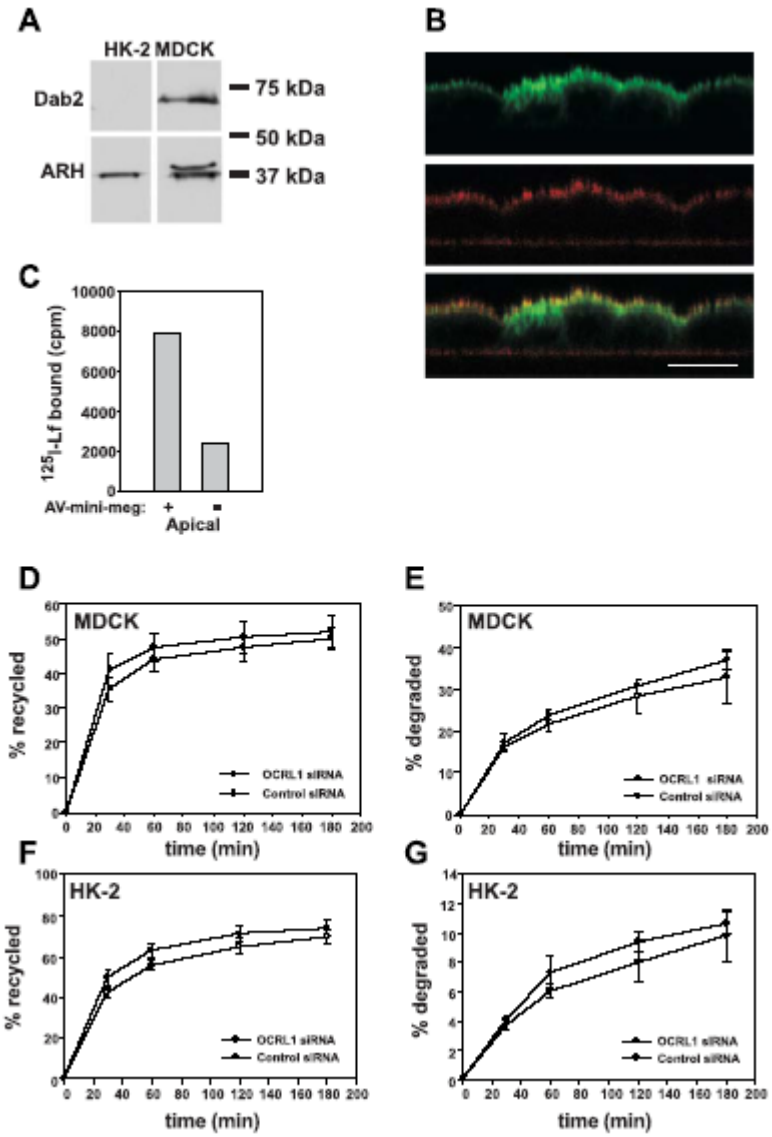

Figure 3.4 OCRL1 knockdown does not affect megalin-mediated uptake and degradation of lactoferrin in MDCK and HK-2 cells. A: Comparable levels of MDCK and HK-2 cell lysates were blotted with antibodies against ARH and Dab-2. The migration of molecular mass standards is indicated on the right. B: Filter-grown MDCK cells were infected with replication-defective recombinant AV encoding V5- and GFP-tagged mini-megalin. Cells were incubated on ice with anti-V5 antibody and secondary antibody to label the surface population of mini-megalin (red), then fixed and processed for confocal microscopy. The total cellular population of mini-megalin

was visualized using the GFP label (green). Scale bar: 10 μm. C: Filter grown MDCK cells infected with control AV or AV encoding mini-megalin were incubated with apically-added ^{125}I-Lf on ice, then washed, solubilized, and cell-associated radioactivity quantitated using a gamma counter MDCK (D,E) or HK-2 (F,G) cells treated with control or OCRL1 siRNA were incubated with ^{125}I-Lf as described in Materials and Methods. MDCK cells were infected with AV-mini-megalin one day before the experiment. The kinetics of Lf recycling (D,F) and degradation (E,G) were quantitated. Similar results were obtained in three independent experiments for each cell type. Figure 3.4A was generated by C.J.G..

We then monitored the postendocytic fate of ^{125}I-Lf internalized apically from control and OCRL1 knockdown MDCK cells infected with AV-mini-megalin. As shown in Figure 3.4 (D and E), we observed no difference in the kinetics of recycling or degradation of this ligand in cells lacking OCRL1 compared with control cells. Moreover, OCRL1 knockdown had no effect on the kinetics of ^{125}I-Lf recycling or degradation mediated by endogenous megalin in HK-2 cells (Figure 3.4F,G).

Because the effect of OCRL1 on megalin-mediated handling of ^{125}I-Lf could be too subtle to detect in a single round of endocytosis, we also examined cumulative degradation of ligand over a prolonged incubation period (Table 3.1). HK-2 cells nucleofected with control or OCRL1 siRNA were incubated overnight with ^{125}I-Lf and release of TCA soluble counts quantitated. No effect of OCRL1 knockdown on the amount of ^{125}I-Lf degraded was observed using this integrated approach. Together,

our studies suggest that uptake and degradation of megalin ligands is unaffected by loss of OCRL1 function in human and canine kidney cells.

Table 3.1 OCRL1 knockdown in HK-2 cells does not affect lactoferrin degradation.

	Control siRNA (cpm)	OCRL1 siRNA (cpm)	OCRL1 KD/Control
Exp.1	44137+/-4035	35952+/-9995	0.81
Exp.2	31216+/-8761	40648+/-5172	1.30
Exp.3	5246+/-2261	4747+/-1704	0.91
Exp.4	3085+/-116	4577+/-1259	1.48
Average	--	--	1.13+/-0.32

HK-2 cells treated with control or OCRL1 siRNA were incubated overnight with ^{125}I-Lf and TCA soluble counts were recovered to quantitate cumulative ^{125}I-Lf degradation. Results from four independent experiments are shown. Experiments one and two were performed using a different batch of ^{125}I-Lf compared with three and four.

A recent study found a small pool of OCRL1 associated with the adaptor APPL1 in clathrin coated pits (170). Because APPL1 also associates through megalin via the adaptor GIPC it was suggested that OCRL1 may play a role in endocytosis of a megalin-containing complex. We therefore directly examined the effect of OCRL1 knockdown on the initial rate of megalin internalization using a biotinylation/stripping approach. HK-2 cells treated with control or OCRL1 siRNA and infected with AV-mini-megalin were biotinylated using sulfo-NHS-SS-biotin on ice and then warmed

to 37^{o}C for 0 or 6 min. At each time point, samples were rapidly chilled, and remaining surface biotin was stripped with the membrane impermeant reducing agent MESNa. Duplicate biotinylated samples were not warmed and left unstripped to measure the total amount of biotinylated megalin at the start of the time course. Cells were solubilized and biotinylated megalin was recovered and analyzed by western blotting. As a control, we also examined the effect of PI5KIβ overexpression on megalin endocytosis kinetics. We have previously demonstrated that overexpression of this enzyme stimulates endocytosis of other apical proteins, presumably by increasing surface levels of PIP_2 (119). As shown in Figure 3.5A, knockdown of OCRL1 had no effect on megalin internalization. In contrast, megalin endocytosis was enhanced upon overexpression of PI5KIβ. Moreover, OCRL1 knockdown had no effect on the internalization kinetics of ^{125}I-IgA internalization mediated by a different surface receptor (the polymeric immunoglobulin receptor, pIgR) expressed using AV in either HK-2 (Figure 3.5B) or MDCK cells (unpublished results of C.M.S.). Like megalin, pIgR endocytosis is clathrin-mediated, but pIgR does not contain ARH/Dab-2 binding motifs. Together, these data suggest that OCRL1 is not directly involved in internalization or postendocytic trafficking of megalin and its ligands, or of other membrane receptors.

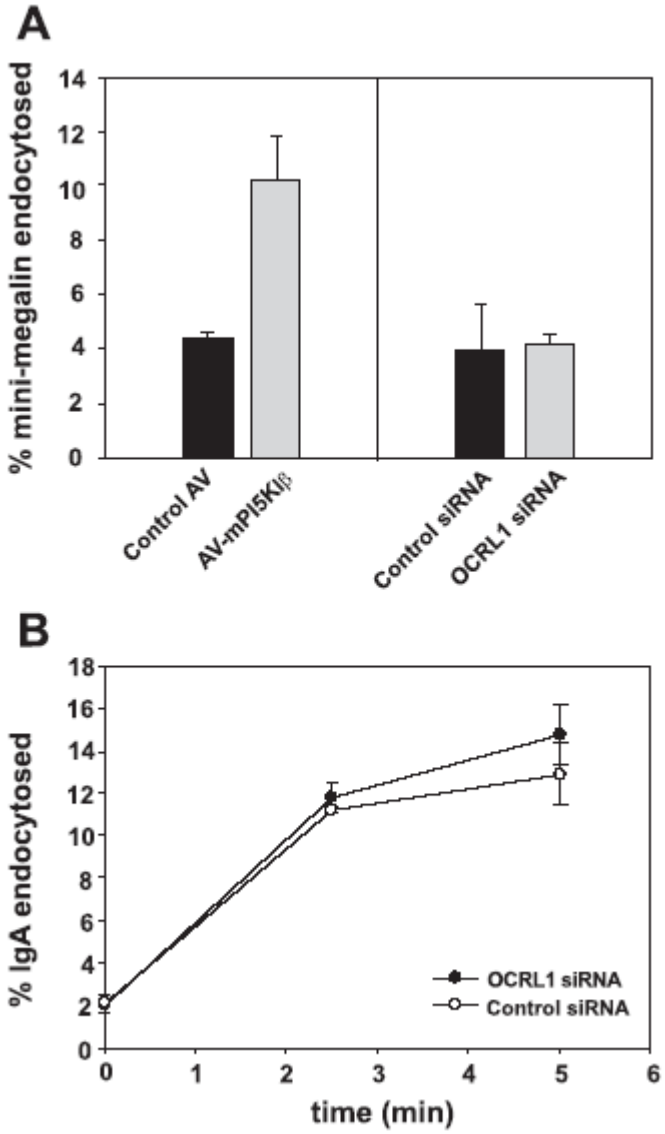

Figure 3.5 OCRL1 knockdown does not affect endocytosis of megalin in HK-2 cells. A: The effect of PI5KIβ overexpression (left panel) or OCRL1 knockdown (right panel) on endocytosis of mini-megalin was quantitated using the biotinylation-based assay described in Materials and Methods. HK-2 cells treated with control or OCRL1 siRNA or infected with control or PI5KIβ expressing AVs as indicated were biotinylated on ice, then warmed to 37^{o}C for zero or six min. Samples were stripped to remove surface biotin and endocytosis was quantitated by Western blotting after recovery of residual biotinylated mini-megalin. One set of zero min samples was left

unstripped so that results could be normalized to total mini-megalin at the surface before warming up. The mean endocytosis (+/-S.E.) from three experiments comparing PI5KIβ overexpression to control AV and four experiments comparing OCRL1 and control siRNA are plotted. B: Endocytosis of ^{125}I-IgA by pIgR-expressing HK-2 cells nucleofected with either control or OCRL1 siRNA was performed as described in Materials and Methods. The mean +/- range of duplicate samples is shown. Similar results were obtained in two experiments. Figure 3.5B was generated by C.M.S..

3.2.4 Lysosomal hydrolase delivery in OCRL1 knockdown cells

Previous studies demonstrated that OCRL1 knockdown in HeLa cells resulted in partial redistribution of the cation-independent mannose 6-phosphate receptor from the TGN to endosomal structures. Moreover, OCRL1 patients are reported to have increased levels of lysosomal hydrolases in their serum (222). To determine whether depletion of OCRL1 affects delivery of lysosomal hydrolases in renal epithelial cells, we quantitated cathepsin D secretion in HK-2 cells treated with control or OCRL1 siRNA. Cells were radiolabeled for 2 h and returned to culture in serum free medium. Media was collected after a 4 h chase and released cathepsin D, recovered after immunoprecipitation and SDS-PAGE, was quantitated using a phosphorimager. As shown in Figure 3.6, knockdown of OCRL1 in HK-2 cells consistently resulted in a roughly 20% increase in cathepsin D secretion. This increase is comparable to that

observed upon incubation of HK-2 cells with ammonium chloride, which inhibits lysosomal delivery of newly synthesized soluble hydrolases (Figure 3.6).

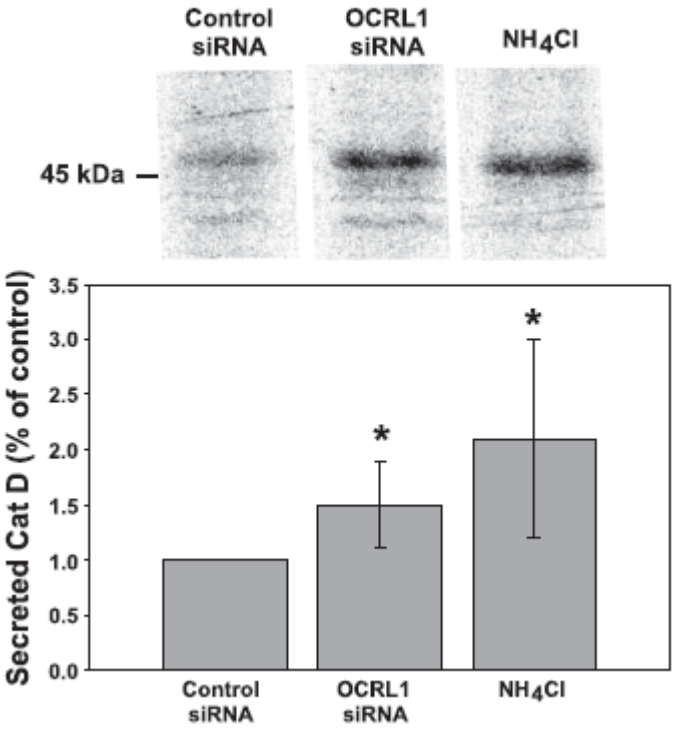

Figure 3.6 Delivery of newly synthesized lysosomal hydrolases is impaired in HK-2 cells lacking OCRL1. HK-2 cells treated with control or OCRL1 siRNA were radiolabeled for two h and chased for four h. NH_4Cl (10 mM) was included in the indicated samples. Radioactive cathepsin D secreted into the media during the chase was quantitated after immunoprecipitation and SDS-PAGE and normalized relative to control. The results from three experiments are plotted. *, P=0.029 by Mann-Whitney Rank Sum test. Samples of cathepsin D immunoprecipitated from the medium in a representative experiment are shown above the graph. Figure 3.6 was generated by C.J.G..

3.3 DISCUSSION

We have optimized conditions to efficiently knock down OCRL1 in both human (HK-2) and canine (MDCK) renal epithelial cells and measured the consequences on cellular PIP_2, actin comet frequency, and biosynthetic and postendocytic delivery. Depletion of OCRL1 did not have a significant effect on cellular PIP_2 levels but increased actin comet formation. However, we did not detect any effects of OCRL1 knockdown on the kinetics of apical biosynthetic delivery of HA or on megalin endocytosis, two trafficking steps that are stimulated when cellular PIP_2 is increased by overexpression of PI5KIβ. In contrast, we observed a significant increase in the secretion of the lysosomal enzyme cathepsin D in cells lacking OCRL1, consistent with previous observations that plasma lysosomal enzymes are elevated in Lowe syndrome patients and with a role for OCRL1 in TGN-endosome trafficking (168,222). Together, our data suggest that a defect in this step in membrane traffic represents the primary manifestation of cells lacking OCRL1. Below we discuss the implications of our findings with respect to the pathogenesis of Lowe syndrome.

3.3.1 Phenotype of OCRL1-depleted cells

Knockdown of OCRL1 using nucleofection was efficient (80-95%) as monitored using both Western blotting and PCR. We were able to amplify endogenous message encoding INPP5B in MDCK but not in HK-2 cells. Knockdown of OCRL1 did not significantly increase cellular PIP_2 levels measured in MDCK cells but had a dramatic effect on the number of cells with detectable actin comets. Fibroblasts from Lowe syndrome patients have previously been demonstrated to have significantly elevated

numbers of actin comets (223); thus acute depletion of OCRL1 (even in cells expressing INPP5B) appears to appropriately mimic key features observed in fibroblast models for the disease. The absence of a dramatic effect on PIP_2 levels upon OCRL1 knockdown is consistent with the localization of OCRL1 to intracellular compartments and suggests that this enzyme normally does not have access to the majority of cellular PIP_2, which is localized to the plasma membrane.

3.3.2 OCRL1 knockdown and biosynthetic delivery

We previously found that increased cellular PIP_2 mediated by overexpression of PI5KIβ resulted in increased actin comet frequency and also enhanced biosynthetic delivery kinetics of the apical protein influenza HA (118). However, in the studies reported here we found no effect on apical protein delivery in cells lacking OCRL1, although we did observe an increase in actin comets. PI5KIβ overexpression results in a considerably larger and statistically significant increase in cellular PIP_2 levels compared with OCRL1 knockdown, so it is possible that a threshold increase in PIP_2 is required to stimulate delivery kinetics detectably. Alternatively, the effects of PIP_2-stimulated HA delivery might not be linked directly to actin comet formation, although the selective modulation of HA delivery we observed upon PI5KIβ expression, inhibition of Arp2/3 activation (118), and N-WASP knockdown (Figure 3.3) would argue against this idea. Finally, actin comets stimulated by OCRL1 knockdown may emanate from sites distinct from those evoked upon PI5KIβ overexpression and may not propel apically-destined carriers.

Although we were unable to assess the effect of OCRL1 knockdown on megalin

biosynthetic traffic, we believe it unlikely that this pathway is affected by OCRL1 depletion. Like HA, a fraction of megalin has been reported to reside in glycolipid enriched microdomains, or lipid rafts (225), though it is not known whether the two take a similar biosynthetic route to the apical membrane. The stimulation in apical delivery we might predict in OCRL1-depleted cells (but did not observe for HA) would be expected to increase surface megalin levels and is intuitively inconsistent with a trafficking defect that would result in proteinuria. Importantly, we did not find any significant difference in the steady state level of mini-megalin at the cell surface of control vs. OCRL1-depleted cells as assessed by western blotting (data not shown).

3.3.3 OCRL1 knockdown does not disrupt megalin trafficking

OCRL1 knockdown did not affect megalin endocytosis as measured by either a biotinylated assay to detect receptor internalization or by following the fate of the radioiodinated ligand ^{125}I-Lf. The latter assay was performed using two model systems: polarized MDCK cells expressing a mini-megalin receptor and human proximal tubule cells that express endogenous megalin. Moreover, we found no effects of OCRL1 knockdown on ligand degradation when we monitored multiple rounds of uptake over a 14-18 h period. In contrast, we found that overexpression of PI5KIβ stimulated the rate of megalin endocytosis. Together, these results suggest the strong possibility that OCRL1 does not directly regulate megalin traffic or function along the endocytic pathway. Recent studies have demonstrated that OCRL1 binds directly to clathrin heavy chain and have observed a small fraction of cellular OCRL1 in association with clathrin coated vesicles (162,168,170,206). Our studies suggest

that the pool of protein associated with the cell surface and very early endocytic vesicles may not have a direct role in modulating endocytosis.

On the one hand, our observations are consistent with the prediction that increased cellular PIP_2 would not alter megalin traffic in a manner that would be expected to compromise low molecular weight protein uptake. On the other hand, the lack of effect of OCRL1 depletion on megalin traffic is somewhat surprising given that effects on endocytosis of fluid phase markers and megalin ligands have been reported in two CLC-5 knockout mouse models of Dent disease (17,213,218). A significant fraction of patients diagnosed with Dent disease have recently been shown to have mutations in OCRL1 rather than in CLC-5 (178), suggesting that the two proteins provide critical functions along the same pathway. There is a decrease in both the overall level and the apical concentration of megalin and cubulin in the proximal tubule of mouse CLC-5 knockouts that leads to a profound decrease in the endocytosis of megalin/cubulin ligands (213,218,219). This effect is not universal, as no defect in apical endocytosis or megalin function is observed in the thyroid of CLC-5 knockout mice (226,227). It is not yet clear how loss of CLC-5 leads to the observed decrease in megalin expression and the consequent low molecular weight proteinuria characteristic of Dent disease patients (214,215). Changes in megalin localization have not been observed in renal biopsies from human patients (228), although both Dent disease and Lowe syndrome patients shed significantly decreased levels of megalin into the urine (18). CLC-5 is largely localized to endocytic compartments and endosome acidification in proximal tubule cells cultured from CLC-5 deficient mice is

reported to be defective (229). A small fraction of CLC-5 also localizes to the cell surface and it has also been suggested that CLC-5 plays an important role in endocytosis at the plasma membrane (216). Importantly, while there is a clear inhibition in the accumulation of ligands and fluid phase markers in proximal tubule cells from CLC-5 knockout vs. control mice (17,219), it is not known whether the rate of endocytosis is affected. By analogy with our studies in OCRL1-depleted cells we predict that no change would be observed in endocytosis kinetics in renal epithelial cells. Unfortunately, we could not address this directly, as we were unable, using multiple approaches, to knock down CLC-5 in any of our renal epithelial cell lines.

3.3.4 OCRL1 knockdown enhances lysosomal enzyme secretion

Knockdown of OCRL1 perturbed lysosomal delivery of newly synthesized cathepsin D. This result is consistent with studies by Choudhury *et al*. demonstrating a partial shift in the steady state distribution of the cation-independent mannose 6-phosphate receptor from the TGN to endosomes in cells transfected with OCRL1 siRNA (168), as well as with the previous observation that Lowe syndrome patients have elevated serum levels of lysosomal hydrolases (222). This finding is also consistent with the primarily TGN/endosomal distribution of OCRL1.

How OCRL1 function regulates the sorting of lysosomal hydrolases is still unknown. OCRL1 interacts with numerous components of the machinery known to be involved in this process, including clathrin and several members of the rab GTPase family, however, there is no evidence that interaction with OCRL1 modulates the function of these proteins (168,230). A more tractable possibility that has been suggested is that

modulation of Golgi or endosomal PIP_2 levels by OCRL1 is important for the recruitment of adaptor proteins required for TGN to endosomal delivery (172). Alternatively, OCRL1 modulation of actin dynamics may be required for the sorting or delivery of lysosomally-destined cargos.

3.3.5 Summary

How does loss of OCRL1 activity lead to the renal manifestations observed in Lowe syndrome patients? Our results would suggest that OCRL1 does not directly modulate the trafficking or function of megalin. Although lysosomal hydrolases bind to and can be internalized by megalin (231), it is unlikely that the slight increase in enzyme secretion we observed would significantly impede megalin binding to other ligands. Together our results suggest that OCRL1 deficiency does not directly cause a defect in megalin trafficking or in the uptake or degradation of megalin ligands. Rather, we hypothesize that proteinuria is a downstream consequence that results from reduced levels of megalin in the renal proximal tubule of Lowe syndrome patients. We did not observe any difference in the binding or uptake of megalin ligands to HK-2 cells in which OCRL1 was acutely depleted compared with control cells, and speculate that the loss of megalin results from chronic alterations in cell signaling in renal cells lacking OCRL1. To this end, it is noteworthy that both OCRL1 and CLC-5 have been suggested to associate with macromolecular complexes that include megalin at the cell surface and that could be involved in cell signaling (170,216,232). Additionally, megalin has been reported to undergo intramembrane proteolysis that generates a tail-containing fragment able to enter the nucleus (8).

Similarly, APPL1 can translocate from endosomes to the nucleus in response to extracellular stimuli such as oxidative stress (233). Indeed, a more global response to loss of OCRL1 function is necessary to explain the other clinical abnormalities associated with Lowe syndrome. Future exploration of these possibilities will clearly be necessary to elucidate the pathway by which loss of OCRL1 function leads to renal disease in patients with Lowe syndrome. **

** Chapter three has been adapted from the published manuscript (174).

4.0 THE ROLE OF OCRL1 IN RENAL EPITHELIAL PRIMARY CILIA

4.1 INTRODUCTION

The three characteristic symptoms of Lowe syndrome are cataracts, mental retardation and renal proximal tubule dysfunction. Lowe patients are usually born with cataracts and develop mental and renal problems early in life (153). Typical renal symptoms include abnormal loss of low-molecular-weight proteins, bicarbonate, phosphate, excessive water and other nutrients (153). More than 120 mutations in *OCRL,* the disease gene, have been described in Lowe patients all over the world (234). Among these mutations, some completely abolish production of the OCRL1 protein while others compromise or eliminate the phosphatase activity or prevent OCRL1 from interacting with other cellular proteins (170,176,235). It has been suggested that these different classes of *OCRL* mutations explain why patients with Lowe syndrome have variable symptom severity.

OCRL1 is primarily localized to the *trans*-Golgi network, although it is also found on endosomal compartments and the plasma membrane (162,167-171). It exists as two splice isoforms termed a and b that differ by a single exon encoding 8 amino acids. The longer isoform a is the only isoform present in the brain while both isoforms are found in all other tissues (206). The OCRL1 protein used in the present study is isoform b, which is an 893-amino-acid protein consisting of a middle 5-phosphatase

domain and a C-terminal RhoGAP-like domain. The interacting proteins of OCRL1 include clathrin, alpha-adaptin, APPL1, Rac, Cdc42 and various Rab GTPases (162,166,170,206,230,235-238). The added 8 amino acids in isoform a are adjacent to one of the putative clathrin boxes [which are consensus five-residue clathrin-binding motifs (239)] and have recently been shown to potentiate clathrin binding over isoform b (206). Thus the two isoforms of OCRL1 may represent two functional pools of this enzyme that participate differentially in clathrin-mediated trafficking events such as endocytosis (206).

Recently a minor group of patients carrying *OCRL* mutations were shown to only develop renal tubular defects and have largely unaffected eyes and intelligence (175-178). Many of these patients were originally diagnosed with Dent disease, another X-linked recessive disorder manifested only by renal tubular dysfunction, and therefore referred to as the Dent 2 patients (175-178). Dent disease is caused by mutations in the gene *CLCN5*, which encodes a voltage-gated chloride/proton antiporter ClC-5. ClC-5 is involved in acidification of endosomes (179-181). Loss of ClC-5 function leads to abnormal pH inside endosomes which, in turn, affects receptor-mediated nutrient uptake by disrupting recycling of receptors, including the multiligand receptor megalin (17,18). This mechanism has been suggested as the pathological reason underlying the renal tubular dysfunction present in Dent patients (17,18). It is not known whether a similar mechanism is associated with Lowe syndrome or Dent 2 disease (although my data from chapter three argue against this possibility, as discussed below). Dent 2 patients do not carry mutations in the *CLCN5*

gene, however renal phenotypes of these patients more closely resemble those found in Dent patients than those in Lowe patients (for example, Dent 2 patients typically do not develop the characteristic Lowe phenotype systematic acidosis) (176). Interestingly, Dent 2 mutations of *OCRL* cluster into a distinct pattern readily distinguishable from the classical Lowe syndrome mutations (176). While all Dent 2 nonsense and frameshift mutations (which result in loss or disruption of large portions of the gene) are within the first 7 exons of the *OCRL* gene, all missense Dent 2 mutations occur in the 5-phosphatase domain spanning exons 9-15 (176). An alternative splice variant of OCRL1 that initiates after exon 7 (likely from a Met in exon 8) has been suggested to exist and partially compensate for loss of OCRL1 in Dent 2 patients with nonsense or frameshift *OCRL* mutations (176). This proposed OCRL1 variant, if verified by future studies, should partially account for the milder Dent 2 phenotypes compared with those found in Lowe patients (176). Interestingly, most known Lowe mutations are present after the *OCRL* exon 7, and presumably able to eliminate the compensatory effect of the hypothetical splice variant (176). How the phosphatase domain enriched missense mutations result in Dent 2 symptoms remains unclear (176).

Extensive studies have been focused on elucidating the pathogenesis of Lowe syndrome with little success so far. There is no mouse model for this disease because *OCRL* knockout mice are completely healthy due to the redundant activity of another PI 5-phosphatase INPP5B (173). This redundancy is absent in humans because of considerably lower INPP5B expression (173,174). Considering the

similarities in renal manifestations between Lowe syndrome and Dent disease (e.g., both Lowe and Dent patients develop low molecular weight proteinuria), our lab and other researchers have investigated the function and traffic of megalin using OCRL1 deficient cells or Lowe patient urine samples (18,174). Megalin is the major receptor responsible for low-molecular-weight protein reabsorption at the renal proximal tubules. Urinary lost of megalin ligands and decrease in megalin shedding have been reported for both Lowe and Dent patients (18,160,240). As mentioned above, megalin malfunction in Dent patients and CLC5 knockout mice has been suggested (17,18). However, our lab has shown that acute loss of OCRL1 mediated by RNAi in cultured dog and human renal epithelial cells does not affect megalin trafficking and ligand uptake (174). Whether chronic signaling defects due to OCRL1 loss-of-function could lead to megalin abnormality remains unclear.

The C-terminus of OCRL1 5-phosphatase domain contains an ASH domain, which is a recently identified conserved module present in a large family of proteins (182). Many ASH-containing proteins are associated with cilia, flagella and the centrosome, indicating the involvement of ASH domain in ciliary regulations and the roles of ASH family proteins in cilia function (182). Interestingly, many ciliopathies are characterized by symptoms in the eyes, the brain and the kidneys, the same organs affected by Lowe syndrome (21,33,34). In addition, OCRL1 has been reported to bind Rab8, a recycling endosome localized small GTPase required for BBsome functions (35,236). The BBsome has been shown to preferentially bind and be recruited to liposomal membranes by $PI(3,4)P_2$ (31). Notably, OCRL1 can hydrolyze PIP_3 to

generate $PI(3,4)P_2$ *in vitro* (never tested *in vivo*) (188,241). Moreover, PIP_3 was recently found to be enriched in recycling endosomes in renal epithelial cells (188,241). These pieces of evidence suggest a possible role of OCRL1 in ciliary functions and a hypothetical involvement of OCRL1 in $PI(3,4)P_2$ mediated recruitment as well as in Rab8 dependent activities of the BBsome on recycling endosomes. Recently, another PI 5-phosphatase, INPP5E, has been implicated in multiple ciliopathies (29,30). Loss of INPP5E function (in knockout animals) causes embryonic or neonatal death in mice (29). The developing kidneys in the mutant mouse embryos contain multiple cysts in which epithelial cells have been found with primary cilia with abnormally dilated ends (29). The relationship between OCRL1 and ciliary pathways has never been addressed. In the studies described here, I used MDCK cells as the model system to investigate the effect of acute OCRL1 loss-of-function on primary cilia morphology. My results indicate that OCRL1 is involved in regulation of kidney epithelial primary cilia length. Studies of other lab members suggest that OCRL1 also regulates lumen formation when MDCK cells are cultured as 3D cysts. Together, our results suggest a novel hypothesis for the renal pathogenesis of Lowe syndrome and for the first time describe a relationship between OCRL1 loss-of-function and ciliopathies.

4.2 RESULTS

4.2.1 Acute depletion of OCRL1 results in elongated primary cilia in MDCK cells

As mentioned above, MDCK cells elaborate single non-motile primary cilia that

protrude from their apical domains. In the present study, cultured type II MDCK cells are used as a model to study kidney tubular epithelial functions. Similar to the ones found on renal epithelial cells *in vivo*, primary cilia of MDCK cells are able to respond to fluid change and produce Ca^{2+} mediated signals (41). After knocking down OCRL1 in polarized MDCK cells grown (for 4-5 days) on permeable filter supports, I imaged the cellular cilia and discovered that these cells had longer primary cilia compared to control cells treated with the firefly luciferase siRNA. Figure 4.1A shows representative XY fields of MDCK cell monolayers where primary cilia are visualized using an anti-acetylated tubulin antibody. Interestingly, in both control and OCRL1 knockdown cell images, the primary cilia observed are not of uniform length. Most cilia appear short and look like 'little dots' while a few longer ones can occasionally be seen. In every experiment, lengths of >100 cilia were randomly quantitated for each siRNA treatment using Volocity software and the data were plotted as length versus percentile. From >10 independent experiments, the cilia in OCRL1 knockdown cells were consistently longer than in control cells. Figure 4.1B shows the graph from one representative experiment. The difference in cilia length between control siRNA and OCRL1 siRNA treated MDCK cells is statistically significant ($P<0.001$ by Mann-Whitney rank sum test).

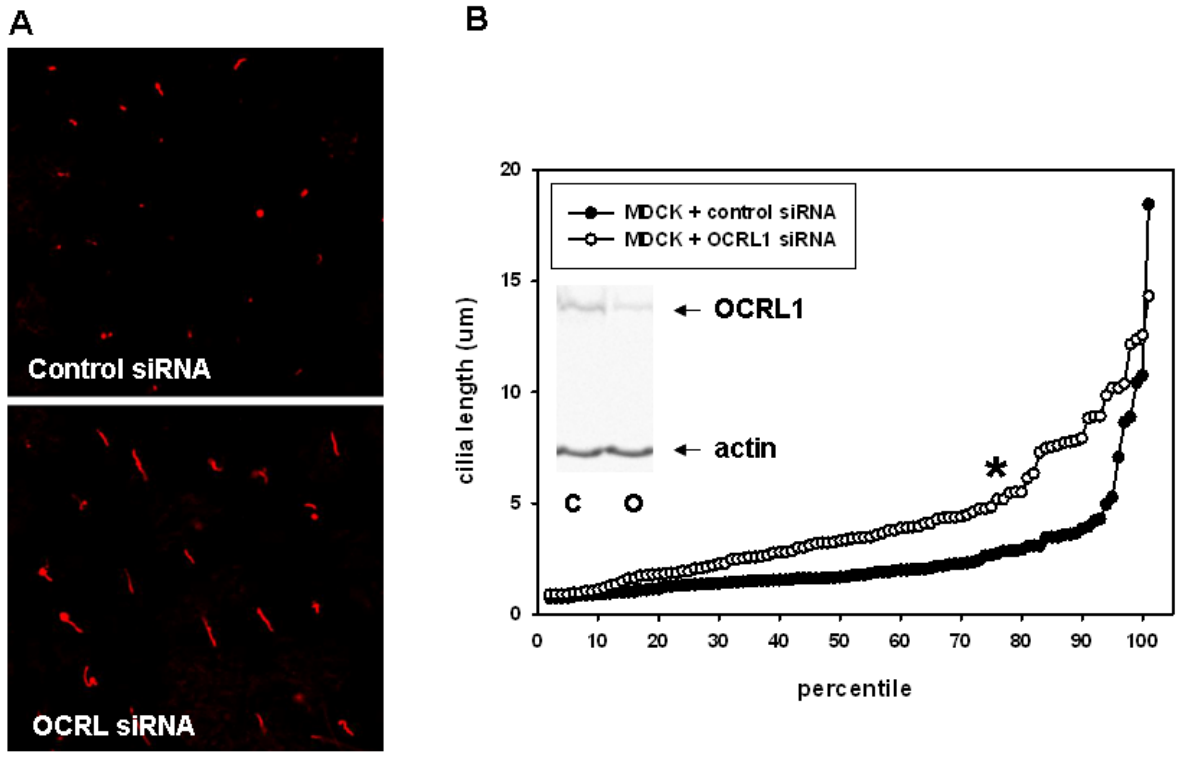

Figure 4.1 SiRNA-mediated OCRL1 knockdown results in elongated primary cilia on polarized MDCK cells. A: representative XY images of MDCK monolayers four days after treated with control or OCRL1 siRNA and subjected to immunofluorescence. Red: acetylated tubulin. B is a distribution graph from a single representative experiment comparing length distributions of primary cilia on MDCK cells treated with different siRNAs. Lengths of >100 cilia in random fields were measured for each treatment. * $P<0.001$ by Mann-Whitney rank sum test. Similar results were seen in >10 independent experiments. The inset of the graph shows the Western blotting result of the same experiment to determine OCRL1 knockdown efficiency (74.8%). C: control siRNA; O: OCRL1 siRNA.

4.2.2 OCRL1-depleted MDCK cells have morphologically normal primary cilia

To examine the morphology of cilia in OCRL1 knockdown versus control cells, I performed scanning electronic microscopy on 5-day filter-grown MDCK cells treated with either OCRL1 or control siRNA in the imaging core of the Pittsburgh Center for Kidney Research (PCKR) with the help of Dr. Gerard Apodaca and Mr. Wily Giovanni Ruiz. Figure 4.2 shows representative SEM images of primary cilia on cells under different treatments. OCRL1 knockdown in polarized MDCK cells did not appear to cause morphological abnormalities in primary cilia. Notably, those MDCK primary cilia discernable by SEM are almost always the longer ones (mostly ≥ 5 μm) and are present only on a minor group of cells. The shorter ones (with lengths < 5 μm), which represent the majority of MDCK cilia population (as manifested by the immunofluorescence studies), are largely not identifiable possibly due to camouflage from the dense apical microvilli (visible in Figure 4.2). Interestingly, MDCK cells treated with OCRL1 siRNA appeared to have more visible cilia compared to cells treated with the control siRNA when imaged by SEM. This is consistent with our quantitation (Figure 4.1) suggesting that OCRL1 knockdown results in overall longer primary cilia in MDCK cells.

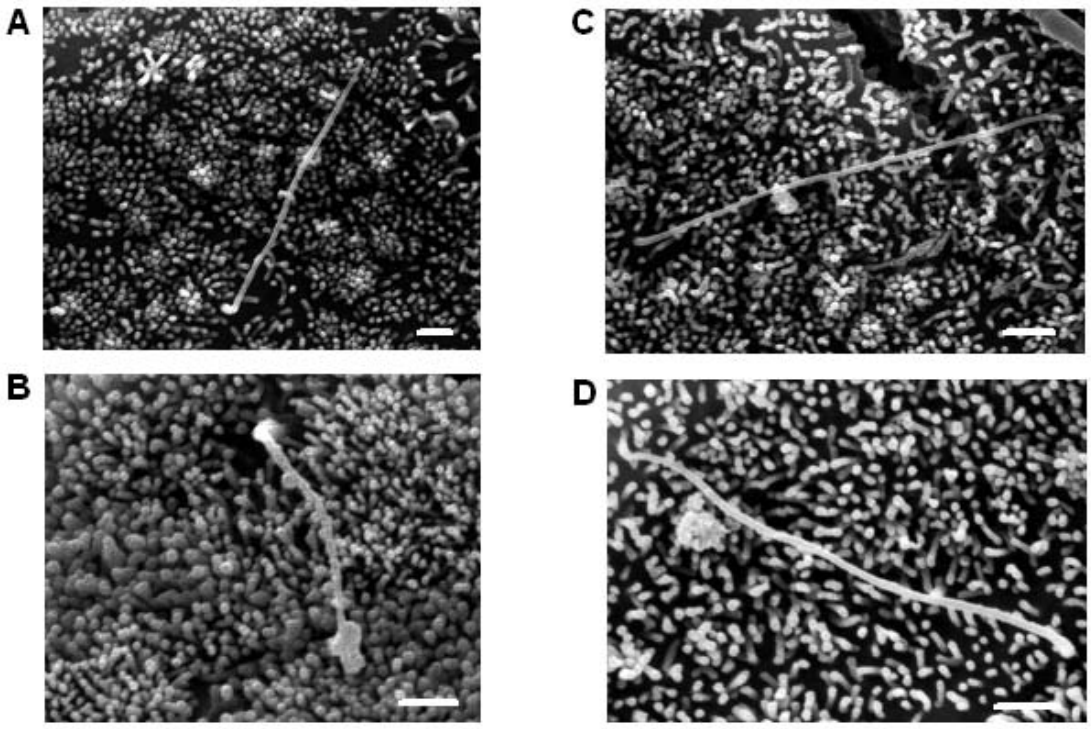

Figure 4.2 MDCK cells with OCRL1 knockdown have morphologically normal primary cilia. SEM images of primary cilia on cells five days after treated with control (A and B) or OCRL1 (C and D) siRNA are shown. Scale bar: one μm

4.2.3 Exogenous wildtype OCRL1 is able to restore normal cilia length in MDCK cells depleted of the endogenous OCRL1

To test whether the cilia length alteration observed was a specific effect of OCRL1 loss-of-function, I designed an N-terminal-GFP tagged siRNA resistant OCRL1 construct (GFP-R-OCRL1) using the pEGFP-C1 vector (Kanr/Neor). If the cilia phenotype was indeed a result of losing endogenous OCRL1, expressing the siRNA-resistant protein should be able to reverse it. When transiently expressed in BSC-1 cells (which are large flat epithelial cells well suited to fluorescence studies) by transfection, GFP-R-OCRL1 correctly localized to the Golgi ribbon (as marked by Giantin) as well as to cytoplasmic puncta partially overlapping with EEA1 (the early endosomal marker) (Figure 4.3A). I then generated MDCK cell lines stably expressing GFP-R-OCRL1 as well as other constructs discussed below. Figure 4.3B,C show data from a representative experiment (from three independent experiments) using MDCK and MDCK GFP-R-OCRL1 stable cells. As in my previous experiments (Figure 4.1), OCRL1 siRNA treatment elongated the primary cilia on MDCK cells ($P<0.001$). When GFP-R-OCRL1 was stably expressed in MDCK cells treated with OCRL1 siRNA, normal cilia length in GFP-positive cells was restored. The cilia-shortening effect of GFP-R-OCRL1 in MDCK cells treated with OCRL1 siRNA is statistically significant ($P<0.001$). The expression of GFP-R-OCRL1 is not affected by OCRL1 siRNA (Figure 4.3B). Similar results were obtained using mixed stable MDCK lines (in which there is a large variation in construct expression level among the different expressing cells) and clonal stable cell lines (in which the single-cell

expression levels are relatively homogeneous and moderate). The effect of GFP-R-OCRL1 expression on primary cilia length of MDCK cells treated with the control siRNA (without OCRL1 knockdown) varied between experiments (data not shown). Future studies are needed to address whether OCRL1 overexpression affects primary cilia length.

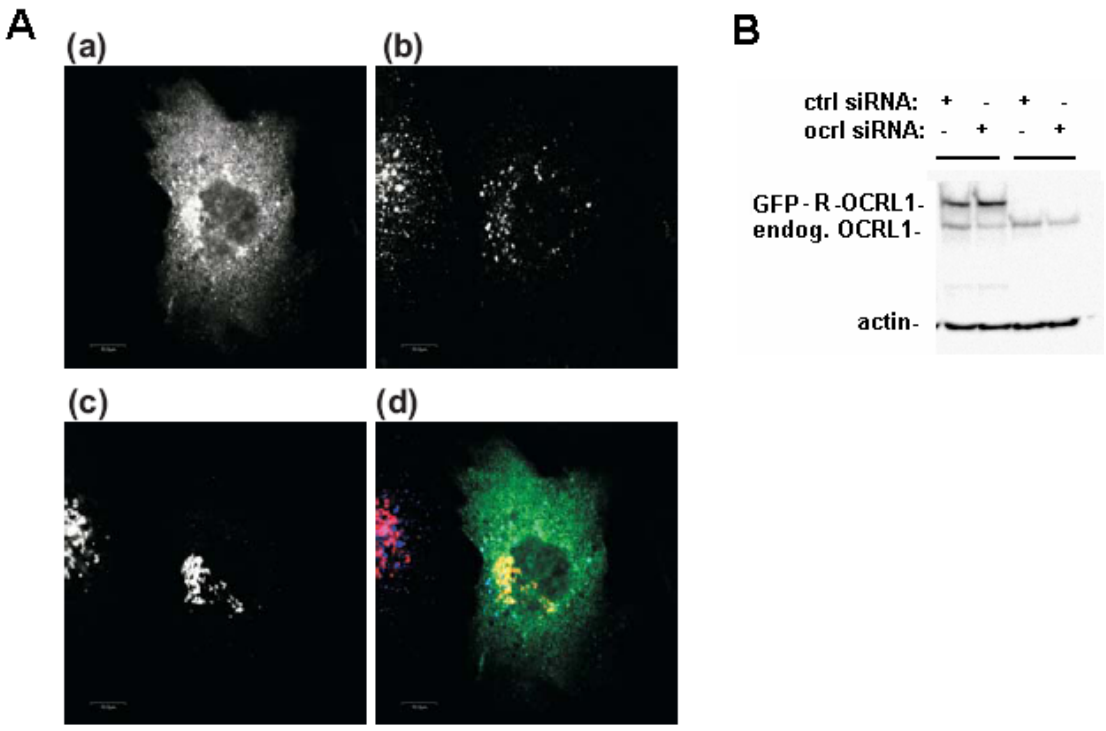
A
(a)
(b)
(c)
(d)
B
ctrl siRNA: + - + -
ocrl siRNA: - + - +
GFP-R-OCRL1-
endog. OCRL1-
actin-

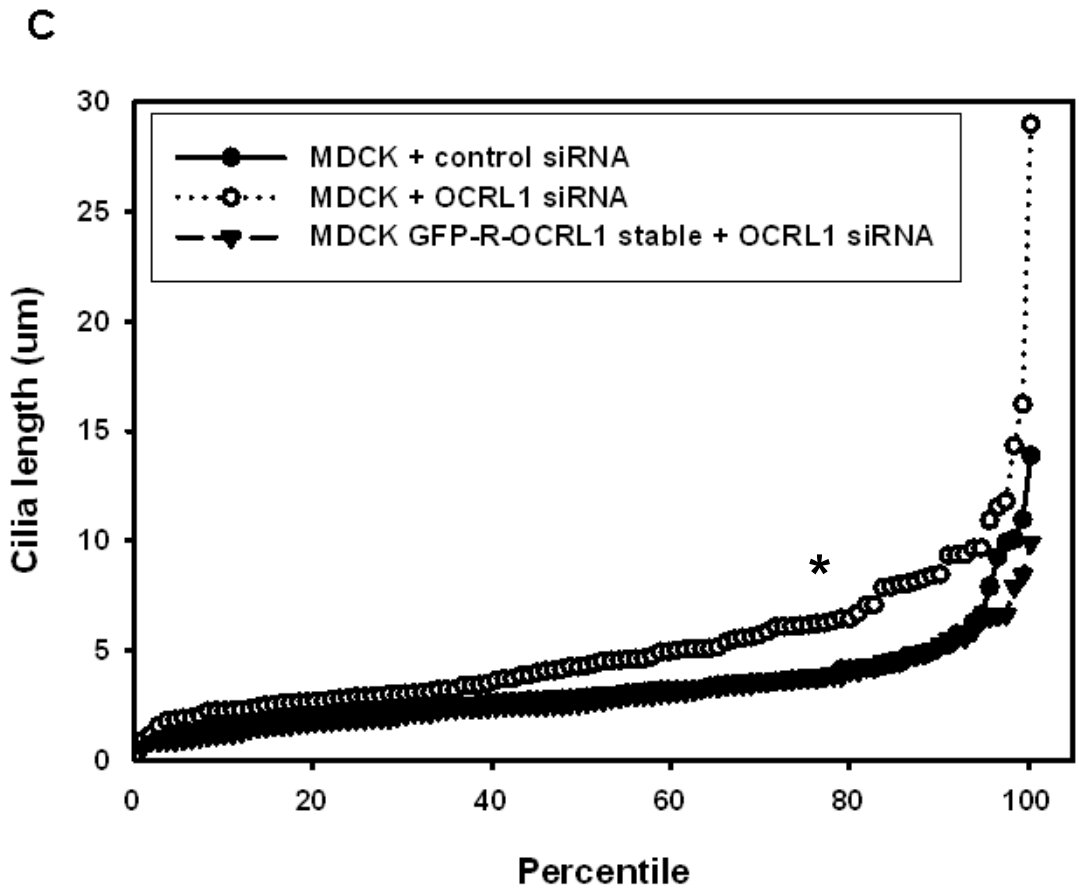
C
MDCK + control siRNA
MDCK + OCRL1 siRNA
MDCK GFP-R-OCRL1 stable + OCRL1 siRNA
Cilia length (um)
Percentile
0
5
10
15
20
25
30
0
20
40
60
80
100
*

Figure 4.3 Exogenously expressed siRNA-resistant wildtype OCRL1 is able to restore normal cilia length in MDCK cells treated with OCRL1 siRNA. A: confocal XY images showing localization of GFP-R-OCRL1 in BSC-1 cells determined by immunofluorescence. (a) GFP; (b) EEA-1; (c); Giantin; (d) merge. Scale bar: 10μm. B: Western blotting to determine knockdown efficiencies of endogenous OCRL1 (54.9% and 52.4% for the parental MDCK (right two lanes) and the MDCK stable line respectively) in the experiment shown in C. Note that siRNA only reduces expression of the endogenous OCRL1, not the GFP tagged exogenous OCRL1. C: Results of one representative experiment showing primary cilia length distributions of MDCK cells treated differently as labeled and processed for immunofluorescence. * $P<0.001$ by Mann-Whitney rank sum test. Similar results were seen in three independent experiments.

4.2.4 Two exogenously expressed OCRL1 point mutants are able to restore normal cilia length in MDCK cells depleted of the endogenous OCRL1

To understand which domain(s) of OCRL1 is responsible for the cilia lengthening effect, I introduced point mutations into GFP-R-OCRL1 and determined the abilities of different mutants to rescue the cilia elongation caused by OCRL1 siRNA. The mutated amino acids are depicted in Figure 1.3. Figure 4.4 shows the result of one mutant, GFP-R-OCRL1 G304E, from a representative experiment of > three total experiments. G304E is a Dent II mutation found in the catalytic domain of OCRL1 and has been predicted to disrupt the phosphatase activity of OCRL1 (176). As shown in Figure 4.4A, the localization pattern of GFP-R-OCRL1 G304E in BSC-1 cells is similar to that of the wildtype protein. Curiously, expression of GFP-R-OCRL1 G304E still restored normal cilia length in MDCK cells treated with OCRL1 siRNA in three independent experiments. Results of one representative experiment are shown in Figure 4.4B,C; the cilia shortening effect of GFP-R-OCRL1 G304E is statistically significant ($P<0.001$). Therefore, the 5-phosphatase activity may not be required for the cilia related functions of OCRL1.

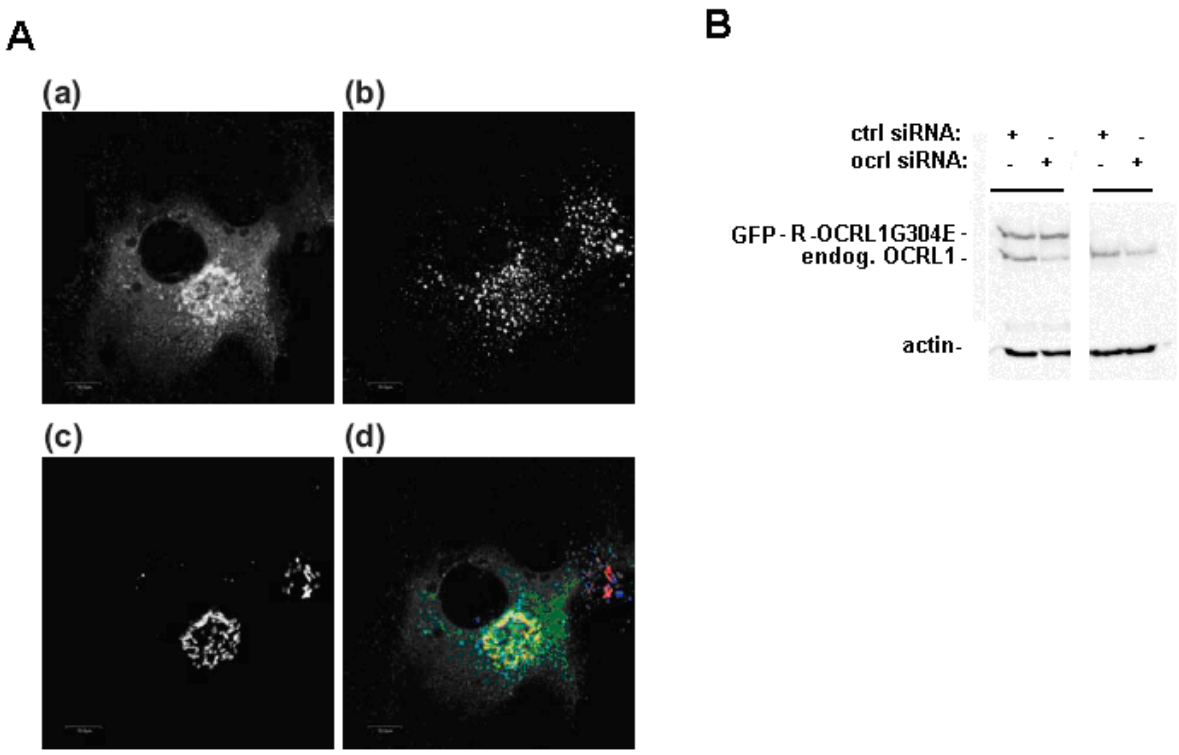
A
(a)
(b)
(c)
(d)
B
ctrl siRNA: + - + -
ocrl siRNA: - + - +
GFP-R-OCRL1G304E -
endog. OCRL1 -
actin-

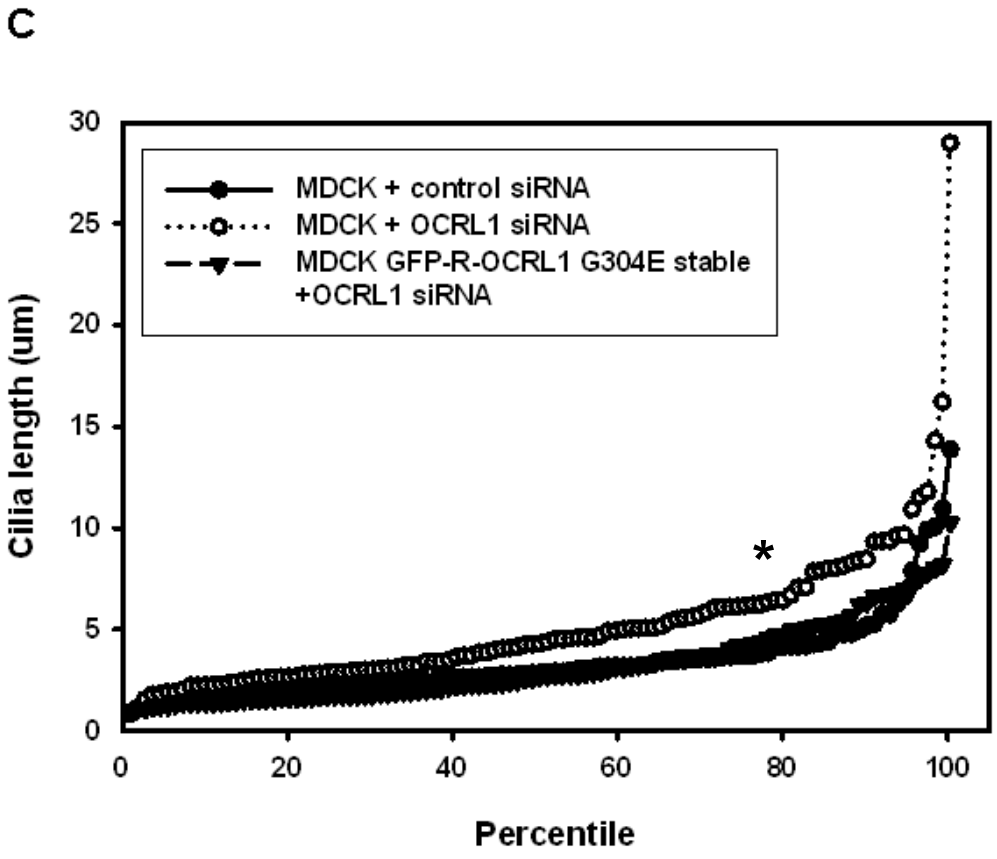
C
MDCK + control siRNA
MDCK + OCRL1 siRNA
MDCK GFP-R-OCRL1 G304E stable
+OCRL1 siRNA
Cilia length (um)
Percentile
0
5
10
15
20
25
30
0
20
40
60
80
100
*

Figure 4.4 Exogenously expressed siRNA-resistant OCRL1 G304E mutant is able to restore normal cilia length in MDCK cells treated with OCRL1 siRNA. A: confocal XY images showing localization of GFP-R-OCRL1 G304E in BSC-1 cells determined by immunofluorescence. (a) GFP; (b) EEA-1; (c); Giantin; (d) merge. Scale bar: 10μm. B: Western blotting to determine knockdown efficiencies of endogenous OCRL1 (54.9% and 49.4% for the parental MDCK (right two lanes) and the MDCK stable line respectively) in the experiment shown in C. Note that siRNA only reduces expression of the endogenous OCRL1, not the GFP tagged exogenous OCRL1 G304E. C: Results of one representative experiment showing primary cilia length distributions of MDCK cells treated differently as labeled and processed for immunofluorescence. * $P<0.001$ by Mann-Whitney rank sum test. Similar results were seen in three independent experiments.

The C-terminal ASH domain of OCRL1 lies between amino acids 570 and 676 (182). Many ASH domain proteins are associated with cilia, making this domain a good candidate for a cilia regulating moiety. Deletion of E585 (within the ASH domain) is a Lowe syndrome mutation that has been shown to eliminate the interaction between OCRL1 and the endosomal adaptor protein APPL1 [(170,235), Figure 1.3]. This point mutation also reduces binding capacity of OCRL1 to the early endosomal marker Rab5 small GTPase (which interacts with APPL1) (170,235,242). I made the DNA construct encoding GFP-R-OCRL1 ΔE585 and expressed the mutant in BSC-1 cells. As shown in Figure 4.5A, unlike the wildtype protein, GFP-R-OCRL1 ΔE585 is largely cytosolic with dramatically reduced Golgi and endosomal association. This cellular localization pattern is consistent with what has been reported before (170,235). I generated a MDCK stable cell line expressing the mutant GFP-R-OCRL1 ΔE585 and repeated the rescue experiment described above using this stable line and a control parental MDCK cell line. Data from three independent experiments indicate that GFP-R-OCRL1 ΔE585 expression reverses the primary cilia elongation on OCRL1 siRNA treated MDCK cells. Results from one representative experiment are shown in Figure 4.5B,C (the cilia shortening effect of GFP-R-OCRL1 ΔE585 in OCRL1 siRNA treated MDCK cells is statistically significant; $P<0.001$). The relatively low level of detectable ΔE585 mutant in Western blots, compared with other GFP-R OCRL1 proteins, reflects the fact that relatively few cells in the stable cell line expressed the heterologous protein.

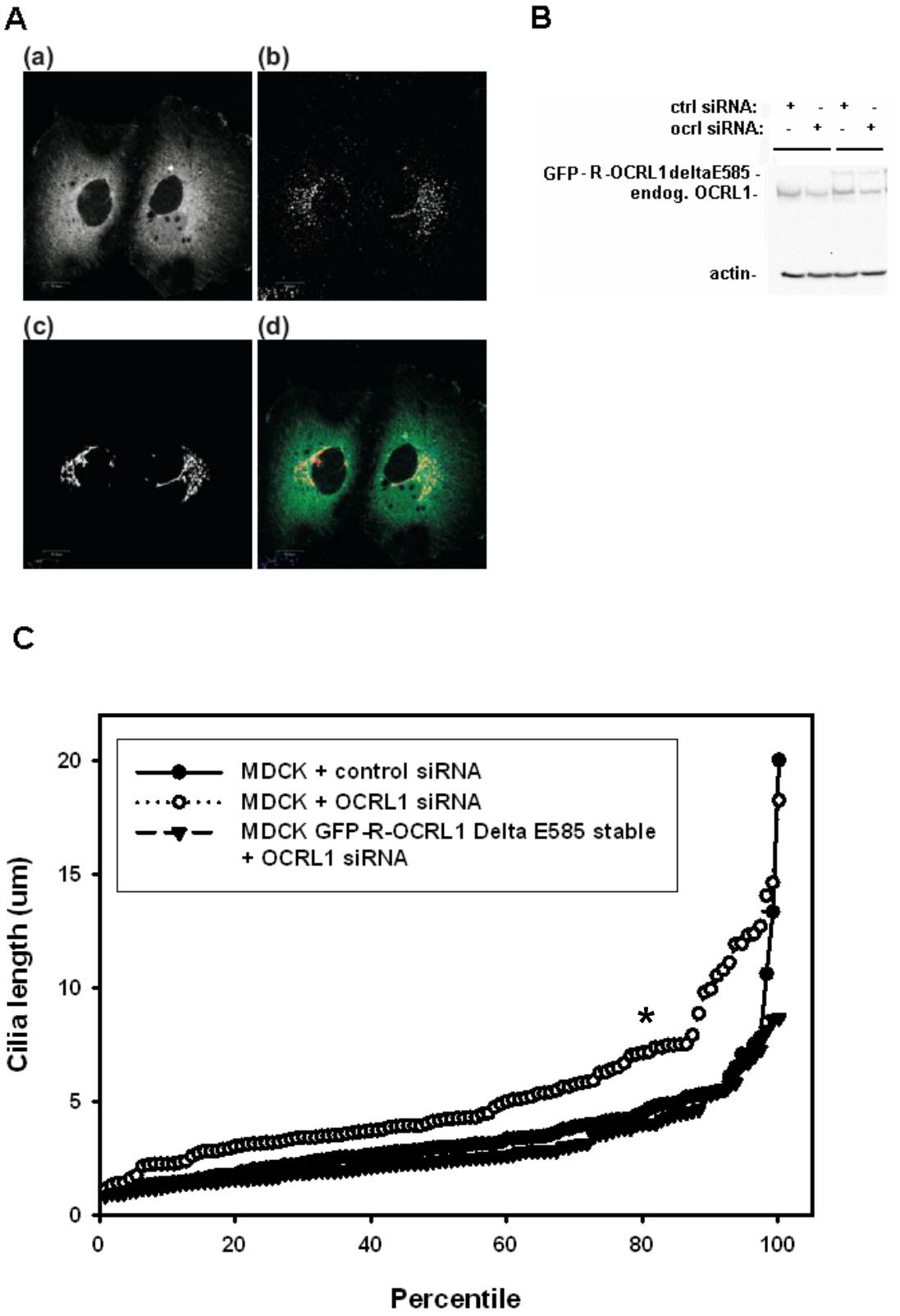

Figure 4.5 Exogenously expressed siRNA-resistant OCRL1 ΔE585 mutant is able to restore normal cilia length in MDCK cells treated with OCRL1 siRNA. A:

confocal XY images showing localization of GFP-R-OCRL1 ΔE585 in BSC-1 cells determined by immunofluorescence. (a) GFP; (b) EEA-1; (c); Giantin; (d) merge. Scale bar: 10μm. B: Western blotting to determine knockdown efficiencies of endogenous OCRL1 (48.8% and 57.6% for the parental MDCK (left two lanes) and the MDCK stable line respectively) in the experiment shown in C. Note that siRNA only reduces expression of the endogenous OCRL1, not the GFP tagged exogenous OCRL1 ΔE585. C: Results of one representative experiment showing primary cilia length distributions of MDCK cells treated differently as labeled and processed for immunofluorescence. * $P<0.001$ by Mann-Whitney rank sum test. Similar results were seen in three independent experiments.

4.2.5 OCRL1 depletion does not have any effect on primary cilia length of human skin fibroblasts

As a cell type control, I knocked down OCRL1 in human skin fibroblasts by Amaxa electroporation. From one experiment in which the knockdown was >90% (Figure 4.6A), no difference in cilia length was observed between control and OCRL1 knockdown cells (Figure 4.6B). This result indicates that the cilia effect I have observed is cell-type specific, which is consistent with the fact that the Lowe syndrome only affects selected organs and that skin function is not affected by this disease.

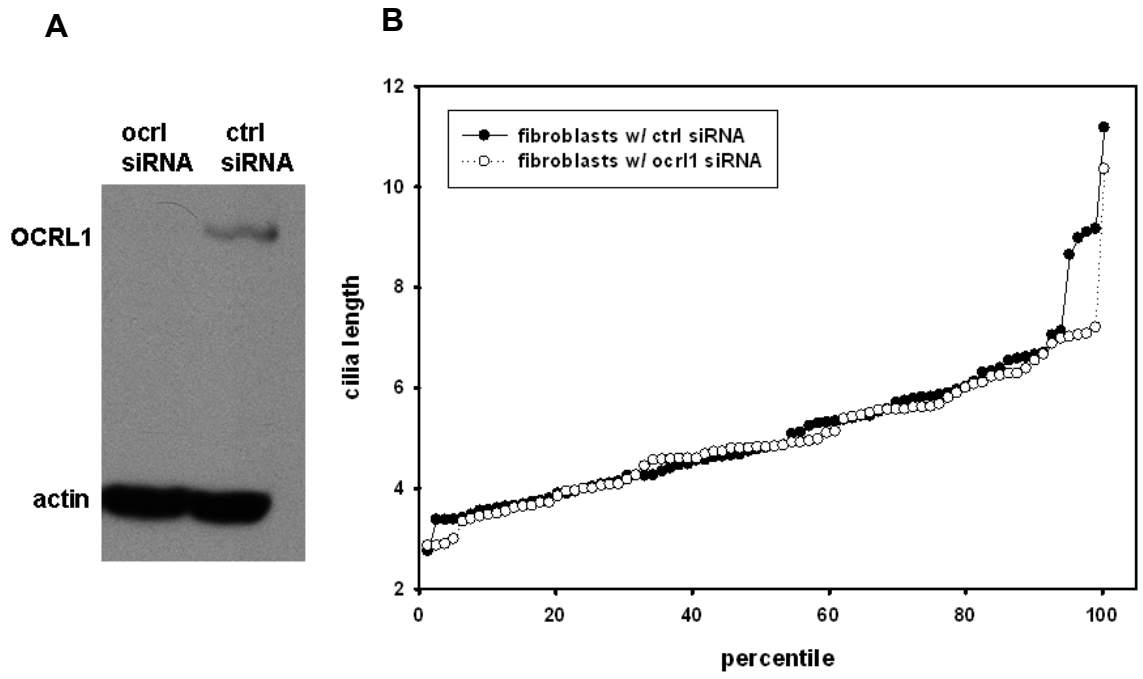

Figure 4.6 SiRNA-mediated OCRL1 knockdown does not affect lengths of primary cilia on human skin fibroblasts. A: Western blotting to determine OCRL1 knockdown efficiency. Human skin fibroblasts were treated with control or OCRL1 siRNA by nucleofection, let recovered for one day, serum starved for three days, and subjected to Western blotting or immunofluorescence staining for acetylated tubulin. B is a distribution graph from a single representative experiment comparing length distributions of cells treated with different siRNAs. Lengths of >100 cilia in random fields were measured for each treatment.

4.3 DISCUSSION

Lowe syndrome is an early-onset multi-organ disorder severely affecting lives of the patients and their family. Since its identification in 1952 (146), people have been trying to find ways to prevent and/or cure this genetic disease, however with limited success. Based on the very dramatic renal symptoms indicating tubular dysfunction and disrupted reabsorption, most studies have so far been focusing on receptor-mediated endocytosis and recycling events in the renal proximal tubule epithelium. However while a pathogenic mechanism involving megalin malfunction has been supported by various evidence from studies on another renal tubular disorder Dent disease (17,18), similar mechanisms remain hypothetical for Lowe syndrome and was argued against by my recent studies using renal epithelial cells with acute OCRL1 depletion [(174); also see chapter three]. Here I have reported a novel function of OCRL1, the Lowe disease protein, in modulating renal epithelial primary cilia length. Given the fact that ciliopathies preferentially affect the kidneys as well as other Lowe syndrome involved organs (21,33,34) and that mutations in another PI phosphatase (INPP5E) have been linked to cilia abnormalities (29,30), my study potentially presents a new possibility for future research on Lowe syndrome and other PI/PIP related diseases.

4.3.1 Relationship between Lowe syndrome and known ciliopathies affecting renal cilia length

In the present study, I have shown that acute RNAi mediated OCRL1 knockdown caused an increase in the overall primary cilia length of cultured polarized MDCK

cells. The (filter-grown) cells imaged were all at the quiescent state, as manifested by nucleus staining (data not shown). Therefore the different cilia length distributions observed were not simply due to distinct cell cycle states. MDCK cilia elongation was a specific effect of OCRL1 knockdown because expression of an siRNA-resistant OCRL1 was able to rescue the phenotype. As mentioned above, the primary cilia on MDCK monolayers resemble intrinsic renal tubular cilia in many aspects, including sensing apical flow changes and initiating Ca^{2+} based signaling cascades (41). Therefore, the cilia related effects I have observed in MDCK cells might resemble the situation *in vivo* and could be indicative of the renal cellular defects associated with OCRL1 mutations in Lowe patients.

Changes in renal cilia length have been documented for various genetic disorders (ciliopathies) including polycystic kidney diseases (PKD), Bardet-Biedl syndrome (BBS), Meckel syndrome (MKS) and others (28,243-251). Mutated genes in these diseases almost always encode cilia resident proteins or regulators of cilia assembly. Variation in cilia length can happen simultaneously in multiple renal tubular segments along the nephron and can also be found in other organs like the pancreas and the liver (247,248,250). Aberrant decrease in cilia length is the dominant phenotype found in ciliopathies affecting the kidneys. Literature indicates that shortening or absence of renal primary cilia has often been attributed to loss of critical factors participating in cilia assembly, maintenance and/or signaling. These factors include IFT proteins [for example Tg737/IFT88, (252)], fibrocystin [the large transmembrane ciliary protein suggested to cooperate with polycystin-2 in the Ca^{2+} signaling;

(253,254)] and kinesins [for example the KIF3A subunit of kinesin-II, the anterograde IFT motor; (244)]. Most of the cilia-eliminating defects result in abnormal cyst formation via mechanisms still under debate (21,244,252-254). Renal cilia lengthening is less frequently observed, compared to cilia shortening, and has been associated with diseases caused by mutations of genes including *MKS3, NPHP3, NEK8* and *BBS4* (28,243,245,246,249). These genes encode protein products with various functions critical for processes ranging from ciliogenesis to cilia related regulation of embryonic development (28,243,245,246,249). How mutations of these genes result in the increase of cilia length remain unknown.

Renal manifestations of the reported cilia elongating diseases (similar to those of the cilia shortening disorders) most often include cystic dysplasia to variable extents (28,243,245,246,249). This is not in line with the cyst-free renal phenotypes of Lowe syndrome. However, at least in the case of *NPHP3* [whose protein product nephrocystin-3 interacts with the ciliary protein inversin and participates in the crucial regulation of both canonical and non-canonical (planar cell polarity or PCP) Wnt signaling cascades during development], selected hypomorphic alleles result in alleviated later-onset (adolescent) nephronophthisis phenotypes including renal tubular atrophy, sclerosis, interstitial fibrosis and renal epithelial basement membrane anomalies with very limited cyst formation (245,246,255). These milder renal phenotypes appear similar to those found in Lowe patients, although comprehensive pathological assessments are needed to compare symptoms of these two disorders in details. If comparable renal manifestations can be verified between Lowe

syndrome and adolescent nephronophthisis, it should suggest that OCRL1 and nephrocystin-3 might participate in the same pathway during developmental regulation.

Genetically heterogeneous PKD disorders (including various forms of nephronophthisis) have long been considered as a group and often studied separately from other renal dysfunctions. It will be interesting if a common pathogenetic mechanism can be identified for both a PKD, like the *NPHP3* defects, and a non-cystic renal disease, like Lowe syndrome. One piece of evidence supporting a role of OCRL1 in embryonic development came from the observation that 20- and 24-week human fetuses with Lowe syndrome developed ocular lens problems/cataracts (153,155). In accordance with this hypothesis, our lab is collaborating with Dr. Neil Hukriede at the PCKR Model Organisms Core (Core D) to examine the effect of OCRL1 loss-of-function on embryonic development of zebrafish *Danio rerio*. This work is being performed by Di Mo in the lab. Preliminary data indicate that OCRL1 expresses early in zebrafish embryos and that knockdown of OCRL1 using a translation-blocking morpholino results in aberrant early development manifested by body axis curvature, hydrocephaly, cardiac edema, smaller eyes, damaged renal clearance and possibly decreased cilia number, consistent with defects in ciliary functions. The zebrafish model has been used successfully in the study of PKDs to identify novel genes related to cystic kidneys (256). Further research on the OCRL1 deficient zebrafish will allow us to evaluate whether it is a viable animal model to study Lowe syndrome.

4.3.2 Lessons from studies on kidney injury and healing

Studies from the Deane lab in Australia have suggested a linkage between renal tubular primary cilia length and renal injuries (257-259). In one study, after introducing an ischemia-reperfusion or a ureteral obstruction injury into the mouse kidneys, they observed an initial decrease of cilia length in multiple tubular segments on the first couple of days post-injury and a subsequent increase of cilia length which clearly surpassed that of the control kidney by day 4-7 post-injury (258). The cilia lengthening phenotype on day 7 post-injury was characterized by an overall shift of the cilia length distribution, resembling what I have seen with the MDCK cells treated with OCRL1 siRNA and returned to culture for 4-5 days. The similar manifestations and time frame suggest the possibility that a common cellular pathway was perturbed by either certain types of renal injuries or OCRL1 loss-of-function. The identity of that pathway is currently unknown and the authors found that day-to-day expression of ciliary proteins PC1, PC2, inversin and IFT52 did not correspond to the change in renal tubular primary cilia length (258). In a separate paper from the same group, the authors showed that the increased cilia length on renal tubules one week after injury retrieved during the later repair process and appeared completely normal six weeks post-injury (257). Due to the limits of cell culture (cells normally become too confluent and undergo apoptosis before siRNAs lose their effects), I was not able to perform similar experiments to look at possible ciliary recovery upon disappearance of OCRL1 knockdown. The correspondence between renal tubular cilia length and the kidney injury/repair status indicates that adjustment of cilia length may represent a cellular

response to renal damage. In the case of Lowe syndrome, chronic loss of OCRL1 possibly imposes a continued stress on the renal tubules and forces the cells to respond by changing cilia length and maybe functioning mode as well. Understanding the cellular mechanism underlying this effect will greatly enhance our knowledge on Lowe syndrome and benefit the therapeutic effort to treat this severe disease.

4.3.3 Elongated primary cilia on OCRL1 depleted MDCK cells are morphologically normal

Under SEM, the structural features of primary cilia on MDCK monolayers treated with OCRL1 siRNA appeared normal compared to control cells. This observation is not surprising because, as reported with the *BBS4*$^{-/-}$ mouse model in which renal tubular primary cilia elongates with normal basal body and axonemal structures (249), changes in cilia length are not necessarily accompanied by structural variations. It seems that ciliary length and shape/structure are differentially regulated by separate groups of cellular proteins. In the case of INPP5E defects, it is currently unknown what mechanism underlies the dilated cilia tips. It could be due to abnormally accumulated and/or structured axonemal materials, pathologically bulged cilia membrane, or even both. Further research is needed to elucidate these mysteries and better explain the coordinated cellular controls over cilia length and shape.

Interestingly, when renal tubular epithelial primary cultures from control and the *BBS4*$^{-/-}$ mice were monitored for cilia growth, those cilia on *BBS4*$^{-/-}$ cells grew more slowly than the wildtype control but ended up longer after a prolonged growth time period (249). This result indicates that certain genetic defects can compromise, but

not abolish, cilia assembly while shifting the growth/turnover equilibrium at the same time. The shifted control of cilia length can potentially be a spontaneous cellular compensating response to reduced ciliary growth rate, although solid evidence is needed to test this possibility. Youssef Rbaibi in the lab is currently measuring the primary cilia re-growth rates on control and OCRL1 depleted MDCK cells upon chemically-induced acute deciliation. It will be very interesting if OCRL1 knockdown results in any change in the rate of *de novo* ciliogenesis on polarized MDCK cells.

4.3.4 Ciliary Ca^{2+} signaling

By growing cells in the 3D Matrigel culture, Youssef Rbaibi in my lab has shown that OCRL1 knockdown also elongates primary cilia on MDCK cells grown as cysts, a condition more closely resembles the renal tubules *in vivo*, Interestingly, he has also discovered that OCRL1 loss-of-function affects cyst morphology and lumen formation, resulting in significantly higher-than-control percentages of cysts with multiple lumens or a filled lumen. Since blunted Ca^{2+} signaling has been linked to changes in the renal tubule morphology in PKDs (20,254,260), our lab is collaborating with Dr. Lisa Satlin and Dr. Rajeev Rohatji at Mount Sinai School of Medicine to measure the Ca^{2+} mediated signaling intensity in control and OCRL1 depleted MDCK cells responding to flow changes. If impaired Ca^{2+} signaling is associated with loss of OCRL1, it may explain the cilia lengthening phenotype in OCRL1 knockdown MDCK cells grown flat and as cysts as well as the observed defects in cyst morphology.

4.3.5 Three possible ciliary roles of OCRL1

What is the possible mechanism of MDCK cilia elongation upon OCRL1 RNAi? OCRL1 does not localize to primary cilia or basal bodies, indicating that it is probably not directly involved in cellular processes happening within cilia. The MKS phenotypes (observed in the *wpk*/MKS3 rat model, MKS human patients as well as MKS1/3 protein knockdown cells) including multi-ciliated renal tubular cells and over-duplicated centrosomes were never observed in my experiments, suggesting that OCRL1 is most likely not involved in cell cycle control or centrosome-mediated initiation of cilia nucleation. As a cytosolic protein, OCRL1 is recruited to cellular membranes by binding to adaptor proteins like APPL1 and Rab5 (170,235). Its correct localization is crucial to its cellular functions because ΔE585, a point mutation outside of the catalytic domain and disrupting the endosomal localization of OCRL1, results in Lowe syndrome (170,235). All known cellular roles of OCRL1 are based on its phosphatase activity and involved in membrane traffic at the TGN and plasma membrane. It preferentially hydrolyzes the D-5 phosphate on PIP_2, although a long wondered question is why the bulk of cellular OCRL1 does not colocalize with the major PIP_2 population at the cell surface. Considering the novel ciliary function of OCRL1 suggested by data from our lab, it is likely that OCRL1 is responsible for regulating PIP_2 and other lipid species at various cellular locations where proteins involved in ciliary pathways are recruited to by interacting with those lipids. According to our current knowledge, three ciliary events are good candidates for the proposed OCRL1 involvement.

First, primary cilia are important regulators of a variety of signaling events during development, including canonical and non-canonical (PCP) Wnt signaling cascades. Many ciliary proteins, including inversin, nephrocystin-3, KIF3A and BBS proteins, can act as “molecular switches” that maintain a balance between the two types of Wnt signaling by potentiating the PCP pathway (261). This effect often involves controlling the membrane versus cytosolic localization of PCP proteins like disheveled (Dvl) (261). Changes in subcellular localization of PCP proteins can potentially be achieved by enzyme (for example OCRL1) -mediated manipulation of membrane lipid composition which subsequently alters the affinity between cellular membranes and lipid binding PCP or adaptor proteins. Alternatively, OCRL1 may regulate localization of other ciliary proteins like the BBS proteins, which in turn manipulates the PCP pathway. Lowe patients do not develop most of the typical PCP phenotypes. However the above mentioned possibly similar renal manifestations of Lowe syndrome and adolescent nephronophthisis (a subset of *NPHP3* defects) may suggest a role of OCRL1 in embryonic development. A lot more research is needed to verify these possibilities and subsequently how can defects in developmental regulation result in cilia elongation.

The second ciliary process possibly involving OCRL1 is BBsome-mediated ciliogenesis. Besides PIP_2, OCRL1 is able to hydrolyze PIP_3 and generate $PI(3,4)P_2$, a lipid shown to recruit the BBsome to membrane compartments (31,32,241,262). $PI(3.4)P_2$ as well as recycling endosome localized Rab8, Rab11 (and possibly other proteins) collaborate to facilitate BBsome-mediated vesicular trafficking of ciliary

membrane proteins to the base of cilia (31,35). OCRL1 localizes to endosomes and interacts with Rab8, making it a possible contributor to $PI(3,4)P_2$ generation on recycling endosomes (235,236). As one of the primary machineries in ciliogenesis and maintenance, the BBsome is most likely involved in the control of cilia length. The potential role of OCRL1 in BBsome recruitment, if verified, may also contribute to the PCP pathway as discussed above. Current efforts in the lab are directed at determining the localization of different BBS proteins in polarized MDCK cells treated with control or OCRL1 siRNA. This experiment is critical for evaluating the role of OCRL1 in BBsome functions. My prediction is that OCRL1 knockdown will disrupt the normal cilliary localization of BBsome subunits. If this prediction is verified by immunofluorescence using antibodies against BBS proteins, my next hypothesis will be that the interaction between OCRL1 and Rab8 plays a role in BBsome functions. To test that hypothesis, critical residues for the OCRL1-Rab8 interaction will need to be identified (preferably in both proteins) and selectively mutated. Whether loss of the OCRL1-Rab8 interaction by mutagenesis affects BBsome functions will need to be determined. OCRL1 mediated $PI(3,4)P_2$ production (from PIP_3) could also contribute to BBsome recruitment/functions, however this possibility has been argued against by the evidence that exogenous OCRL1 with the catalytic domain mutation G304E was still able to restore normal cilia length in cells depleted of the endogenous enzyme.

The third candidate renal ciliary event possibly regulated by OCRL1 is the mechanosensing signaling cascade. As mentioned previously, we are collaborating to measure and compare flow-induced Ca^{2+} responses in control and OCRL1

knockdown MDCK cells to determine whether OCRL1 depletion causes impaired Ca^{2+} signaling. If it does, further experiments will be needed to examine if selected signaling proteins are mislocalized or aberrantly down-regulated and if OCRL1-mediated lipid metabolism contributes to normal positioning/functioning of these proteins.

The above three possibilities are not mutually exclusive. On the contrary, the complicated nature of cellular (as well as ciliary) events usually gives rise to partial overlapping among different pathways. It is highly possible that OCRL1 and/or some of its downstream effectors are involved in multiple ciliary regulations which cooperate for a tight and delicate control over cilia length, structure and functions. This hypothesis will be tested by future studies by our lab as well as other researchers worldwide.

4.3.6 Exogenously expressed OCRL1 with G304E or ΔE585 point mutation retains the ability to restore normal cilia length in MDCK cells depleted of the endogenous OCRL1

It was somewhat surprising that both disease-causing mutants tested, OCRL1 G304E and OCRL1 ΔE585, retained the ability to normalize cilia length in OCRL1 siRNA treated MDCK cells when expressed as siRNA-resistant proteins. As mentioned above, since G304E is a mutation within the 5-phosphatase domain (176), the catalytic activity of OCRL1 may not be required for control of cilia length. This does not rule out possibilities that OCRL1 phosphatase activity is required for other ciliary processes and/or non-ciliary pathways regulated separately. Alternatively,

considering the milder phenotypes of Dent 2 disease compared to those associated with Lowe syndrome, the Dent 2 G304E mutation may not completely abolish the catalytic activity. Therefore, it is probable that the residual phosphatase activity is adequate for the maintenance of cilia length but not enough for selected other cellular functions (whose impairment eventually results in Dent 2 disease). The phosphatase activities of different OCRL1 mutants will be measured by other people in my lab.

In the case of the ΔE585 mutation, which disrupts normal cellular localization of OCRL1, other cellular processes (ciliary or nonciliary) should be affected and responsible for human Lowe syndrome development while the cilia length control machinery remains intact.

4.3.7 Identification of the cilia length control motif(s) within OCRL1

To determine which segment(s) of OCRL1 is responsible for the regulation of cilia length, I have generated domain truncations within this enzyme by mutagenesis. Youssef Rbaibi in the lab will determine, when expressed in polarized MDCK cells treated with OCRL1 siRNA, which construct(s) (GFP-tagged and siRNA-resistant) fails to rescue the lengthened primary cilia to identify the domain required for the cilia length regulation. My prediction of the identified portion is the ASH domain, which is conserved among various ciliary proteins (182). If that is the case, detailed mutagenesis experiments will then be needed to dissect out the sequence motif within OCRL1 that controls renal epithelial primary cilia length.

4.3.8 Summary

To summarize, my recent data have correlated the Lowe syndrome protein OCRL1 to the control of primary cilia length in polarized MDCK cells. A relationship between OCRL1 and cilia has never been studied before, but it is indirectly supported by several pieces of evidence as discussed above. Symptoms of Lowe syndrome show similarities to a variety of cilia defects. Structural and functional analyses of OCRL1 also suggest a role of this enzyme in multiple ciliary pathways. A lot more research is needed to further explore the unanswered questions derived from this new discovery, to examine whether Lowe syndrome is, at least partially, a ciliopathy and to identify novel therapeutic targets needed to prevent and/or cure this severe genetic disease.

5.0 CONCLUSION

PI and PIPs play critical roles in many fundamental cellular processes. Their synthesis and turnover are spatially and temporally controlled by a large group of PI kinases and phosphatases. My thesis focuses on the metabolic regulations of PIP_2, a versatile PIP participating in various cellular functions ranging from signaling and membrane traffic. In polarized epithelial cells, PIP_2 is enriched at the apical plasma membrane, although smaller dynamic populations of this lipid are also present in other membrane compartments. PIP_2 is primarily produced via phosphorylation of PI4P by type I PI5Ks. The three PI5KI isoforms (α, β, and γ) exhibit non-overlapping plasma membrane distributions and non-redundant cellular functions in polarized renal epithelia. PIP_2 hydrolysis is mediated by several phosphatases and phospholipases, one of which is OCRL1, the disease protein of Lowe syndrome. By studying the apical targeting mechanism of PI5KIβ in polarized epithelial cells, and by examining the pathogenesis of Lowe syndrome using cultured renal epithelial cells depleted of OCRL1, I have made some interesting discoveries. These discoveries should contribute to our knowledge on PI/PIP related regulations and human diseases.

5.1 POLARIZED TARGETING OF PI5KIβ

In chapter two, I have shown that the three isoforms of type I PI5K exhibit non-overlapping plasma membrane distributions in polarized renal epithelial cells. While the α and γ661 isoforms are enriched on the lateral cell surface, albeit to distinct extents, PI5KIβ strikingly localizes to the apical plasma membrane. My experiments suggest that the apical localization of PI5KIβ is nonsaturable over a broad range of expression, suggesting that lipid components are likely involved in targeting of this kinase. My data also indicate that PIP_2 is not required for apical targeting of PI5KIβ, and neither is the lipid kinase activity of the enzyme. One possible lipid contributor of PI5KIβ targeting is PA, which interacts with the kinase *in vitro* (263). Future experiments are needed to verify this possibility by determining the distribution of PA in polarized epithelial cells, and by examining whether loss of PA disrupts apical targeting of PI5KIβ.

Because chronic expression disrupts polarized localization of PI5KIβ, the AV-based system has been used to transiently express PI5KIβ constructs in cultured epithelial monolayers. We are now in the process of generating AVs encoding truncation mutants of PI5KIβ. These mutants are critical for identification of the apical targeting signal(s) as well as specific interacting partners of PI5KIβ. I predict that the relatively more flexible N- and C- terminal tails are involved in the polarized localization of PI5KIβ. Meanwhile, we are also generating AVs encoding domain chimeras of the β and γ661 isoforms. More chimeras will be made once the apical targeting sequence of PI5KIβ is narrowed down to a transplantable region. These chimeric proteins will

be used in functional studies to understand differential regulations of PIP_2-related events, including endocytosis, on apical versus basolateral plasma membrane domains. These experiments should provide important information on how PI5KIβ is involved in specific apical cellular events and how PIP_2 synthesis is compartmentally regulated in polarized epithelia.

5.2 LOWE SYNDROME PATHOGENESIS

5.2.1 Megalin function in the kidney

In chapter three, I evaluated the long suspected role of megalin in Lowe syndrome development. Renal epithelial cells were used as the model and megalin trafficking events were studied in control cells or cells with acute RNAi mediated OCRL1 depletion. Surprisingly, upon OCRL1 knockdown, I was not able to detect any defect in megalin endocytosis, recycling or uptake of a megalin ligand, although the total cellular PIP_2 level was slightly elevated. Delivery of newly synthesized lysosomal hydrolases was impaired by loss of OCRL1, consistent with patient studies and with the observation by other groups that OCRL1 knockdown affected cellular distribution of cation-independent mannose 6-phosphate receptor (168), therefore supporting the viability of our cell-based model system.

Lowe patients develop characteristic renal tubular dysfunction manifested by phenotypes including aberrant urinary loss of many megalin ligands. My observation that acute loss of OCRL1 did not interfere with megalin function in renal epithelial cells does not rule out the possibility that chronic signaling defects could disrupt

megalin pathways in the long run to produce Lowe symptoms. One candidate mechanism to mediate chronic signaling, the primary ciliary pathway, has been addressed in chapter four of my thesis.

5.2.2 Renal epithelial cilia functions

By immunofluorescence, I found that siRNA-mediated OCRL1 knockdown caused increased variability in the length of primary cilia on polarized renal epithelial cells. This phenotype was characterized by significantly higher median cilia length value in cells treated with OCRL1 siRNA compared to that in cells treated with control siRNA. I confirmed that the observed effect could be rescued by expression of exogenous wildtype (siRNA-resistant) OCRL1 and was therefore specifically related to loss of this enzyme. Elongated cilia on MDCK monolayers did not exhibit morphological abnormalities when imaged by SEM, indicating that different ciliary properties (length, structure, and etc.) are controlled separately. I also found that OCRL1 regulation of cilia length appeared tissue specific because OCRL1 knockdown in human skin fibroblasts had no effect on the primary cilia length (consistent with the fact that skin is typically not affected by Lowe syndrome). A linkage between OCRL1 and ciliary functions has never been proposed before. By studying the literature, I have found phenotypic similarities between Lowe syndrome and known ciliopathies, including those affecting renal cilia length (21,33,34,245,246,255). Renal cilia elongation has also been associated with selected types of renal injury, although detailed mechanisms remain unclear.

Sequence analysis of OCRL1 has revealed an ASH domain (~100 amino acid long)

sandwiched between the PI 5-phosphatase homology domain and the Rho-GAP like domain (182). The ASH domain is found in more than a dozen human proteins and several other proteins specific for non-human species (182). Most ASH-domain-containing proteins localize and function in cellular cilia/flagella or centrosomes, indicating that this conserved domain might be involved in cilia-related processes (182). Interestingly, defects in two ASH-domain-containing proteins, ASPM and Hydin, have been associated with brain disorders potentially caused by cilia dysfunction (182,264-269). Mutations in ASPM (a centrosomal protein) or Hydin (a ciliary protein) have been suggested to compromise functions of ependymal cilia in the brain, therefore disrupting cilia-directed cerebrospinal fluid flow and causing brain disease (primary microcephaly for defective ASPM, and hydrocephalus for defective Hydin) (182,264-270).The fact that ASH-domain-containing proteins are involved in cilia-related disorders supports the proposed role of this domain in ciliary functions. ASH domain has been suggested to mediate microtubule binding (182,271). This possibility will be tested in our lab by immunofluorescence studies to determine if OCRL1 colocalizes with centrosome/basal body markers.

Notably, like in the case of *OCRL*, disease-causing mutations of *ASPM* scatter within full-length of the gene (176,267). This indicates that different domains of OCRL1 or ASPM collaborate tightly to form a functional protein. It is therefore possible that, for example, the OCRL1 ASH domain mediates localization of the protein to recycling endosomes, or other cellular compartments, where additional domains of OCRL1 regulate ciliary and non-ciliary pathways. Likewise, the

suggestion (by my experiment using siRNA-resistant OCRL1 bearing the G304E mutation) that catalytic activity of OCRL1 does not contribute to cilia length control does not rule out the possibility that the phosphatase domain is designated for other cellular responsibilities of the OCRL1 protein. In the case of Lowe syndrome, it is likely that activities of different OCRL1 domains lead to converging cellular responses, and that disruption of any upstream step by mutating a certain domain of OCRL1 eventually leads to .a same combination of phenotypes in Lowe patients. To determine specific functions of OCRL1 domains, I have recently generated truncation mutants of OCRL1 to examine whether loss of each domain affects ciliary and membrane trafficking events (known to involve OCRL1). Future experiments are needed to elucidate the role of individual domains in OCRL1-regulated pathways.

Based on our current understanding, I propose that OCRL1 is most possibly involved in one or more of the three ciliary processes including the developmental regulation, Ca^{2+} signaling, and BBsome-mediated ciliogenesis. Our lab is currently addressing all three possibilities by experiments in different model systems and in collaboration with other researchers. My experiments indicate that neither of the two disease-causing point mutations tested, G304E and △E585, interferes with the role of OCRL1 in control of cilia length. The truncation mutants of OCRL1 (discussed above) will be used in future experiments to identify critical sequence motifs involved in renal primary cilia length regulation.

5.2.3 Connecting megalin trafficking and primary cilia functions

Dr. De Camilli's group has shown that, when combined, the ASH and Rho-Gap like domains collaborate to bind endocytic adaptors at distinct internalization stages and facilitate endosomal maturation (183). Their data also indicate that binding to endosomal adaptors contributes to regulation of the interaction between OCRL1 and clathrin (183). Considering the previously discussed ciliary role of ASH domain, it is possible that the OCRL1 ASH domain exhibits dual functions to regulate ciliary pathways and, additionally, endocytic processes (in the context of the Rho-GAP like domain) at the same time. If that is the case, endocytosis and primary cilia functions might not be as separated as they seem to be. Rather, Lowe syndrome possibly results from defects in both pathways, consistent with our previous prediction that proteinuria could be due to aberrant-(ciliary)-signaling-mediated chronic megalin (endocytic) dysfunction. It is likely that OCRL1 mutations disrupt a delicate network that consists of selected endocytic as well as ciliary proteins. This network is likely coordinated by ASH and other OCRL1 domains in collaboration, and may involves additional (possibly ASH-domain-containing) proteins that similarly participate in both ciliary and endocytic processes. According to my data, defective megalin endocytosis or recycling is most likely not a direct consequence of OCRL1 loss-of-function. However, in the long run, disrupted ciliary functions and endocytic regulations (in the network described above) could contribute to profound damage in the post-endocytic machineries, which in turn might compromise megalin mediated ligand uptake and cause proteinuria.

To summarize, combining results from chapters three and four, it seems that the pathogenesis of Lowe syndrome is much more complicated than previously expected. The renal tubular dysfunction found in Lowe patients should most likely be attributed to multiple pathways that connect a variety of signaling cascades to membrane traffic at various cellular compartments. Processes involving renal primary cilia and endocytic regulations possibly play roles during development of renal defects in Lowe patients. Future studies are needed to elucidate details about this complexity.

6.0 MATERIALS AND METHODS

6.1 CELL CULTURE

MDCK cells (type II) were cultured in MEM (Sigma) supplemented with 10% FBS (Atlanta Biologicals), 100 units/mL penicillin and 100 µg/mL streptomycin. Four hundred µg/mL geneticin (G418) was included in the culture media of stable lines. Mouse cortical collecting duct (mCCD) cells were grown in 50% HAM-F12 medium (Gibco), 50% DMEM without phenol red low glucose medium (Gibco), 5 µg/mL insulin, 0.02 µg/mL dexamethasone, 0.01 µg/mL selenium, 5 µg/mL transferrin, 2mM L-glutamine, 10^{-9} M triiodothyronine, 20mM Hepes, 2.2 % D-Glucose, 2% Decomplemented FBS, 100 unit s/mL penicillin and 100 µg/mL streptomycin. Both cell types were passaged at confluence. To obtain a polarized monolayer, cells were plated on 12-transwell permeable supports (12mm diameter polycarbonate, Costar) at a super-confluent density of 0.5 - 0.8 million per well and cultured for 4-5 days in growth media at 37 °C in the presence of 5% CO_2.

Human kidney proximal tubule HK-2 cells were obtained from ATCC and grown in DMEM-F12 medium (Sigma) supplemented with 5 µg/mL insulin, 0.02 µg/mL dexamethasone, 0.01 µg/mL selenium, 0.05 µg/mL transferrin, 2mM L-glutamine, 10% FBS, 100 units/mL penicillin and 100 µg/mL streptomycin. HK-2 cells were passaged when 80-90% confluent. Human skin fibroblasts were cultured in DMEM

(Sigma) with 10% FBS and passaged at confluence. BSC-1 (African green monkey kidney epithelial) cells were cultured in DMEM (sigma) with 10% FBS and passaged at confluence.

6.2 SIRNA KNOCKDOWN

All siRNA constructs were purchased from Dharmacon. A target sequence (GGTTCCCTGCCATTTTTCA) that efficiently knocks down OCRL1 was kindly provided by Alex Ungewickell (Washington University). There is an intentional single-nucleotide mismatch at the 3' end of the sense sequence that enhances the efficiency of target mRNA degradation (272). This siRNA efficiently knocks down OCRL1 in HK-2, human skin fibroblast, and MDCK cells. SiRNA targeting canine N-WASP (GGCGAGACCCCCCAAATGC) was based on a published siRNA targeting rat N-WASP (273). SiRNA directed against firefly luciferase was used as a control.

In chapter three, siRNAs were introduced into MDCK and HK-2 cells using nucleofection as follows: Cells cultured in growth media in 10 cm dishes were maintained so that a 50-60% density was achieved on the day of siRNA treatment. Cells were trypsinized from the dishes, counted using a hemocytometer, pelleted by centrifugation, and resuspended in Ingenio electroporation solution (Mirus; 4 million cells/100 µL solution). Suspended cells were mixed with control or OCRL1-specific siRNA (10 µg of siRNA per 4 million cells), transferred into Ingenio cuvettes (0.2 cm gap, Mirus; 100 µL cell suspension/cuvette) and electroporated in an Amaxa nucleofector II (Lonza) using the program T20. After nucleofection, cells were

immediately plated and cultured in growth media for three days before use. Knockdown of OCRL1 was confirmed for all experiments by western blotting or by RT-PCR (described below). Knockdown efficiency was typically >95% in MDCK cells and ~80% in HK-2 cells.

SiRNA transfection of human skin fibroblasts (chapter four) was performed by nucleofection using the protocol described above with minor modifications. The modifications are: 0.5 million cells together with 2 μg siRNA (OCRL1 mismatch siRNA or control firefly luciferase siRNA) and 100μL Ingenio solution were used for each cuvette/reaction and every reaction was split into 2 wells on 12-well culture dishes with coverslips in them. Amaxa program U-023 or T-016 (these 2 programs produce equally well knockdowns) was used. Fibroblasts were starved for three days, starting from the following day of electroporation, in growth medium with 0.5% FBS to facilitate cilia formation. Cells were then fixed for immunofluorescence on day 4 after the nucleofection. Control and OCRL1 knockdown cells from a duplicate pair of wells were collected in each experiment for Western blotting to determine the knockdown efficiency.

SiRNA transfection of MDCK cells in chapter four was performed using lipofectamine 2000 (Invitrogen) as reported before (274). On the day of transfection, semi-confluent MDCK cells grown on plastic were trypsinized and resuspended in the growth medium at the concentration of 2.4 million cells per mL. Meanwhile, siRNA oligos and lipofectamine 2000 were incubated separately in OPTI-MEMI (Gibco) for 5 min at room temperature before they were combined and incubated for 30-45 min. 2.7

μg siRNA, 10 μL lipofectamine 2000 and 500 μL OPTI-MEMI were used for every 4 12-transwells. After the incubation, 125 μL transfection mixture and 333 μL cells (approximately 0.8 million cells) were added to the top chamber of a 12-transwell and gently mixed by pipetting up and down for a few times. 1mL growth medium was then added to the bottom chamber of the transwell. The medium was replaced the next day and cells were cultured for 4-5 days before fixed for subsequent experiments (immunofluorescence and scanning electron microscopy). Cells from a duplicate pair of control and OCRL1 knockdown samples were collected in every experiment for Western blotting to determine the knockdown efficiency.

6.3 DNA CONSTRUCTS AND ADENOVIRUSES

The full-length mouse PI5KIβ gene was cloned into the pEGFP-N1 (Clontech) plasmid vector and tagged with the HA epitope at the N-terminus of the gene (the GFP tag is at the C-terminus). The megalin minireceptor consisting of the ligand binding domain 4, transmembrane domain and cytoplasmic tail of megalin [M4 in (13)] was kindly provided by Dr. Marilyn Farquhar (UCSD) and modified by adding an extracellular V5 epitope tag and cytoplasmic GFP. The construct was subcloned into the pAdtet adenoviral expression vector. Wobble mutations were generated in the siRNA target sequence of OCRL1 (the original RNAi target region described above was therefore changed into AGTACCGTGTCACTTCTCG), using the Qiagen QuikChange® II XL Site-Directed Mutagenesis Kit, to render siRNA-resistance. The same mutagenesis kit was used to introduce G304E and △E585 point mutations.

SiRNA-resistant OCRL1 constructs, including wildtype OCRL1, OCRL1G304E, and OCRL1△E585, were subcloned into the pEGFP-C1 vector using the XhoI and XmaI restriction enzyme sites.

The pAdtet adenoviral expression vector and protocols to generate replication-deficient adenoviruses (AV) using pAdtet-based constructs were described previously (118,275). AVs used in my dissertation research include those encoding HA (tag) – PI5KIβ (mouse), HA (tag) – PI5KIα (mouse), HA (tag) – PI5KIγ661 (human), HA (tag) – PI5KIβ D203A (mouse), HA (tag) – PI5KIβ D227A (mouse), HA (tag) – PI5KIβ K138A (mouse), HA (tag) – PI5KIβ D203A,D227A (mouse), GFP-PHPLCδ (the PH domain of PLC isoform δ tagged with GFP), OCRL1, influenza hemagglutinin (HA), or rabbit polymeric immunoglobulin receptor (pIgR).

6.4 ADENOVIRAL INFECTION

Adenoviral infection of filter-grown MDCK cells and HK-2 cells was as described previously for cells growing on transwells or plastic dishes, respectively (276,277). MDCK cells used in my dissertation studies stably maintain the tetracycline transactivator required for expression of most of our lab's AV-encoded proteins. Adenovirus expressing this transactivator was included during infection of HK-2 cells.

Adenoviral infection of mCCD cells grown on transwell filters or coverslips were done according to protocols similar to those described for infecting MDCK cells on filters or plastic dishes, respectively (276,277) with a few changes. The changes are: 1) mCCD cells were infected 2 days prior to any experiment and 1ng/mL doxycycline

was added to the growth medium on the day of infection to prevent exogenous protein expression. Cells (mostly tight junctions) recovered overnight and doxycycline was removed 1 day before experiments to allow cellular expression of AV-encoded proteins. Transepithelial resistance (TER) of mCCD cells was measured on the day of each experiment to ensure that the cells were properly polarized. 2) AV-tetracycline transactivator was included during infection of mCCD cells. 3) During infection of filter-grown mCCD cells, which formed tighter monolayers compared to type II MDCK cells, viruses (in Ca^{2+}- free phosphate buffered saline (PBS) containing 1mM Mg^{2+}) were added to both the apical (150μL) and the basolateral (50μL drops) chambers of 12-well transwells.

The virally expressed exogenous proteins were detected either by immunofluorescence or by Western blotting.

6.5 WESTERN BLOTTING ANTIBODIES

The Western blotting to detect OCRL1 knockdown was performed using primary antibodies including an affinity-purified monoclonal antibody directed against OCRL1 (1:1000; a generous gift of Drs. Robert Nussbaum and Sharon Suchy) and a mouse monoclonal anti β-actin antibody (1:5000; Sigma; used as the loading control).

The Western blotting to detect virally expressed proteins was performed using primary antibodies including a mouse monoclonal anti HA tag antibody (1:1000; Covance), a mouse monoclonal anti GFP antibody (1:2000; Invitrogen) and the β-actin antibody described above.

Mouse anti-ARH and rabbit anti-Dab2 antibodies for Western blotting were generously provided by Dr. Linton Traub.

Secondary antibodies used included a horseradish peroxidase (HRP) conjugated sheep anti mouse IgG antibody (1:5000; Amersham, GE) and an HRP conjugated donkey anti rabbit IgG antibody (1:5000; Amersham, GE).

6.6 RT-PCR

The Ambion RNAqueous phenol-free total RNA isolation kit was used to extract RNA from mCCD, HK-2 and HeLa cell lysates, and RNA concentration was determined after DNase treatment using absorbance at 260 nm. Reactions containing 1 µg of RNA, 2 µl of Oligo(dT) primer (50 µM stock) and nuclease-free water in a total volume of 12 µl were mixed gently, spun briefly, heated for 3 min at 72°C, and set immediately on ice. Two µl of 10x RT buffer, 4 µl dNTP mix, 1 µl of RNAse inhibitor, and 1 µl Moloney Murine Leukemia Virus reverse transcriptase (or water, for control samples) were added. The solution was then mixed gently and incubated at 42 °C for 1 h, followed by incubation at 92 °C for 10 min to inactivate the RT enzyme. A 3 µl aliquot of this reaction was mixed with 2.5 µl each sense and antisense primers (1 mg/ml), 5 µl of 10x PCR buffer, 0.5 µl of enzyme mix (GeneAmp High Fidelity PCR System, Applied Biosystems) 5 µl of DMSO, and 26.5 µl of PCR-grade water. The solution was pipetted into a 0.6 mL thin walled tube and placed into a Bio-Rad thermocycler. After a 1 min incubation at 95°C, the reaction was cycled 35 times at 95°C for 30 sec, 52°C for 30 sec, and 72°C for 30 sec. Reactions were then incubated for a final 5 min

at 72°C and held at 4°C. Five µl of this reaction was loaded on a 2% agarose gel and product sizes measured against a Track-It ladder (Invitrogen). The agarose gel was stained with ethidium bromide and imaged under Ultraviolet (UV) light. The primers used are listed in Table 6.1. Actin primers were included as positive controls in all experiments to confirm efficient RNA recovery.

Table 6.1 RT-PCR primer sequences.

Primer	Sense Sequence	Antisense Sequence	Product Size
Actin	accttcaactccatcatgaag	ctgctggaaggtggacag	231
PI5K1α	cactgtctccccttcctctg	aggaacaatgtccagccagt	246
PI5K1β	gtatcctccatcagccagga	tggaaggtaacccttgctg	247
PI5K1γ	aaggaggagggtgcaggagt	gggagggagagaacaaggtt	276
Human INPP5B	cagatgtgagccaccacgc	gcgtggtggttcatgcctg	329
Canine INPP5B	ggaagccctgccagagcctgt	acgctgacggtcacttggagt	274
Human OCRL1	cactgacctgggatctttg	ccagctgaatccgaaatcc	321

6.7 GENERATION OF STABLE CELL LINES

MDCK cells were transfected with plasmids encoding HA-PI5KIβ-GFP or GFP tagged OCRL1 constructs using the lipofectamine 2000 reagent (Invitrogen) according to the manufecturer's guide. After the transfection, cells were grown in normal media overnight, split the next day, plated sparsely on 15cm-diameter culture dishes and subsequently selected by including G418 in the growth medium. Mixed MDCK stable lines were obtained by keeping and expanding transfected cells under constant selection. To generate clonal stable lines, single colonies of G418 resistant cells were recovered, expanded and screened by immunofluorescence. Clones with relatively high percentages of GFP-construct expressors (20-70% depending on the construct) were saved.

One MDCK clone expressing HA-PI5KIβ-GFP at a relatively high level (30%-40% of the cells were expressing the GFP-signal when originally screened ~2 weeks post-transfection) was sorted by flow cytometry (fluorescence-activated cell sorting, FACS) with the help of Mr. Timothy Sturgeon at the University of Pittsburgh Center for Vaccine Research (CVR) and split into a higher-expressor population and a lower expressor population based on single cell GFP signal levels.

Among the saved MDCK clones stably expressing GFP-OCRL1 constructs, those exhibiting mostly low to moderate single-cell expression levels (therefore relatively low variation in the single cell GFP intensity) were used in the immunofluorescence studies.

6.8 DNA TRANSFECTION

The transfection of BSC-1 cells with plasmids encoding different GFP-tagged siRNA-resistant OCRL1 constructs was performed using the Lipofectamine 2000 reagent (Invitrogen) in Opti-MEM reduced serum medium (GIBCO) according to the manufacturer' guides. Cells were plated on 12-well culture dishes with a glass coverslip in every well and were cultured in antibiotics-free growth medium. Cells were transfected at 80-90% confluence and were fixed for immunofluorescence after 24 h.

6.9 IMMUNOFLUORESCENCE ON CULTURED CELLS AND ANTIBODIES USED

Filter or coverslip-grown cells were fixed with 4% paraformaldehyde (with 100 mM sodium cacodylate, 3 mM $CaCl_2$, 3 mM $MgCl_2$ and 3 mM KCl; pH 7.4) for 15 min (5 min at 37℃ followed by 10 min at room temperature), quenched in PBS with 20 mM glycine and 75 mM NH_4Cl for 5 min at ambient temperature, permeablized using 0.1% TritonX-100 in the quench solution for 10 min while gently shaken, blocked in PBS with 1% gelatin (from cold water fish skin, Sigma) and 0.1% saponin for 10 min at 37℃, and probed with proper primary and secondary antibodies diluted in PBS with 0.5% gelatin and 0.025% saponin (1 h at ambient temperature for primary and secondary antibody incubations). After thorough washes, squares of transwell filters (cut out from the transwells) or coverslips were mounted on glass slides using Prolong Gold antifade reagent with DAPI (Invitrogen). Mounted slides were dried overnight at room temperature and imaged on a confocal fluorescence microscope.

Confocal XZ and XY images were analyzed and quantitated using the MetaMorph software (Molecular Devices).

In chapter two, primary antibodies used included a monoclonal mouse anti HA tag antibody (1:500; Covance), a polyclonal goat anti PI5KIβ antibody (L-17; 1:50; Santa Cruz), and a monoclonal rat anti ZO-1 antibody (in the form of hybridoma medium used at a dilution of 1:10). Secondary antibodies used were donkey anti goat as well as goat anti mouse or rat antibodies conjugated to appropriate fluorophores (1:500; Invitrogen).

In chapter three, primary antibodies used included the OCRL1 antibody described in section 6.5 (1:100; to detect the endogenous protein), a polyclonal rabbit anti-furin antibody (1:200; Thermo Affinity Bioreagents), and a mouse monoclonal anti-V5 antibody (1:200; Invitrogen). Secondary antibodies used included Alexa488 or 647-conjugated goat anti mouse or rabbit antibodies (1:500; Invitrogen). Surface megalin minireceptor was detected by incubation of cells on ice with primary (anti-V5) and secondary antibodies prior to fixation.

In chapter four, primary antibodies used included a mouse monoclonal anti-acetylated tubulin antibody (1:400; Sigma), a rabbit anti-Giantin antibody (1:200; a gift of Dr. Adam Lindstedt, Carnegie Mellon University), and a mouse monoclonal anti-EEA1 antibody (1:1000; BD Transduction). Goat anti-mouse/rabbit secondary antibodies tagged with appropriate fluorophores (1:500; Invitrogen) were utilized to produce visible fluorescent signals under a fluorescence microscope.

6.10 CILIA LENGTH QUANTITATION

Primary cilia (and centrosomes in the cytosol) were specifically highlighted and identified by using the anti-acetylated tubulin antibody in MDCK and human fibroblast cells. XY images of cilia on cells were taken on a Leica DM6000B upright fluorescence microscope. The length of cilia in random fields was quantitated using Volocity software, sorted ascendingly (by value) and plotted against percentile.

6.11 IMMUNOFLUORESCENCE ON TISSUE SAMPLES AND ANTIBODIES USED

Rat kidney cortical tissue pieces were fixed in 4% paraformaldehyde in PBS for 3 h at room temperature, washed for 3X5 min with PBS, quenched in 0.2 M NH_4Cl in PBS for 14 min at room temperature, washed again for 3X5 min with PBS, and soaked in 30% sucrose in PBS (with 0.02% sodium azide to prevent bacterial contamination) until all pieces had sunk to bottom of the container. The cryoprotected tissue pieces were then frozen in optimal cutting temperature (OCT) compound at approximately -25℃ and sliced into 4 μm sections in a cryostat.

Tissue slices placed on glass slides were incubated in PBS at room temperature for 30 min. Samples were kept wet for all subsequent steps to prevent damage. After the PBS incubation, kidney slices were permeabilized with 1% SDS in PBS for 4 min, washed for 3X5 min with PBS, and blocked in PBS with 1% BSA and 0.02% sodium azide for 15 min at room temperature. Subsequently, tissue slices were incubated in a polyclonal goat anti-PI5KIβ antibody (L-17; 1:50; Santa Cruz) (or no primary antibody as the negative control) diluted in Dako antibody diluent (background reducing; Dako

North America) for 1 h 15 min at room temperature in a humid chamber, washed 2X5 min with high salt PBS (HSPBS; 18 g NaCl per liter added to 1XPBS to break weak electrostatic interactions of antibodies with nonspecific charges) followed by 1X5 min with PBS, and incubated in an Alexa Fluor 488 donkey anti-goat IgG (H+L) (1:500; Invitrogen) secondary antibody diluted in Dako antibody diluent for 1 h at room temperature in a humid chamber. After antibody incubations, samples were washed 2X5 min with HSPBS and 1X5 min with PBS before mounted with coverslips. Slides were dried overnight and imaged using a confocal microscope.

6.12 QUANTITATION OF ACTIN COMETS

GFP-actin expressing MDCK cells treated with OCRL1 or control siRNA were plated onto filters for two days before being transferred to Bioptech 0.17 mm ΔT dishes for an additional day prior to imaging using an Olympus IX-81 (Melville, NY) equipped with an UltraView spinning disc confocal head (PerkinElmer Life Sciences) and an argon-ion, argon-krypton, and helium-cadmium laser combiner. Three minute movies were taken of random fields with either an Olympus 60X PlanApo (NA 1.40) or a 100X UPlanApo (NA 1.35) oil immersion objective. Movies were reviewed multiple times to determine the percentage of cells with actin comets.

6.13 QUANTITATION OF PIP_2

MDCK cells treated with either control or OCRL1 siRNA were plated onto filters for three days. Phospholipids were labeled with ^{32}P-orthophosphate, extracted, and analyzed by TLC to determine relative phospholipids levels as described in (278).

6.14 APICAL BIOSYNTHETIC DELIVERY KINETICS OF HA

MDCK cells (treated with control siRNA or siRNA directed against OCRL1 or N-WASP as noted) were seeded onto Transwell filters for three days. Cells were then infected with AV-HA, and where indicated, with control AV or AV-PI5KI β . The following day, cells were starved in methionine-free medium, pulsed with [^{35}S]-methionine (Easy Tag Express protein labeling mix; Perkin-Elmer), and chased for 2 h. Apical delivery was measured using a cell surface trypsinization assay as described in (275).

6.15 ^{125}I-LACTOFERRIN BINDING TO MDCK CELLS

Human lactoferrin (Sigma) was iodinated to a specific activity of 1500-2000 cpm/ng using the ICl method. Filter-grown MDCK cells were incubated for 1 h on ice with HEPES buffered-MEM containing ^{125}I-lactoferrin (approximately 1,200,000 cpm/well). For competition experiments, >100-fold surplus cold lactoferrin or BSA (negative control, Sigma) was included. After the incubation, cells were washed thoroughly with ice cold medium, solubilized, and cell-associated radioactivity quantitated using a γ-counter (Packard).

6.16 ^{125}I-LACTOFERRIN DEGRADATION AND RECYCLING IN MDCK OR HK-2 CELLS

Filter-grown MDCK cells (infected with AV-mini-megalin) or HK-2 cells on plastic were incubated on ice for 1 h with medium containing ^{125}I-lactoferrin (approximately 1,200,000 cpm/well; added apically to MDCK cells). Cells were washed thoroughly with ice cold medium and then warmed up to 37°C to allow ligand-uptake for various time periods. At each time point, the medium was collected. The cells were harvested after the final time point and solubilized. Tricholoroacetic acid (TCA) was added to the medium at a final concentration of 10% and the samples were incubated for 20 min on ice. After centrifugation, TCA soluble and insoluble ^{125}I was quantitated using a γ-counter, and degraded/recycled lactoferrin determined (TCA-soluble/insoluble ^{125}I cpm divided by the total ^{125}I cpm recovered in the cells and medium).

6.17 ACCUMULATED ^{125}I-LACTOFERRIN DEGRADATION IN HK-2 CELLS

Non-polarized HK-2 cells treated with control or OCRL1 siRNA were incubated in GIBCO Opti-MEM I reduced-serum medium (Invitrogen) containing ^{125}I-lactoferrin (approximately 200,000 cpm/well) in a 37°C incubator overnight (14-18 h). Blank wells containing ^{125}I-lactoferrin in medium (no cells) were incubated under the same conditions to determine non-specific ^{125}I-Lf degradation (background). After the incubation, the medium was collected and TCA precipitated as described above.

Cells were solubilized and subjected to the Dc protein assay (Bio-Rad). The amount of ^{125}I-lactoferrin degraded in each sample was calculated as TCA soluble counts above background normalized to total protein levels.

6.18 ENDOCYTOSIS OF MINI-MEGALIN

Endocytosis of mini-megalin was assessed using a biotinylation-based assay performed using the protocol previously described for MUC1 (279). Briefly, HK-2 cells infected with AV-mini-megalin (and either co-infected with AV-PI5KIβ or control AV, or treated with OCRL1 or control siRNA) were biotinylated on ice using sulfo-NHS-SS-biotin (Pierce). Cells were then rapidly warmed to 37^{o}C for 0 or 6 min (one of the experiments comparing control and PI5KIβ AVs was warmed for only 5 min.) Biotin on the cell surface was stripped with 2-mercaptoethane sulfonate (MESNa) before cells were solubilized in a HEPES buffered detergent solution (60mM octyl-β-D-glucopyranoside, 50mM NaCl, 10mM HEPES, 0.1% SDS, pH 7.4). Duplicate 0’ samples were left unstripped to quantitate total biotinylated mini-megalin at the cell surface. Biotinylated proteins were recovered after immunoprecipitation with avidin-conjugated beads and analyzed by western blotting (to detect the V5 tag on mini-megalin) after SDS-PAGE. The percentage of mini-megalin endocytosis at each time point was calculated as the % of total biotinylated signal remaining at 6 min minus the % remaining at 0’ (background).

6.19 ENDOCYTOSIS OF ^{125}I-IGA

Iodination of IgA was performed essentially as described in (280). HK-2 cells nucleofected with control or OCRL1 siRNA were plated in 12-well dishes and infected with AV-pIgR after 2 days. The following day, cells were incubated with ^{125}I-IgA for 1 h on ice, then washed extensively with ice cold medium to remove unbound radioligand. The cells were then incubated in pre-warmed medium in a 37°C waterbath for 0, 2.5, or 5 min, then rapidly chilled. To remove ^{125}I-IgA from the cell surface, cells were incubated for 30 min on ice with 100 µg/ml L-1-tosylamide-2-phenylethylchloromethyl-ketone-treated trypsin (Sigma), then stripped with 150 mM glycine buffer, pH 2.3 for 15 min on ice. Finally cells were solubilized in 50 mM Tris-HCl, 2% Nonidet P-40, 0.4% deoxycholate, 62.5 mM EDTA, pH 7.4 and cell-associated radioactivity determined using a gamma counter. Internalized ^{125}I-IgA was quantitated relative to total ^{125}I-IgA (recovered in the cells, trypsin and glycine strips, and the medium).

6.20 QUANTITATION OF CATHEPSIN D SECRETION

HK-2 cells were cultured for three days after nucleofection with either control or OCRL1 siRNA. Cells were then pulse labeled with [^{35}S]-methionine and chased for 4 h. NH_4Cl (10 mM) was included in some samples as a positive control. Following the chase both the cells and the media were harvested and immunoprecipitated using an anti-cathepsin D antibody (Upstate). Radioactive cathepsin D secreted into the medium during the chase was quantitated following separation by SDS-PAGE.

6.21 SCANNING ELECTRON MICROSCOPY

SiRNA transfection was performed on MDCK cells as described above. Five days after the transfection, control or OCRL1 siRNA treated polarized cells grown on transwell filters were fixed in (0.5% glutaraldehyde + 2% paraformaldehyde + 0.5 mM $MgCl_2$ + 1 mM $CaCl_2$ in 200 mM sodium cacodylate buffer, pH 7.4) for 30 min to 1 h at room temperature and washed with 100 mM sodium cacodylate buffer, pH 7.4, for 5 min. Subsequently, cells were fixed again with 1.5% OsO_4 in 100 mM sodium cacodylate buffer, pH 7.4, for 1 h at 4℃ on an ice tray while gently shaken in a fume hood, rinsed repeatedly with deionized water, and washed 1X5 min in deionized water while gently shaken. Following fixation, cells were dehydrated by soaked through an alcohol gradient (made with deionized water), consisting of 40%, 50%, 75%, 80%, 90% and 95% ethanol solutions, on ice for 5 min with each alcohol solution. Cells were then put through an extreme dehydration process by incubated in 100% ethanol for 2X10 min at room temperature. Dehydrated samples were critical point dried on a Samdri®-PVT-3D machine (Tousimis) and sputter coated using gold palladium in a Cressington Sputter Coater before imaged in a JEOL JSM-T300 scanning electron microscope (SEM).

BIBLIOGRAPHY

1. Ovalle, W. K., Nahirney, P.C. (2008) *Netter's Essential Histology*, Elsevier Inc.

2. Junqueira, L. C., Carneiro, J. (2003) *Basic Histology*, 10th ed., The McGraw-Hill Companies, Inc.

3. Kierszenbaum, A. L. (2007) *Histology and Cell Biology - An Introduction to Pathology*, 2nd ed., Mosby, Inc., an affiliate of Elsevier Inc.

4. Muto, S., Hata, M., Taniguchi, J., Tsuruoka, S., Moriwaki, K., Saitou, M., Furuse, K., Sasaki, H., Fujimura, A., Imai, M., Kusano, E., Tsukita, S., and Furuse, M. (2010) *Proc Natl Acad Sci U S A* **107**, 8011-8016

5. Elkouby-Naor, L., and Ben-Yosef, T. (2010) *Int Rev Cell Mol Biol* **279**, 1-32

6. Christensen, E. I., and Birn, H. (2002) *Nat Rev Mol Cell Biol* **3**, 256-266

7. Verroust, P. J., and Christensen, E. I. (2002) *Nephrol Dial Transplant* **17**, 1867-1871

8. Biemesderfer, D. (2006) *Kidney Int* **69**, 1717-1721

9. Zou, Z., Chung, B., Nguyen, T., Mentone, S., Thomson, B., and Biemesderfer, D. (2004) *J Biol Chem* **279**, 34302-34310

10. Christensen, E. I., and Gburek, J. (2004) *Pediatr Nephrol* **19**, 714-721

11. Goldstein, J. L., Brown, M. S., Anderson, R. G., Russell, D. W., and Schneider, W. J. (1985) *Annu Rev Cell Biol* **1**, 1-39

12. Krieger, M., and Herz, J. (1994) *Annu Rev Biochem* **63**, 601-637

13. Takeda, T., Yamazaki, H., and Farquhar, M. G. (2003) *Am J Physiol Cell Physiol* **284**, C1105-1113

14. Christensen, E. I., and Verroust, P. J. (2002) *Pediatr Nephrol* **17**, 993-999

15. Moestrup, S. K., Kozyraki, R., Kristiansen, M., Kaysen, J. H., Rasmussen, H. H., Brault, D., Pontillon, F., Goda, F. O., Christensen, E. I., Hammond, T. G., and Verroust, P. J. (1998) *J Biol Chem* **273**, 5235-5242

16. Kozyraki, R., Fyfe, J., Verroust, P. J., Jacobsen, C., Dautry-Varsat, A., Gburek, J., Willnow, T. E., Christensen, E. I., and Moestrup, S. K. (2001) *Proc Natl Acad Sci U S A* **98**, 12491-12496

17. Piwon, N., Gunther, W., Schwake, M., Bosl, M. R., and Jentsch, T. J. (2000) *Nature* **408**, 369-373

18. Norden, A. G., Lapsley, M., Igarashi, T., Kelleher, C. L., Lee, P. J., Matsuyama, T., Scheinman, S. J., Shiraga, H., Sundin, D. P., Thakker, R. V., Unwin, R. J., Verroust, P., and Moestrup, S. K. (2002) *J Am Soc Nephrol* **13**, 125-133

19. Santo, Y., Hirai, H., Shima, M., Yamagata, M., Michigami, T., Nakajima, S., and Ozono, K. (2004) *Pediatr Nephrol* **19**, 612-615

20. Berbari, N. F., O'Connor, A. K., Haycraft, C. J., and Yoder, B. K. (2009) *Curr Biol* **19**, R526-535

21. Lancaster, M. A., and Gleeson, J. G. (2009) *Curr Opin Genet Dev* **19**, 220-229

22. Veland, I. R., Awan, A., Pedersen, L. B., Yoder, B. K., and Christensen, S. T. (2009) *Nephron Physiol* **111**, p39-53

23. Satir, P., and Christensen, S. T. (2008) *Histochem Cell Biol* **129**, 687-693

24. Gerdes, J. M., Davis, E. E., and Katsanis, N. (2009) *Cell* **137**, 32-45

25. Han, Y. G., and Alvarez-Buylla, A. (2010) *Curr Opin Neurobiol* **20**, 58-67

26. Oishi, I., Kawakami, Y., Raya, A., Callol-Massot, C., and Izpisua Belmonte, J. C. (2006) *Nat Genet* **38**, 1316-1322

27. Seeley, E. S., and Nachury, M. V. (2010) *J Cell Sci* **123**, 511-518

28. Tammachote, R., Hommerding, C. J., Sinders, R. M., Miller, C. A., Czarnecki, P. G., Leightner, A. C., Salisbury, J. L., Ward, C. J., Torres, V. E., Gattone, V. H., 2nd, and Harris, P. C. (2009) *Hum Mol Genet* **18**, 3311-3323

29. Jacoby, M., Cox, J. J., Gayral, S., Hampshire, D. J., Ayub, M., Blockmans, M., Pernot, E., Kisseleva, M. V., Compere, P., Schiffmann, S. N., Gergely, F., Riley, J. H., Perez-Morga, D., Woods, C. G., and Schurmans, S. (2009) *Nat Genet* **41**, 1027-1031

30. Bielas, S. L., Silhavy, J. L., Brancati, F., Kisseleva, M. V., Al-Gazali, L., Sztriha, L., Bayoumi, R.

A., Zaki, M. S., Abdel-Aleem, A., Rosti, R. O., Kayserili, H., Swistun, D., Scott, L. C., Bertini, E., Boltshauser, E., Fazzi, E., Travaglini, L., Field, S. J., Gayral, S., Jacoby, M., Schurmans, S., Dallapiccola, B., Majerus, P. W., Valente, E. M., and Gleeson, J. G. (2009) *Nat Genet* **41**, 1032-1036

31. Jin, H., White, S. R., Shida, T., Schulz, S., Aguiar, M., Gygi, S. P., Bazan, J. F., and Nachury, M. V. (2010) *Cell* **141**, 1208-1219

32. Jin, H., and Nachury, M. V. (2009) *Curr Biol* **19**, R472-473

33. Gunay-Aygun, M. (2009) *Am J Med Genet C Semin Med Genet* **151C**, 296-306

34. Cardenas-Rodriguez, M., and Badano, J. L. (2009) *Am J Med Genet C Semin Med Genet* **151C**, 263-280

35. Knodler, A., Feng, S., Zhang, J., Zhang, X., Das, A., Peranen, J., and Guo, W. (2010) *Proc Natl Acad Sci U S A* **107**, 6346-6351

36. Hellman, N. E., Liu, Y., Merkel, E., Austin, C., Le Corre, S., Beier, D. R., Sun, Z., Sharma, N., Yoder, B. K., and Drummond, I. A. (2010) *Proc Natl Acad Sci U S A* **107**, 18499-18504

37. Katz, S. M., and Morgan, J. J. (1984) *Ultrastruct Pathol* **6**, 285-294

38. Duffy, J. L., and Suzuki, Y. (1968) *Am J Pathol* **53**, 609-616

39. Hassan, M. O., and Subramanyan, S. (1995) *Ultrastruct Pathol* **19**, 201-203

40. Ong, A. C., and Wagner, B. (2005) *Am J Kidney Dis* **45**, 1096-1099

41. Praetorius, H. A., and Spring, K. R. (2003) *J Membr Biol* **191**, 69-76

42. Di Paolo, G., and De Camilli, P. (2006) *Nature* **443**, 651-657

43. Roth, M. G. (2004) *Physiol Rev* **84**, 699-730

44. Hokin, M. R. (1968) *Arch Biochem Biophys* **124**, 280-284

45. Mikoshiba, K. (2006) *J Neurochem* **97**, 1627-1633

46. Streb, H., Irvine, R. F., Berridge, M. J., and Schulz, I. (1983) *Nature* **306**, 67-69

47. Taylor, C. W., Taufiq Ur, R., and Pantazaka, E. (2009) *Chaos* **19**, 037102

48. Diambra, L., and Marchant, J. S. (2009) *Chaos* **19**, 037103

49. Berridge, M. J. (2009) *Biochim Biophys Acta* **1793**, 933-940

50. Nishizuka, Y. (1995) *FASEB J* **9**, 484-496

51. Hiles, I. D., Otsu, M., Volinia, S., Fry, M. J., Gout, I., Dhand, R., Panayotou, G., Ruiz-Larrea, F., Thompson, A., Totty, N. F., and et al. (1992) *Cell* **70**, 419-429

52. Schu, P. V., Takegawa, K., Fry, M. J., Stack, J. H., Waterfield, M. D., and Emr, S. D. (1993) *Science* **260**, 88-91

53. Herman, P. K., and Emr, S. D. (1990) *Mol Cell Biol* **10**, 6742-6754

54. Stack, J. H., Herman, P. K., Schu, P. V., and Emr, S. D. (1993) *EMBO J* **12**, 2195-2204

55. Martin-Belmonte, F., Gassama, A., Datta, A., Yu, W., Rescher, U., Gerke, V., and Mostov, K. (2007) *Cell* **128**, 383-397

56. Lemmon, M. A. (2008) *Nat Rev Mol Cell Biol* **9**, 99-111

57. Puertollano, R. (2004) *EMBO Rep* **5**, 942-946

58. Traub, L. M., and Wendland, B. (2010) *Nature* **465**, 556-557

59. Traub, L. M. (2009) *Nat Rev Mol Cell Biol* **10**, 583-596

60. Brett, T. J., and Traub, L. M. (2006) *Curr Opin Cell Biol* **18**, 395-406

61. Chernomordik, L. (1996) *Chem Phys Lipids* **81**, 203-213

62. Wymann, M. P., and Pirola, L. (1998) *Biochim Biophys Acta* **1436**, 127-150

63. Vanhaesebroeck, B., Leevers, S. J., Panayotou, G., and Waterfield, M. D. (1997) *Trends Biochem Sci* **22**, 267-272

64. Volinia, S., Dhand, R., Vanhaesebroeck, B., MacDougall, L. K., Stein, R., Zvelebil, M. J., Domin, J., Panaretou, C., and Waterfield, M. D. (1995) *EMBO J* **14**, 3339-3348

65. Woscholski, R., Kodaki, T., McKinnon, M., Waterfield, M. D., and Parker, P. J. (1994) *FEBS Lett* **342**, 109-114

66. Stack, J. H. a. E., S.D. (1995) *J. Biol. Chem.* **269**, 31552-31562

67. Domin, J., Gaidarov, I., Smith, M. E., Keen, J. H., and Waterfield, M. D. (2000) *J Biol Chem* **275**, 11943-11950

68. Gaidarov, I., Smith, M. E., Domin, J., and Keen, J. H. (2001) *Mol Cell* **7**, 443-449

69. Joly, M., Kazlauskas, A., and Corvera, S. (1995) *J Biol Chem* **270**, 13225-13230

70. Jones, S. M., and Howell, K. E. (1997) *J Cell Biol* **139**, 339-349

71. Martys, J. L., Wjasow, C., Gangi, D. M., Kielian, M. C., McGraw, T. E., and Backer, J. M. (1996) *J Biol Chem* **271**, 10953-10962

72. Shpetner, H., Joly, M., Hartley, D., and Corvera, S. (1996) *J Cell Biol* **132**, 595-605

73. Spiro, D. J., Boll, W., Kirchhausen, T., and Wessling-Resnick, M. (1996) *Mol Biol Cell* **7**, 355-367

74. Flanagan, C. A., Schnieders, E. A., Emerick, A. W., Kunisawa, R., Admon, A., and Thorner, J. (1993) *Science* **262**, 1444-1448

75. Yoshida, S., Ohya, Y., Goebl, M., Nakano, A., and Anraku, Y. (1994) *J Biol Chem* **269**, 1166-1172

76. Nakagawa, T., Goto, K., and Kondo, H. (1996) *J Biol Chem* **271**, 12088-12094

77. Wong, K., and Cantley, L. C. (1994) *J Biol Chem* **269**, 28878-28884

78. Balla, T., Downing, G. J., Jaffe, H., Kim, S., Zolyomi, A., and Catt, K. J. (1997) *J Biol Chem* **272**, 18358-18366

79. Meyers, R., and Cantley, L. C. (1997) *J Biol Chem* **272**, 4384-4390

80. Nakagawa, T., Goto, K., and Kondo, H. (1996) *Biochem J* **320 (Pt 2)**, 643-649

81. Audhya, A., Foti, M., and Emr, S. D. (2000) *Mol Biol Cell* **11**, 2673-2689

82. Hama, H., Schnieders, E. A., Thorner, J., Takemoto, J. Y., and DeWald, D. B. (1999) *J Biol Chem* **274**, 34294-34300

83. Walch-Solimena, C., and Novick, P. (1999) *Nat Cell Biol* **1**, 523-525

84. Godi, A., Pertile, P., Meyers, R., Marra, P., Di Tullio, G., Iurisci, C., Luini, A., Corda, D., and De Matteis, M. A. (1999) *Nat Cell Biol* **1**, 280-287

85. Wong, K., Meyers dd, R., and Cantley, L. C. (1997) *J Biol Chem* **272**, 13236-13241

86. Trotter, P. J., Wu, W. I., Pedretti, J., Yates, R., and Voelker, D. R. (1998) *J Biol Chem* **273**,

13189-13196

87. Han, G. S., Audhya, A., Markley, D. J., Emr, S. D., and Carman, G. M. (2002) *J Biol Chem* **277**, 47709-47718

88. Shelton, S. N., Barylko, B., Binns, D. D., Horazdovsky, B. F., Albanesi, J. P., and Goodman, J. M. (2003) *Biochem J* **371**, 533-540

89. Wei, Y. J., Sun, H. Q., Yamamoto, M., Wlodarski, P., Kunii, K., Martinez, M., Barylko, B., Albanesi, J. P., and Yin, H. L. (2002) *J Biol Chem* **277**, 46586-46593

90. Wang, Y. J., Wang, J., Sun, H. Q., Martinez, M., Sun, Y. X., Macia, E., Kirchhausen, T., Albanesi, J. P., Roth, M. G., and Yin, H. L. (2003) *Cell* **114**, 299-310

91. Bazenet, C. E., Ruano, A. R., Brockman, J. L., and Anderson, R. A. (1990) *J Biol Chem* **265**, 18012-18022

92. Ling, L. E., Schulz, J. T., and Cantley, L. C. (1989) *J Biol Chem* **264**, 5080-5088

93. Boronenkov, I. V., and Anderson, R. A. (1995) *J Biol Chem* **270**, 2881-2884

94. Castellino, A. M., Parker, G. J., Boronenkov, I. V., Anderson, R. A., and Chao, M. V. (1997) *J Biol Chem* **272**, 5861-5870

95. Divecha, N., Truong, O., Hsuan, J. J., Hinchliffe, K. A., and Irvine, R. F. (1995) *Biochem J* **309 (Pt 3)**, 715-719

96. Rameh, L. E., Tolias, K. F., Duckworth, B. C., and Cantley, L. C. (1997) *Nature* **390**, 192-196

97. Zhang, X., Loijens, J. C., Boronenkov, I. V., Parker, G. J., Norris, F. A., Chen, J., Thum, O., Prestwich, G. D., Majerus, P. W., and Anderson, R. A. (1997) *J Biol Chem* **272**, 17756-17761

98. Fruman, D. A., Meyers, R. E., and Cantley, L. C. (1998) *Annu Rev Biochem* **67**, 481-507

99. Kunz, J., Fuelling, A., Kolbe, L., and Anderson, R. A. (2002) *J Biol Chem* **277**, 5611-5619

100. Boronenkov, I. V., Loijens, J. C., Umeda, M., and Anderson, R. A. (1998) *Mol Biol Cell* **9**, 3547-3560

101. Hinchliffe, K. A., Irvine, R. F., and Divecha, N. (1996) *EMBO J* **15**, 6516-6524

102. Itoh, T., Ijuin, T., and Takenawa, T. (1998) *J Biol Chem* **273**, 20292-20299

103. Hinchliffe, K. A., Ciruela, A., Letcher, A. J., Divecha, N., and Irvine, R. F. (1999) *Curr Biol* **9**,

983-986

104. Ciruela, A., Hinchliffe, K. A., Divecha, N., and Irvine, R. F. (2000) *Biochem J* **346 Pt 3**, 587-591

105. Kunz, J., Wilson, M. P., Kisseleva, M., Hurley, J. H., Majerus, P. W., and Anderson, R. A. (2000) *Mol Cell* **5**, 1-11

106. Rozenvayn, N., and Flaumenhaft, R. (2001) *J Biol Chem* **276**, 22410-22419

107. Sbrissa, D., Ikonomov, O. C., and Shisheva, A. (1999) *J Biol Chem* **274**, 21589-21597

108. Sbrissa, D., Ikonomov, O. C., and Shisheva, A. (2002) *J Biol Chem* **277**, 6073-6079

109. Cooke, F. T., Dove, S. K., McEwen, R. K., Painter, G., Holmes, A. B., Hall, M. N., Michell, R. H., and Parker, P. J. (1998) *Curr Biol* **8**, 1219-1222

110. Gary, J. D., Wurmser, A. E., Bonangelino, C. J., Weisman, L. S., and Emr, S. D. (1998) *J Cell Biol* **143**, 65-79

111. Yamamoto, A., DeWald, D. B., Boronenkov, I. V., Anderson, R. A., Emr, S. D., and Koshland, D. (1995) *Mol Biol Cell* **6**, 525-539

112. Ikonomov, O. C., Sbrissa, D., Mlak, K., Kanzaki, M., Pessin, J., and Shisheva, A. (2002) *J Biol Chem* **277**, 9206-9211

113. Ishihara, H., Shibasaki, Y., Kizuki, N., Katagiri, H., Yazaki, Y., Asano, T., and Oka, Y. (1996) *J Biol Chem* **271**, 23611-23614

114. Ling, K., Bairstow, S. F., Carbonara, C., Turbin, D. A., Huntsman, D. G., and Anderson, R. A. (2007) *J Cell Biol* **176**, 343-353

115. Padron, D., Wang, Y. J., Yamamoto, M., Yin, H., and Roth, M. G. (2003) *J Cell Biol* **162**, 693-701

116. Loijens, J. C., and Anderson, R. A. (1996) *J Biol Chem* **271**, 32937-32943

117. Barbieri, M. A., Heath, C. M., Peters, E. M., Wells, A., Davis, J. N., and Stahl, P. D. (2001) *J Biol Chem* **276**, 47212-47216

118. Guerriero, C. J., Weixel, K. M., Bruns, J. R., and Weisz, O. A. (2006) *J Biol Chem* **281**, 15376-15384

119. Weixel, K. M., Edinger, R. S., Kester, L., Guerriero, C. J., Wang, H., Fang, L., Kleyman, T. R., Welling, P. A., Weisz, O. A., and Johnson, J. P. (2007) *J Biol Chem* **282**, 36534-36542

120. Bairstow, S. F., Ling, K., Su, X., Firestone, A. J., Carbonara, C., and Anderson, R. A. (2006) *J Biol Chem* **281**, 20632-20642

121. Krauss, M., Kukhtina, V., Pechstein, A., and Haucke, V. (2006) *Proc Natl Acad Sci U S A* **103**, 11934-11939

122. Desrivieres, S., Cooke, F. T., Parker, P. J., and Hall, M. N. (1998) *J Biol Chem* **273**, 15787-15793

123. Homma, K., Terui, S., Minemura, M., Qadota, H., Anraku, Y., Kanaho, Y., and Ohya, Y. (1998) *J Biol Chem* **273**, 15779-15786

124. Winzeler, E. A., Shoemaker, D. D., Astromoff, A., Liang, H., Anderson, K., Andre, B., Bangham, R., Benito, R., Boeke, J. D., Bussey, H., Chu, A. M., Connelly, C., Davis, K., Dietrich, F., Dow, S. W., El Bakkoury, M., Foury, F., Friend, S. H., Gentalen, E., Giaever, G., Hegemann, J. H., Jones, T., Laub, M., Liao, H., Liebundguth, N., Lockhart, D. J., Lucau-Danila, A., Lussier, M., M'Rabet, N., Menard, P., Mittmann, M., Pai, C., Rebischung, C., Revuelta, J. L., Riles, L., Roberts, C. J., Ross-MacDonald, P., Scherens, B., Snyder, M., Sookhai-Mahadeo, S., Storms, R. K., Veronneau, S., Voet, M., Volckaert, G., Ward, T. R., Wysocki, R., Yen, G. S., Yu, K., Zimmermann, K., Philippsen, P., Johnston, M., and Davis, R. W. (1999) *Science* **285**, 901-906

125. Itoh, T., Ishihara, H., Shibasaki, Y., Oka, Y., and Takenawa, T. (2000) *J Biol Chem* **275**, 19389-19394

126. Sbrissa, D., Ikonomov, O. C., and Shisheva, A. (2000) *Biochemistry* **39**, 15980-15989

127. Chen, M. Z., Zhu, X., Sun, H. Q., Mao, Y. S., Wei, Y., Yamamoto, M., and Yin, H. L. (2009) *J Biol Chem* **284**, 23743-23753

128. Lacalle, R. A., Peregil, R. M., Albar, J. P., Merino, E., Martinez, A. C., Merida, I., and Manes, S. (2007) *J Cell Biol* **179**, 1539-1553

129. Arioka, M., Nakashima, S., Shibasaki, Y., and Kitamoto, K. (2004) *Biochem Biophys Res Commun* **319**, 456-463

130. Vicinanza, M., D'Angelo, G., Di Campli, A., and De Matteis, M. A. (2008) *EMBO J* **27**, 2457-2470

131. Guo, S., Stolz, L. E., Lemrow, S. M., and York, J. D. (1999) *J Biol Chem* **274**, 12990-12995

132. Krauss, M., and Haucke, V. (2007) *EMBO Rep* **8**, 241-246

133. Nicot, A. S., and Laporte, J. (2008) *Traffic* **9**, 1240-1249

134. Huang, J., and Klionsky, D. J. (2007) *Cell Cycle* **6**, 1837-1849

135. Petiot, A., Ogier-Denis, E., Blommaart, E. F., Meijer, A. J., and Codogno, P. (2000) *J Biol Chem* **275**, 992-998

136. Vivanco, I., and Sawyers, C. L. (2002) *Nat Rev Cancer* **2**, 489-501

137. Zeng, X., Overmeyer, J. H., and Maltese, W. A. (2006) *J Cell Sci* **119**, 259-270

138. Narkis, G., Ofir, R., Landau, D., Manor, E., Volokita, M., Hershkowitz, R., Elbedour, K., and Birk, O. S. (2007) *Am J Hum Genet* **81**, 530-539

139. Marion, E., Kaisaki, P. J., Pouillon, V., Gueydan, C., Levy, J. C., Bodson, A., Krzentowski, G., Daubresse, J. C., Mockel, J., Behrends, J., Servais, G., Szpirer, C., Kruys, V., Gauguier, D., and Schurmans, S. (2002) *Diabetes* **51**, 2012-2017

140. Soeda, Y., Tsuneki, H., Muranaka, H., Mori, N., Hosoh, S., Ichihara, Y., Kagawa, S., Wang, X., Toyooka, N., Takamura, Y., Uwano, T., Nishijo, H., Wada, T., and Sasaoka, T. (2010) *Mol Endocrinol* **24**, 1965-1977

141. Baumgartener, J. W. (2003) *Curr Drug Targets Immune Endocr Metabol Disord* **3**, 291-298

142. Metzner, A., Precht, C., Fehse, B., Fiedler, W., Stocking, C., Gunther, A., Mayr, G. W., and Jucker, M. (2009) *Gene Ther* **16**, 570-573

143. Kimura, T., Suzuki, A., Fujita, Y., Yomogida, K., Lomeli, H., Asada, N., Ikeuchi, M., Nagy, A., Mak, T. W., and Nakano, T. (2003) *Development* **130**, 1691-1700

144. Chibon, F., Primois, C., Bressieux, J. M., Lacombe, D., Lok, C., Mauriac, L., Taieb, A., and Longy, M. (2008) *J Med Genet* **45**, 657-665

145. Ooms, L. M., Horan, K. A., Rahman, P., Seaton, G., Gurung, R., Kethesparan, D. S., and Mitchell, C. A. (2009) *Biochem J* **419**, 29-49

146. Lowe, C. U., Terrey, M., and Mac, L. E. (1952) *AMA Am J Dis Child* **83**, 164-184

147. Attree, O., Olivos, I. M., Okabe, I., Bailey, L. C., Nelson, D. L., Lewis, R. A., McInnes, R. R., and Nussbaum, R. L. (1992) *Nature* **358**, 239-242

148. Silver, D. N., Lewis, R. A., and Nussbaum, R. L. (1987) *J Clin Invest* **79**, 282-285

149. Reilly, D. S., Lewis, R. A., Ledbetter, D. H., and Nussbaum, R. L. (1988) *Am J Hum Genet* **42**, 748-755

150. Reilly, D. S., Lewis, R. A., and Nussbaum, R. L. (1990) *Genomics* **8**, 62-70

151. Hodgson, S. V., Heckmatt, J. Z., Hughes, E., Crolla, J. A., Dubowitz, V., and Bobrow, M. (1986) *Am J Med Genet* **23**, 837-847

152. Mueller, O. T., Hartsfield, J. K., Jr., Gallardo, L. A., Essig, Y. P., Miller, K. L., Papenhausen, P. R., and Tedesco, T. A. (1991) *Am J Hum Genet* **49**, 804-810

153. Al-Uzri, A., Steiner, R.D., Wasserstein, M.P., Fenton, C.L. (2009) Oculocerebrorenal Dystrophy (Lowe Syndrome).

154. Schurman, S. J., and Scheinman, S. J. (2009) *Nat Rev Nephrol* **5**, 529-538

155. Gaary, E. A., Rawnsley, E., Marin-Padilla, J. M., Morse, C. L., and Crow, H. C. (1993) *J Ultrasound Med* **12**, 234-236

156. McSpadden, K. (2000) *Living with Lowe Syndrome: A Guide for Families, Friends and Professionals*, 3rd ed., Lowe Syndrome Association, Inc

157. Lewis, R. A., Nussbaum, R.L., Brewer, E.D. (2008) Lowe Syndrome.

158. Charnas, L. R., Bernardini, I., Rader, D., Hoeg, J. M., and Gahl, W. A. (1991) *N Engl J Med* **324**, 1318-1325

159. Kleta, R. (2008) *Clin J Am Soc Nephrol* **3**, 1244-1245

160. Vilasi, A., Cutillas, P. R., Maher, A. D., Zirah, S. F., Capasso, G., Norden, A. W., Holmes, E., Nicholson, J. K., and Unwin, R. J. (2007) *Am J Physiol Renal Physiol* **293**, F456-467

161. Tricot, L., Yahiaoui, Y., Teixeira, L., Benabdallah, L., Rothschild, E., Juquel, J. P., Satre, V., Grunfeld, J. P., and Chauveau, D. (2003) *Nephrol Dial Transplant* **18**, 1923-1925

162. Ungewickell, A., Ward, M. E., Ungewickell, E., and Majerus, P. W. (2004) *Proc Natl Acad Sci U S A* **101**, 13501-13506

163. Suchy, S. F., Olivos-Glander, I. M., and Nussabaum, R. L. (1995) *Hum Mol Genet* **4**, 2245-2250

164. Zhang, X., Jefferson, A. B., Auethavekiat, V., and Majerus, P. W. (1995) *Proc Natl Acad Sci U S A* **92**, 4853-4856

165. Peck, J., Douglas, G. t., Wu, C. H., and Burbelo, P. D. (2002) *FEBS Lett* **528**, 27-34

166. Lichter-Konecki, U., Farber, L. W., Cronin, J. S., Suchy, S. F., and Nussbaum, R. L. (2006) *Mol*

Genet Metab **89**, 121-128

167. Dressman, M. A., Olivos-Glander, I. M., Nussbaum, R. L., and Suchy, S. F. (2000) *J Histochem Cytochem* **48**, 179-190

168. Choudhury, R., Diao, A., Zhang, F., Eisenberg, E., Saint-Pol, A., Williams, C., Konstantakopoulos, A., Lucocq, J., Johannes, L., Rabouille, C., Greene, L. E., and Lowe, M. (2005) *Mol Biol Cell* **16**, 3467-3479

169. Olivos-Glander, I. M., Janne, P. A., and Nussbaum, R. L. (1995) *Am J Hum Genet* **57**, 817-823

170. Erdmann, K. S., Mao, Y., McCrea, H. J., Zoncu, R., Lee, S., Paradise, S., Modregger, J., Biemesderfer, D., Toomre, D., and De Camilli, P. (2007) *Dev Cell* **13**, 377-390

171. Faucherre, A., Desbois, P., Nagano, F., Satre, V., Lunardi, J., Gacon, G., and Dorseuil, O. (2005) *Hum Mol Genet* **14**, 1441-1448

172. Lowe, M. (2005) *Traffic* **6**, 711-719

173. Janne, P. A., Suchy, S. F., Bernard, D., MacDonald, M., Crawley, J., Grinberg, A., Wynshaw-Boris, A., Westphal, H., and Nussbaum, R. L. (1998) *J Clin Invest* **101**, 2042-2053

174. Cui, S., Guerriero, C. J., Szalinski, C. M., Kinlough, C. L., Hughey, R. P., and Weisz, O. A. (2010) *Am J Physiol Renal Physiol* **298**, F335-345

175. Bokenkamp, A., Bockenhauer, D., Cheong, H. I., Hoppe, B., Tasic, V., Unwin, R., and Ludwig, M. (2009) *J Pediatr* **155**, 94-99

176. Shrimpton, A. E., Hoopes, R. R., Jr., Knohl, S. J., Hueber, P., Reed, A. A., Christie, P. T., Igarashi, T., Lee, P., Lehman, A., White, C., Milford, D. V., Sanchez, M. R., Unwin, R., Wrong, O. M., Thakker, R. V., and Scheinman, S. J. (2009) *Nephron Physiol* **112**, p27-36

177. Cho, H. Y., Lee, B. H., Choi, H. J., Ha, I. S., Choi, Y., and Cheong, H. I. (2008) *Pediatr Nephrol* **23**, 243-249

178. Hoopes, R. R., Jr., Shrimpton, A. E., Knohl, S. J., Hueber, P., Hoppe, B., Matyus, J., Simckes, A., Tasic, V., Toenshoff, B., Suchy, S. F., Nussbaum, R. L., and Scheinman, S. J. (2005) *Am J Hum Genet* **76**, 260-267

179. Ludwig, M., Doroszewicz, J., Seyberth, H. W., Bokenkamp, A., Balluch, B., Nuutinen, M., Utsch, B., and Waldegger, S. (2005) *Hum Genet* **117**, 228-237

180. Picollo, A., and Pusch, M. (2005) *Nature* **436**, 420-423

181. Scheel, O., Zdebik, A. A., Lourdel, S., and Jentsch, T. J. (2005) *Nature* **436**, 424-427

182. Ponting, C. P. (2006) *Bioinformatics* **22**, 1031-1035

183. Swan, L. E., Tomasini, L., Pirruccello, M., Lunardi, J., and De Camilli, P. (2010) *Proc Natl Acad Sci U S A* **107**, 3511-3516

184. (2010) Tight junction. *Wikipedia*

185. Gumbiner, B. (1987) *Am J Physiol* **253**, C749-758

186. Gassama-Diagne, A., Yu, W., ter Beest, M., Martin-Belmonte, F., Kierbel, A., Engel, J., and Mostov, K. (2006) *Nat Cell Biol* **8**, 963-970

187. Thompson, A., Nessler, R., Wisco, D., Anderson, E., Winckler, B., and Sheff, D. (2007) *Mol Biol Cell* **18**, 2687-2697

188. Fields, I. C., King, S. M., Shteyn, E., Kang, R. S., and Folsch, H. (2010) *Mol Biol Cell* **21**, 95-105

189. Thieman, J. R., Mishra, S. K., Ling, K., Doray, B., Anderson, R. A., and Traub, L. M. (2009) *J Biol Chem* **284**, 13924-13939

190. Yamamoto, M., Chen, M. Z., Wang, Y. J., Sun, H. Q., Wei, Y., Martinez, M., and Yin, H. L. (2006) *J Biol Chem* **281**, 32630-32638

191. Naim, H. Y., Dodds, D. T., Brewer, C. B., and Roth, M. G. (1995) *J Cell Biol* **129**, 1241-1250

192. Park, S. J., Itoh, T., and Takenawa, T. (2001) *J Biol Chem* **276**, 4781-4787

193. Moritz, A., De Graan, P. N., Gispen, W. H., and Wirtz, K. W. (1992) *J Biol Chem* **267**, 7207-7210

194. Stace, C., Manifava, M., Delon, C., Coadwell, J., Cockcroft, S., and Ktistakis, N. T. (2008) *Adv Enzyme Regul* **48**, 55-72

195. Delon, C., Manifava, M., Wood, E., Thompson, D., Krugmann, S., Pyne, S., and Ktistakis, N. T. (2004) *J Biol Chem* **279**, 44763-44774

196. Nishioka, T., Frohman, M. A., Matsuda, M., and Kiyokawa, E. (2010) *J Biol Chem* **285**, 35979-35987

197. Brindley, D. N., Pilquil, C., Sariahmetoglu, M., and Reue, K. (2009) *Biochim Biophys Acta* **1791**, 956-961

198. Grimsey, N., Han, G. S., O'Hara, L., Rochford, J. J., Carman, G. M., and Siniossoglou, S. (2008) *J Biol Chem* **283**, 29166-29174

199. Brindley, D. N., and Pilquil, C. (2009) *J Lipid Res* **50 Suppl**, S225-230

200. Brindley, D. N. (2004) *J Cell Biochem* **92**, 900-912

201. Pyne, S., Long, J. S., Ktistakis, N. T., and Pyne, N. J. (2005) *Biochem Soc Trans* **33**, 1370-1374

202. Pyne, S., Kong, K. C., and Darroch, P. I. (2004) *Semin Cell Dev Biol* **15**, 491-501

203. Brindley, D. N., and Waggoner, D. W. (1998) *J Biol Chem* **273**, 24281-24284

204. (2010) Phosphatidic acid. *Wikipedia*

205. Tolias, K. F., Hartwig, J. H., Ishihara, H., Shibasaki, Y., Cantley, L. C., and Carpenter, C. L. (2000) *Curr Biol* **10**, 153-156

206. Choudhury, R., Noakes, C. J., McKenzie, E., Kox, C., and Lowe, M. (2009) *J Biol Chem* **284**, 9965-9973

207. Lin, T., Orrison, B. M., Leahey, A. M., Suchy, S. F., Bernard, D. J., Lewis, R. A., and Nussbaum, R. L. (1997) *Am J Hum Genet* **60**, 1384-1388

208. Zhang, X., Hartz, P. A., Philip, E., Racusen, L. C., and Majerus, P. W. (1998) *J Biol Chem* **273**, 1574-1582

209. Charnas, L. R., and Gahl, W. A. (1991) *Adv Pediatr* **38**, 75-107

210. Vicinanza, M., D'Angelo, G., Di Campli, A., and De Matteis, M. A. (2008) *Cell Mol Life Sci* **65**, 2833-2841

211. Taunton, J., Rowning, B. A., Coughlin, M. L., Wu, M., Moon, R. T., Mitchison, T. J., and Larabell, C. A. (2000) *J Cell Biol* **148**, 519-530

212. Utsch, B., Bokenkamp, A., Benz, M. R., Besbas, N., Dotsch, J., Franke, I., Frund, S., Gok, F., Hoppe, B., Karle, S., Kuwertz-Broking, E., Laube, G., Neb, M., Nuutinen, M., Ozaltin, F., Rascher, W., Ring, T., Tasic, V., van Wijk, J. A., and Ludwig, M. (2006) *Am J Kidney Dis* **48**, 942 e941-914

213. Christensen, E. I., Devuyst, O., Dom, G., Nielsen, R., Van der Smissen, P., Verroust, P., Leruth, M., Guggino, W. B., and Courtoy, P. J. (2003) *Proc Natl Acad Sci U S A* **100**, 8472-8477

214. Devuyst, O., Jouret, F., Auzanneau, C., and Courtoy, P. J. (2005) *Nephron Physiol* **99**, p69-73

215. Guggino, S. E. (2007) *Nat Clin Pract Nephrol* **3**, 449-455

216. Hryciw, D. H., Ekberg, J., Pollock, C. A., and Poronnik, P. (2006) *Int J Biochem Cell Biol* **38**, 1036-1042

217. Su, T., Cariappa, R., and Stanley, K. (1999) *FEBS Lett* **453**, 391-394

218. Wang, S. S., Devuyst, O., Courtoy, P. J., Wang, X. T., Wang, H., Wang, Y., Thakker, R. V., Guggino, S., and Guggino, W. B. (2000) *Hum Mol Genet* **9**, 2937-2945

219. Wang, Y., Cai, H., Cebotaru, L., Hryciw, D. H., Weinman, E. J., Donowitz, M., Guggino, S. E., and Guggino, W. B. (2005) *Am J Physiol Renal Physiol* **289**, F850-862

220. Coon, B. G., Mukherjee, D., Hanna, C. B., Riese, D. J., 2nd, Lowe, M., and Aguilar, R. C. (2009) *Hum Mol Genet* **18**, 4478-4491

221. Williams, C., Choudhury, R., McKenzie, E., and Lowe, M. (2007) *J Cell Sci* **120**, 3941-3951

222. Ungewickell, A. J., and Majerus, P. W. (1999) *Proc Natl Acad Sci U S A* **96**, 13342-13344

223. Allen, P. G. (2003) *Nat Cell Biol* **5**, 972-979

224. Nagai, M., Meerloo, T., Takeda, T., and Farquhar, M. G. (2003) *Mol Biol Cell* **14**, 4984-4996

225. Marzolo, M. P., Yuseff, M. I., Retamal, C., Donoso, M., Ezquer, F., Farfan, P., Li, Y., and Bu, G. (2003) *Traffic* **4**, 273-288

226. Maritzen, T., Lisi, S., Botta, R., Pinchera, A., Fanelli, G., Viacava, P., Marcocci, C., and Marino, M. (2006) *Thyroid* **16**, 725-730

227. van den Hove, M. F., Croizet-Berger, K., Jouret, F., Guggino, S. E., Guggino, W. B., Devuyst, O., and Courtoy, P. J. (2006) *Endocrinology* **147**, 1287-1296

228. Moulin, P., Igarashi, T., Van der Smissen, P., Cosyns, J. P., Verroust, P., Thakker, R. V., Scheinman, S. J., Courtoy, P. J., and Devuyst, O. (2003) *Kidney Int* **63**, 1285-1295

229. Hara-Chikuma, M., Wang, Y., Guggino, S. E., Guggino, W. B., and Verkman, A. S. (2005) *Biochem Biophys Res Commun* **329**, 941-946

230. Hyvola, N., Diao, A., McKenzie, E., Skippen, A., Cockcroft, S., and Lowe, M. (2006) *EMBO J* **25**, 3750-3761

231. Nielsen, R., Courtoy, P. J., Jacobsen, C., Dom, G., Lima, W. R., Jadot, M., Willnow, T. E., Devuyst, O., and Christensen, E. I. (2007) *Proc Natl Acad Sci U S A* **104**, 5407-5412

232. Pollock, C. A., and Poronnik, P. (2007) *Curr Opin Nephrol Hypertens* **16**, 359-364

233. Miaczynska, M., Christoforidis, S., Giner, A., Shevchenko, A., Uttenweiler-Joseph, S., Habermann, B., Wilm, M., Parton, R. G., and Zerial, M. (2004) *Cell* **116**, 445-456

234. (2008) OCRL. in *Genes- Genetics Home Reference*

235. McCrea, H. J., Paradise, S., Tomasini, L., Addis, M., Melis, M. A., De Matteis, M. A., and De Camilli, P. (2008) *Biochem Biophys Res Commun* **369**, 493-499

236. Fukuda, M., Kanno, E., Ishibashi, K., and Itoh, T. (2008) *Mol Cell Proteomics* **7**, 1031-1042

237. Mao, Y., Balkin, D. M., Zoncu, R., Erdmann, K. S., Tomasini, L., Hu, F., Jin, M. M., Hodsdon, M. E., and De Camilli, P. (2009) *EMBO J* **28**, 1831-1842

238. Shin, H. W., Hayashi, M., Christoforidis, S., Lacas-Gervais, S., Hoepfner, S., Wenk, M. R., Modregger, J., Uttenweiler-Joseph, S., Wilm, M., Nystuen, A., Frankel, W. N., Solimena, M., De Camilli, P., and Zerial, M. (2005) *J Cell Biol* **170**, 607-618

239. ter Haar, E., Harrison, S. C., and Kirchhausen, T. (2000) *Proc Natl Acad Sci U S A* **97**, 1096-1100

240. Cutillas, P. R., Chalkley, R. J., Hansen, K. C., Cramer, R., Norden, A. G., Waterfield, M. D., Burlingame, A. L., and Unwin, R. J. (2004) *Am J Physiol Renal Physiol* **287**, F353-364

241. Schmid, A. C., Wise, H. M., Mitchell, C. A., Nussbaum, R., and Woscholski, R. (2004) *FEBS Lett* **576**, 9-13

242. van der Bliek, A. M. (2005) *Nat Cell Biol* **7**, 548-550

243. Smith, L. A., Bukanov, N. O., Husson, H., Russo, R. J., Barry, T. C., Taylor, A. L., Beier, D. R., and Ibraghimov-Beskrovnaya, O. (2006) *J Am Soc Nephrol* **17**, 2821-2831

244. Lin, F., Hiesberger, T., Cordes, K., Sinclair, A. M., Goldstein, L. S., Somlo, S., and Igarashi, P. (2003) *Proc Natl Acad Sci U S A* **100**, 5286-5291

245. Olbrich, H., Fliegauf, M., Hoefele, J., Kispert, A., Otto, E., Volz, A., Wolf, M. T., Sasmaz, G., Trauer, U., Reinhardt, R., Sudbrak, R., Antignac, C., Gretz, N., Walz, G., Schermer, B., Benzing, T., Hildebrandt, F., and Omran, H. (2003) *Nat Genet* **34**, 455-459

246. Bergmann, C., Fliegauf, M., Bruchle, N. O., Frank, V., Olbrich, H., Kirschner, J., Schermer, B.,

Schmedding, I., Kispert, A., Kranzlin, B., Nurnberg, G., Becker, C., Grimm, T., Girschick, G., Lynch, S. A., Kelehan, P., Senderek, J., Neuhaus, T. J., Stallmach, T., Zentgraf, H., Nurnberg, P., Gretz, N., Lo, C., Lienkamp, S., Schafer, T., Walz, G., Benzing, T., Zerres, K., and Omran, H. (2008) *Am J Hum Genet* **82**, 959-970

247. Cano, D. A., Murcia, N. S., Pazour, G. J., and Hebrok, M. (2004) *Development* **131**, 3457-3467

248. Woollard, J. R., Punyashtiti, R., Richardson, S., Masyuk, T. V., Whelan, S., Huang, B. Q., Lager, D. J., vanDeursen, J., Torres, V. E., Gattone, V. H., LaRusso, N. F., Harris, P. C., and Ward, C. J. (2007) *Kidney Int* **72**, 328-336

249. Mokrzan, E. M., Lewis, J. S., and Mykytyn, K. (2007) *Nephron Exp Nephrol* **106**, e88-96

250. Williams, S. S., Cobo-Stark, P., James, L. R., Somlo, S., and Igarashi, P. (2008) *Pediatr Nephrol* **23**, 733-741

251. Zhang, M. Z., Mai, W., Li, C., Cho, S. Y., Hao, C., Moeckel, G., Zhao, R., Kim, I., Wang, J., Xiong, H., Wang, H., Sato, Y., Wu, Y., Nakanuma, Y., Lilova, M., Pei, Y., Harris, R. C., Li, S., Coffey, R. J., Sun, L., Wu, D., Chen, X. Z., Breyer, M. D., Zhao, Z. J., McKanna, J. A., and Wu, G. (2004) *Proc Natl Acad Sci U S A* **101**, 2311-2316

252. Pazour, G. J. (2004) *J Am Soc Nephrol* **15**, 2528-2536

253. Kim, I., Fu, Y., Hui, K., Moeckel, G., Mai, W., Li, C., Liang, D., Zhao, P., Ma, J., Chen, X. Z., George, A. L., Jr., Coffey, R. J., Feng, Z. P., and Wu, G. (2008) *J Am Soc Nephrol* **19**, 455-468

254. Wang, S., Zhang, J., Nauli, S. M., Li, X., Starremans, P. G., Luo, Y., Roberts, K. A., and Zhou, J. (2007) *Mol Cell Biol* **27**, 3241-3252

255. Omran, H., Haffner, K., Burth, S., Fernandez, C., Fargier, B., Villaquiran, A., Nothwang, H. G., Schnittger, S., Lehrach, H., Woo, D., Brandis, M., Sudbrak, R., and Hildebrandt, F. (2001) *J Am Soc Nephrol* **12**, 107-113

256. Marshall, W. F. (2004) *Curr Biol* **14**, R913-914

257. Verghese, E., Ricardo, S. D., Weidenfeld, R., Zhuang, J., Hill, P. A., Langham, R. G., and Deane, J. A. (2009) *J Am Soc Nephrol* **20**, 2147-2153

258. Verghese, E., Weidenfeld, R., Bertram, J. F., Ricardo, S. D., and Deane, J. A. (2008) *Nephrol Dial Transplant* **23**, 834-841

259. Wang, L., Weidenfeld, R., Verghese, E., Ricardo, S. D., and Deane, J. A. (2008) *J Anat* **213**, 79-85

260. Nauli, S. M., Alenghat, F. J., Luo, Y., Williams, E., Vassilev, P., Li, X., Elia, A. E., Lu, W., Brown, E. M., Quinn, S. J., Ingber, D. E., and Zhou, J. (2003) *Nat Genet* **33**, 129-137

261. Simons, M., and Mlodzik, M. (2008) *Annu Rev Genet* **42**, 517-540

262. Xu, Y., Seet, L. F., Hanson, B., and Hong, W. (2001) *Biochem J* **360**, 513-530

263. Honda, A., Nogami, M., Yokozeki, T., Yamazaki, M., Nakamura, H., Watanabe, H., Kawamoto, K., Nakayama, K., Morris, A. J., Frohman, M. A., and Kanaho, Y. (1999) *Cell* **99**, 521-532

264. Robinson, M. L., Allen, C. E., Davy, B. E., Durfee, W. J., Elder, F. F., Elliott, C. S., and Harrison, W. R. (2002) *Mamm Genome* **13**, 625-632

265. Lechtreck, K. F., Delmotte, P., Robinson, M. L., Sanderson, M. J., and Witman, G. B. (2008) *J Cell Biol* **180**, 633-643

266. Davy, B. E., and Robinson, M. L. (2003) *Hum Mol Genet* **12**, 1163-1170

267. Bond, J., Scott, S., Hampshire, D. J., Springell, K., Corry, P., Abramowicz, M. J., Mochida, G. H., Hennekam, R. C., Maher, E. R., Fryns, J. P., Alswaid, A., Jafri, H., Rashid, Y., Mubaidin, A., Walsh, C. A., Roberts, E., and Woods, C. G. (2003) *Am J Hum Genet* **73**, 1170-1177

268. Desir, J., Cassart, M., David, P., Van Bogaert, P., and Abramowicz, M. (2008) *Am J Med Genet A* **146A**, 1439-1443

269. Shen, J., Eyaid, W., Mochida, G. H., Al-Moayyad, F., Bodell, A., Woods, C. G., and Walsh, C. A. (2005) *J Med Genet* **42**, 725-729

270. Sawamoto, K., Wichterle, H., Gonzalez-Perez, O., Cholfin, J. A., Yamada, M., Spassky, N., Murcia, N. S., Garcia-Verdugo, J. M., Marin, O., Rubenstein, J. L., Tessier-Lavigne, M., Okano, H., and Alvarez-Buylla, A. (2006) *Science* **311**, 629-632

271. Saunders, R. D., Avides, M. C., Howard, T., Gonzalez, C., and Glover, D. M. (1997) *J Cell Biol* **137**, 881-890

272. Gong, D., and Ferrell, J. E., Jr. (2004) *Trends Biotechnol* **22**, 451-454

273. Kempiak, S. J., Yamaguchi, H., Sarmiento, C., Sidani, M., Ghosh, M., Eddy, R. J., Desmarais, V., Way, M., Condeelis, J., and Segall, J. E. (2005) *J Biol Chem* **280**, 5836-5842

274. Mo, D., Potter, B. A., Bertrand, C. A., Hildebrand, J. D., Bruns, J. R., and Weisz, O. A. (2010) *Am J Physiol Renal Physiol* **299**, F1178-1184

275. Henkel, J. R., Gibson, G. A., Poland, P. A., Ellis, M. A., Hughey, R. P., and Weisz, O. A. (2000)

J Cell Biol **148**, 495-504

276. Henkel, J. R., Apodaca, G., Altschuler, Y., Hardy, S., and Weisz, O. A. (1998) *Mol Biol Cell* **9**, 2477-2490

277. Henkel, J. R., Popovich, J. L., Gibson, G. A., Watkins, S. C., and Weisz, O. A. (1999) *J Biol Chem* **274**, 9854-9860

278. Bruns, J. R., Ellis, M. A., Jeromin, A., and Weisz, O. A. (2002) *J Biol Chem* **277**, 2012-2018

279. Altschuler, Y., Kinlough, C. L., Poland, P. A., Bruns, J. B., Apodaca, G., Weisz, O. A., and Hughey, R. P. (2000) *Mol Biol Cell* **11**, 819-831

280. Breitfeld, P. P., Casanova, J. E., Harris, J. M., Simister, N. E., and Mostov, K. E. (1989) *Methods Cell Biol* **32**, 329-337